OPTIMIZATION OF DOPPLER PROCESSING BY USING BANK OF MATCHED FILTERS

A THESIS SUBMITTED TO
THE GRADUATE SCHOOL OF NATURAL AND APPLIED SCIENCES
OF
MIDDLE EAST TECHNICAL UNIVERSITY

BY

ONUR AKTOP

IN PARTIAL FULFILLMENT OF THE REQUIREMENTS
FOR
THE DEGREE OF MASTER OF SCIENCE
IN
ELECTRICAL AND ELECTRONICS ENGINEERING

SEPTEMBER 2005

Approval of the Graduate School of Natural and Applied Sciences

_____
Prof. Dr. Canan ÖZGEN
Director

I certify that this thesis satisfies all the requirements as a thesis for the degree of Master of Science.

_____
Prof. Dr. İsmet ERKMEN
Head of Department

This is to certify that we have read this thesis and that in our opinion it is fully adequate, in scope and quality, as a thesis for the degree of Master of Science.

_____
Prof. Dr. Yalçın TANIK
Supervisor

Examining Committee Members

Prof. Dr. Mete SEVERCAN	(METU, EE)	_____
Prof. Dr. Yalçın TANIK	(METU, EE)	_____
Assoc. Prof. Dr. Sencer KOÇ	(METU, EE)	_____
Assist. Prof. Dr. Ali Özgür YILMAZ	(METU, EE)	_____
Aykut ARIKAN, M. Sc. in EE	(ASELSAN)	_____

I hereby declare that all information in this document has been obtained and presented in accordance with academic rules and ethical conduct. I also declare that, as required by these rules and conduct, I have fully cited and referenced all material and results that are not original to this work.

Name, Last name : ONUR AKTOP

Signature :

ABSTRACT

OPTIMIZATION OF DOPPLER PROCESSING BY
USING BANK OF MATCHED FILTERS

AKTOP, Onur
M.S., Department of Electrical and Electronics Engineering
Supervisor: Prof. Dr. Yalçın TANIK

September 2005, 139 pages

In radars, matched filters are used in the receiver of the system. Since the target velocity is not known a priori, degradation occurs due to mismatch of the return signal and the matched filter. The performance of the radar can be improved by using a bank of matched filters. The first topic investigated in this work is optimization of the bank of matched filter structure. Two methods are proposed for the design of the parallel filter structure and computations are performed with both methods.

The output signal of a radar receiver filter consists not only of the main peak from the target but also of range sidelobes. In a multi-target radar environment, the sidelobes of one large target may appear as a smaller target at another range, or the integrated sidelobes from targets or clutter may mask all the information of another target. The second part of this thesis discusses the methods for decreasing the sidelobe level of the receiver output. Two methods are studied for this purpose. The first is the classical amplitude weighting and the second is the use of an inverse filter that

minimizes total sidelobe energy. Both methods decrease the sidelobe levels while bringing a mismatch loss and main peak broadening. For the inverse filter case it is observed that the effect of inverse filter becomes evident as the filter length is increased beyond some point.

Finally, the effects of quantization on video signal and the receiver filter coefficients are evaluated. It is observed that 16 bits quantization is sufficient for all kinds of receiver filters tested.

Keywords: Pulse Doppler radar, Doppler mismatch, P4 code, amplitude weighting, inverse filter

ÖZ

DOPPLER İŞLEMENİN UYUMLU SÜZGEÇ ÖBEĞİ KULLANILARAK ENİYİLEŞTİRİLMESİ

AKTOP, Onur
Yüksek Lisans, Elektrik ve Elektronik Mühendisliği Bölümü
Tez Yöneticisi: Prof. Dr. Yalçın TANIK

Eylül 2005, 139 sayfa

Radarlarda uyumlu süzgeçler sistemin alıcılarında kullanılmaktadır. Hedefin hızı önceden bilinmediğinden sistemde kullanılan uyumlu süzgeç ile hedeften gelen işaretin birbirlerine uyumsuzluğundan dolayı sistemde kayıp oluşmaktadır. Radarın başarımı uyumlu süzgeç öbeği kullanılarak artırılabilir. Bu tezdeki çalışma uyumlu süzgeç öbeği yapısının eniyileştirilmesi ile başlamaktadır. Süzgeç öbeği yapısı için iki yöntem önerilmiş ve benzetimler yapılarak bu yöntemlerin başarımları bulunmuştur.

Radar alıcı süzgecinin çıkış işareti sadece yankı alımı için kullanılan asıl tepeyi içermemekte, bunun yanında yan lopları da bulunmaktadır. Birden çok hedef barındıran bir ortamda, büyük bir hedefin yan lopları başka bir hedefin asıl tepesi gibi gözükebilmekte; bir çok hedefin birleşik yan lobu veya parazitler ise başka bir hedefi tamamen gölgeleyebilmektedir. Bu tezin ikinci kısmı radarın alıcı çıkışındaki yan lop seviyesinin düşürülmesiyle ilgili çalışmaları içerir. Bu amaçla iki yöntem üzerinde durulmuştur; bunlardan ilki klasik genlik ağırlıklandırması, diğeri ise ters süzgeç kullanarak toplam yan

lop enerjisinin asgari düzeye indirilmesidir. Her iki yöntem de yan lop seviyesini düşürürken uyumsuzluktan kaynaklanan kayıba ve asıl tepenin genişlemesine neden olur. Ters süzgeç yönteminde filtrenin öneminin filtre uzunluğu belirli bir değeri geçtikten sonra ortaya çıktığı gözlenmiştir.

Son olarak hedeften gelen yankı işaretinin ve süzgeç katsayılarının kuvantalanmasının radarın başarımına etkileri değerlendirilmiştir. Kuvantalamanın 16 parçadan yapılmasının test edilen tüm alıcı süzgeçleri için yeterli olduğu görülmüştür.

Anahtar Kelimeler: Darbeli Doppler radarı, Doppler uyumsuzluğu, P4 kodu, genlik ağırlıklandırması, ters süzgeç

To my parents,

who always support me in all aspects of my life

ACKNOWLEDGEMENTS

I appreciate Prof. Dr. Yalçın Tanık for his guidance, support and valuable contributions throughout the study.

I express my deepest gratitude to my mother Saniye Aktop, my father Süleyman Aktop and my brother Armağan Aktop for their trust and encouragements throughout my education life.

TABLE OF CONTENTS

LIST OF TABLES

TABLE

LIST OF FIGURES

FIGURE

LIST OF ABBREVIATIONS

ACF	Autocorrelation Function
A/D	Analog to Digital
FM	Frequency Modulation
ibw	Inverse Bandwidth
IF	Inverse Filter
ISL	Integrated Sidelobe Level
LFMW	Linear Frequency Modulation Waveform
MF	Matched Filter
MLB	Main Lobe Broadening
P_D	Probability of Detection
P_{FA}	Probability of False Alarm
PSL	Peak Sidelobe Level
SNR	Signal to Noise Ratio
TSSWA	Two Sample Sliding Window Averager
TSSWD	Two Sample Sliding Window Differencer
WGN	White Gaussian Noise
WMF	Windowed Matched Filter

CHAPTER 1

INTRODUCTION

1.1. Problem Definition

Radar is an electromagnetic system for the detection and location of objects that operates by transmitting electromagnetic signals and receiving echoes from reflective objects (targets) within its volume of coverage. It extracts the location of the objects in space about the radar, the time rate of change of the objects' location in space and in some cases identifies the objects as being a particular one of a number of classes using the information from the echo signal. Radar is an acronym for RAdio Detection And Ranging [1].

Generally, the return signal and the transmitted signals are not the same in a radar system. The difference in signals comes from the radial velocity of the target causing a Doppler frequency shift in the echo signal received by the radar. The Doppler shift phenomenon is used to discriminate real targets from the background clutter such as precipitation, chaff, sea or ground [2]. This phenomenon also gives rise to a signal-to-noise-ratio (SNR) loss in the receiving filter of the radar. The resulting SNR loss in the receiver can be very significant depending on the parameters of the radar and the target radial velocity.

The echo signal coming from a reflective object is filtered in the receiver system of the radar to determine if a target is present or not in the radars operating environment. The output signal of a radar receiver filter consists not only of the main peak used for echo detection but also of time (range) sidelobes. In a multi-target radar environment, the time sidelobes of one large target may appear as a smaller target at another range, or the integrated sidelobes from targets or clutter may mask all the information of another target. Because of this, it is generally desirable that the time sidelobes of the autocorrelation function (ACF) of the transmitted waveform be reduced to the lowest level possible [2].

In modern radars, analog-to-digital (A/D) converters are used in different stages of the whole system. Quantization errors exist in the system because of the finite bit representation of the coefficients of a radar receiver filter and quantization of the received analog signal. The quantization error can increase the sidelobes of the ACF, decrease the probability of detection (P_D) or increase the probability of false alarm (P_{FA}) of the radar depending on the quantization levels used.

1.2. Scope of the Thesis

In this thesis, the first problem considered is the minimization of the SNR loss which is a result of the Doppler shift in the received echo signal. The parameters that cause the SNR loss are obtained first and a parallel filter method is proposed as a solution to the problem. The minimum number of parallel filters that satisfies the desired SNR loss is obtained. The center frequencies of the filters are also calculated. In the literature a study on this subject could not be found.

The second problem considered is the reduction of time sidelobes of the ACF. Different solutions to this problem are considered. The first method is

the use of an amplitude weighting window in the matched filter of the radar. The benefits and drawbacks of this method for different weighting windows are obtained and compared. In [9], the amplitude weighting method is discussed briefly. The results of $\cos^n$ function on pedestal k, Taylor n_{bar} = 6 and Chebyshev windowing functions are given. However, the performance of windowing functions with Doppler shifted echo signal is not investigated. The second method proposed is the use of an inverse filter that minimizes the sidelobe energy. The results of the latter method are obtained and compared with the results of the previous one. In [17], both methods are discussed. Classical amplitude weighting performances of Hanning, Hamming, Chebyshev and Taylor windowing functions are obtained. Inverse filtering method is also studied with different input code lengths and different inverse filter lengths. Again the performance of the methods with Doppler shifted echo signal is not discussed. The difference of the study in this thesis from [9, 17] is that both methods are investigated in detail with Doppler shift responses. The performances of 25 window functions are obtained and the best functions are determined. The performances of window functions that have variable parameters are also obtained and the best parameter values are determined. The Doppler shift performances of the best window functions, as well as inverse filter approach are also obtained.

The last concern of this thesis is the effects of quantization on radar receiver performance. Finite bit representation of receiver filter coefficients and quantization of analog input signal is taken into account and the effect of this on ACF sidelobes is considered. The results are obtained and compared for different receiver filters (matched, inverse) and different weighting windows. Also for a desired P_D and P_{FA}, the extra input SNR required is calculated for different receiver filters and for different levels of quantization. In [12], the effects of quantization on sidelobe levels for Frank code are given briefly. An analysis of the effect of quantization on performance of weighting windows or inverse filter could not be found in the literature. Also, a study on the effect of quantization on detection probabilities of these methods is not present in the literature.

1.3. Outline of the Thesis

In chapter 2; a review of fundamental radar signal processing concepts is given. Matched filter theory, pulse compression, polyphase codes and the radar ambiguity function are roughly mentioned in this chapter.

The parallel filter method for minimization of mismatch loss in the receiver filter is investigated in Chapter 3. The details of the proposed system are given for both odd and even number of parallel filters.

Chapter 4 investigates the weighting techniques for sidelobe suppression. The effects of different weighting windows are compared.

In chapter 5, sidelobe suppression problem is approached by inverse filter method. The results obtained in this chapter are also compared with the results of previous chapter.

The effect of quantization on the performance of the radar system is discussed for various receiver filters in Chapter 6.

CHAPTER 2

REVIEW OF FUNDAMENTAL CONCEPTS

2.1. Matched Filter Theory

The basic concept of matched filters evolved from the effort to obtain a better theoretical understanding of the factors leading to optimum performance of a radar system. The optimum linear processing of radar signals is performed by the matched filter technique. The raw radar data which is assumed to be corrupted by white Gaussian noise available at the radar receiver is transformed into a suitable form with the matched filtering technique for performing optimum detection decisions such as target / no target; or for estimating target parameters such as range, velocity, acceleration with minimum errors [3].

The characteristics of matched filters can be designated by either a frequency response function or a time response function, each being related to the other by a Fourier transform operation. In the frequency domain the matched filter transfer function, $H(f)$, is the complex conjugate function of the spectrum of the signal that is to be processed in the optimum fashion. Thus the transfer function of a matched filter has the form

$$H(f) = kS^{*}(f)e^{-j2\pi fT_d} \tag{2.1}$$

where $S(f)$ is the spectrum of the transmitted signal $s(t)$, k is a constant for normalization, and T_d is a delay constant required to make the filter physically realizable. Except for the amplitude and delay factors of the form $ke^{-j2\pi fT_d}$, the transfer function of a matched filter is the complex conjugate of the spectrum of the signal to which it is matched. Because of this a matched filter is sometimes called a "*conjugate*" filter [4].

The time domain relationship between the transmitted signal and its matched filter is obtained by taking the inverse Fourier transform of $H(f)$. This leads to the result that the impulse response of a matched filter is a replica of the time inverse of the signal function. Thus, if $h(t)$ represents the matched filter impulse response, the general relationship in time domain equivalent to (2.1) is

$$h(t) = ks(T_d - t) \tag{2.2}$$

Then, the output of the matched filter is obtained as

$$y(t) = \int_0^\infty h(\tau)s(t-\tau)d\tau \tag{2.3}$$

or

$$y(t) = \int_{-\infty}^\infty H(f)S(f)e^{j2\pi ft}df\ . \tag{2.4}$$

(2.4) is the inverse Fourier transform of $Y(f)$ and (2.3) is the convolution of $h(t)$ and $s(t)$. Consequently the output of the matched filter is

$$y(t) = \int_0^\infty s(T_d-\tau)s(t-\tau)d\tau \tag{2.5}$$

or

$$y(t) = \int_{-\infty}^{\infty} |S(f)|^2 e^{j2\pi f(t-T_d)} df \,. \tag{2.6}$$

(2.6) is the inverse Fourier transform of the signal energy spectral density $|S(f)|^2$ and (2.5) is the correlation of the input signal $s(t)$. Hence, matched filtering is equivalent to correlation processing [3]. This indicates that the matched filter may be implemented as a cross correlator between the echo from a target and a time-delayed and Doppler-shifted replica of the transmitted signal [2].

The characteristics of the matched filter can be derived using three different approaches:

Signal / Noise criterion
Likelihood ratio criterion
Inverse probability criterion

The signal/noise ratio criterion assumes that the optimum predetection system maximizes the SNR at one instant of time at the output of the signal processor [3]. The signal / noise approach was developed independently by several individuals [5, 6]. Assuming the basic definition

$$SNR = \frac{(peak\ (instantaneous)\ output\ voltage)^2}{rms\ noise\ power} \tag{2.7}$$

North [5] determined that the matched filter maximized this ratio yielding

$$SNR_{max} = \frac{2\ x\ received\ signal\ energy}{noise\ power\ per\ unit\ bandwidth} \tag{2.8}$$

(2.8) also implies that the ability to detect a radar signal is only a function of the energy it contains and the noise power density [3]. Features of the signal as peak power, time duration, wave shape and bandwidth do not enter the expression.

The likelihood criterion defines the optimum predetection filter as the one that processes the received signal in such a way as to provide an evaluation of the ratio of two conditional probabilities, which are signal plus noise or noise only cases [3]. This criterion was formulated from considerations of the theories for statistical decision and parameter estimation, developed by Wald [7], Neyman and Pearson [8], and others.

The inverse probability criterion describes the ideal receiver as the one that processes the received signal so as to produce an a posteriori probability distribution as an output [9]. This approach is based on Shannon's information theory, and was first developed by Woodward and Davies [10], and later expanded by Woodward [11].

2.2. Radar Ambiguity Function

For a radar system, it is evident that a particular waveform for transmission must first be specified before an optimum detection system can be implemented. Because of this requirement, the radar designer is always faced with the task of specifying an appropriate signal for his particular application. This signal is usually defined as the one which will lead to the least amount of uncertainty and ambiguity when the radar return signal is interpreted for information about range, velocity and the number of true targets in the radar's environment [3].

The successful extraction of information about range and velocity is determined by the measuring accuracy of the radar. The performance of the

radar system, in both respects, is accurately indicated by Woodward's ambiguity function [3]. The ambiguity function is defined as the response of the matched filter radar receiver to a target displaced in range delay τ and Doppler frequency φ from a reference target. The ambiguity function is given as $|X(\tau,\varphi)|^2$ where [1]:

$$|X(\tau,\varphi)| = \int_{-\infty}^{\infty} u(t)u^*(t+\tau)e^{-j2\pi\varphi t}\,dt \tag{2.9}$$

where $u(t)$ is the transmitted waveform. The ambiguity function is closely related to the matched filtered output waveform and is simply the squared magnitude of the time-reversed matched filter response. Because of this the ambiguity function is a measure of the ability of the radar system to distinguish similar coded waveforms at the receiver that differ in time of arrival and / or frequency shift.

It can be shown through Parseval's theorem that $X(\tau,\varphi)$ can also be expressed in terms of $U(f)$, the Fourier transform of $u(t)$, thus:

$$|X(\tau,\varphi)| = \int_{-\infty}^{\infty} U^*(f)U(f+\varphi)e^{-j2\pi f\tau}\,df \tag{2.10}$$

In the ambiguity diagram notation $\tau = 0$ and $\varphi = 0$ correspond to the time and Doppler frequency displacement of target of interest; i.e. the ambiguity diagram origin is centered on the target location in the range - Doppler frequency plane. For the case of matched filter reception, the origin of the ambiguity function may be thought of as the output of the matched filter that is tuned in time delay and frequency shift to the signal reflected from an idealized point source target. In this case τ becomes the time delay relative to the target position, and φ becomes the Doppler relative to the target Doppler [2].

The most significant aspect of the ambiguity diagram in the context of signal design is that the total potential ambiguity does not change from one signal to the next. This property is known as the *radar uncertainty principle* or sometimes as the *law of conservation of ambiguity*. It leads to the conclusion that the total potential ambiguity is the same for all signals those posses the same energy. It is the most important ambiguity function constraint since it implies that all signals are equally good (or bad) as long as they are not compared against a specific radar environment [9]. The preferable procedure for signal design would be to align the ambiguity distribution so that the regions of potential ambiguity occur where, a priori, undesirable target parameters are not expected, and to derive the signal from this distribution by means of an inverse transform. Unfortunately, this transform is not unique. Further, even if a unique transform could be formulated there is no guarantee that the signal derived from this will be realizable. The usual procedure is therefore to examine the ambiguity function of a variety of signals for the one that yields the best fit for the operational environment [3].

If $|X(\tau,\varphi)|^2$ is an ambiguity function then the volume invariance property can be shown as:

$$\int_{-\infty}^{\infty}\int_{-\infty}^{\infty}|X(\tau,\varphi)|^2 d\tau d\varphi = |X(0,0)|^2 \tag{2.11}$$

2.2.1. Ambiguity Function Examples

The significance and general properties of the ambiguity function are discussed generally in the previous section. In this section examples of ambiguity functions are given.

Figure 2.1 and Figure 2.2 show the ambiguity function of a Frank [13] and P4 [15] codes of length 100.

Range axis is given in code length and the frequency axis is given in code duration multiplied with target Doppler Shift. For the plots the parameters given below are used:

$c = 3x10^8 m/s$

$f_0 = 9.5GHz$

$\delta R = 15m$

$N = 100$

$V_{R,max} = 1500 m/s$

where c is the speed of electromagnetic wave propagation, f_0 is the center frequency of the radar, δR is the range resolution of the radar, N is the code length and V_R is the radial target velocity.

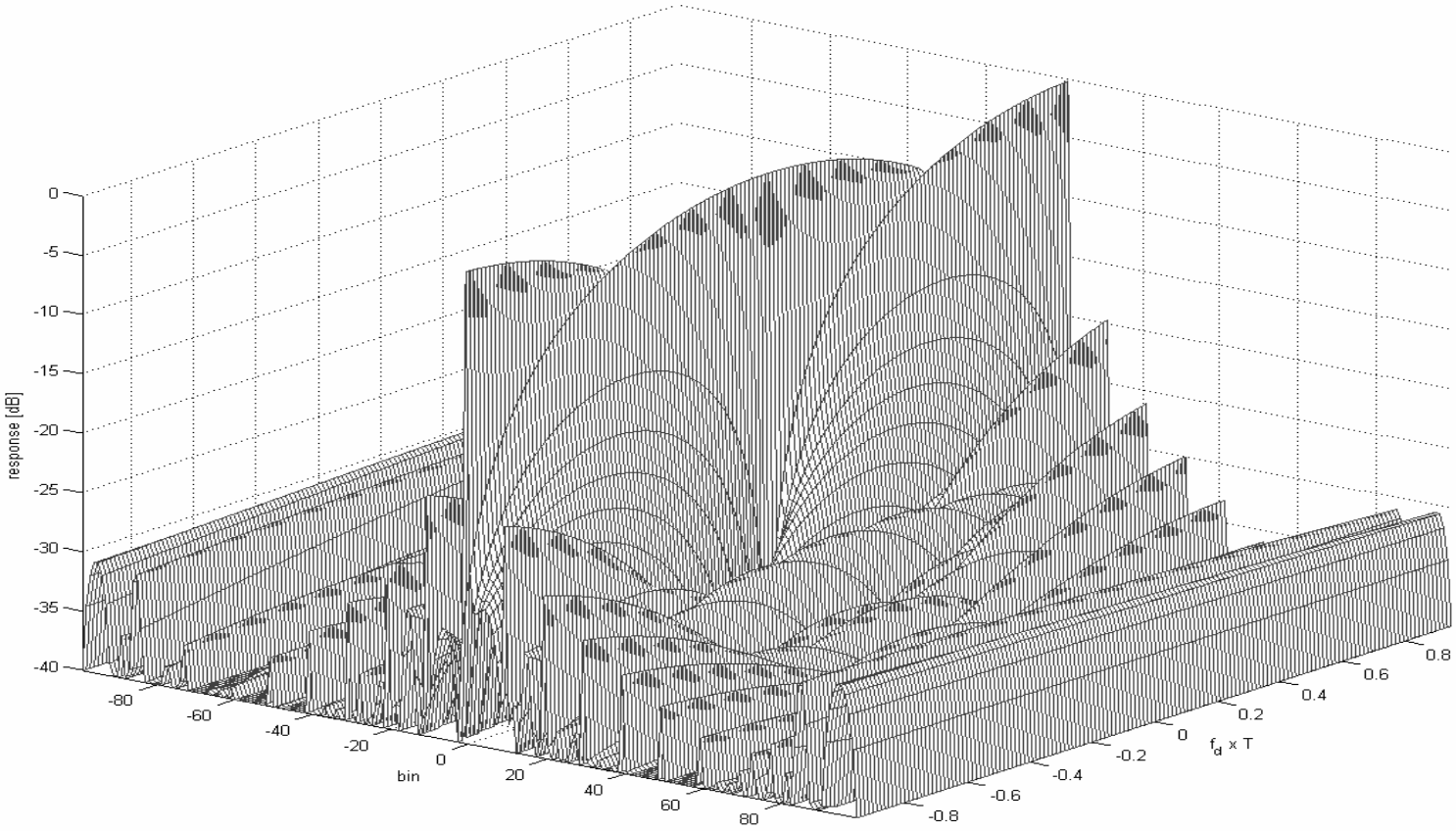

Figure 2.1: Ambiguity function of a 100 element Frank code

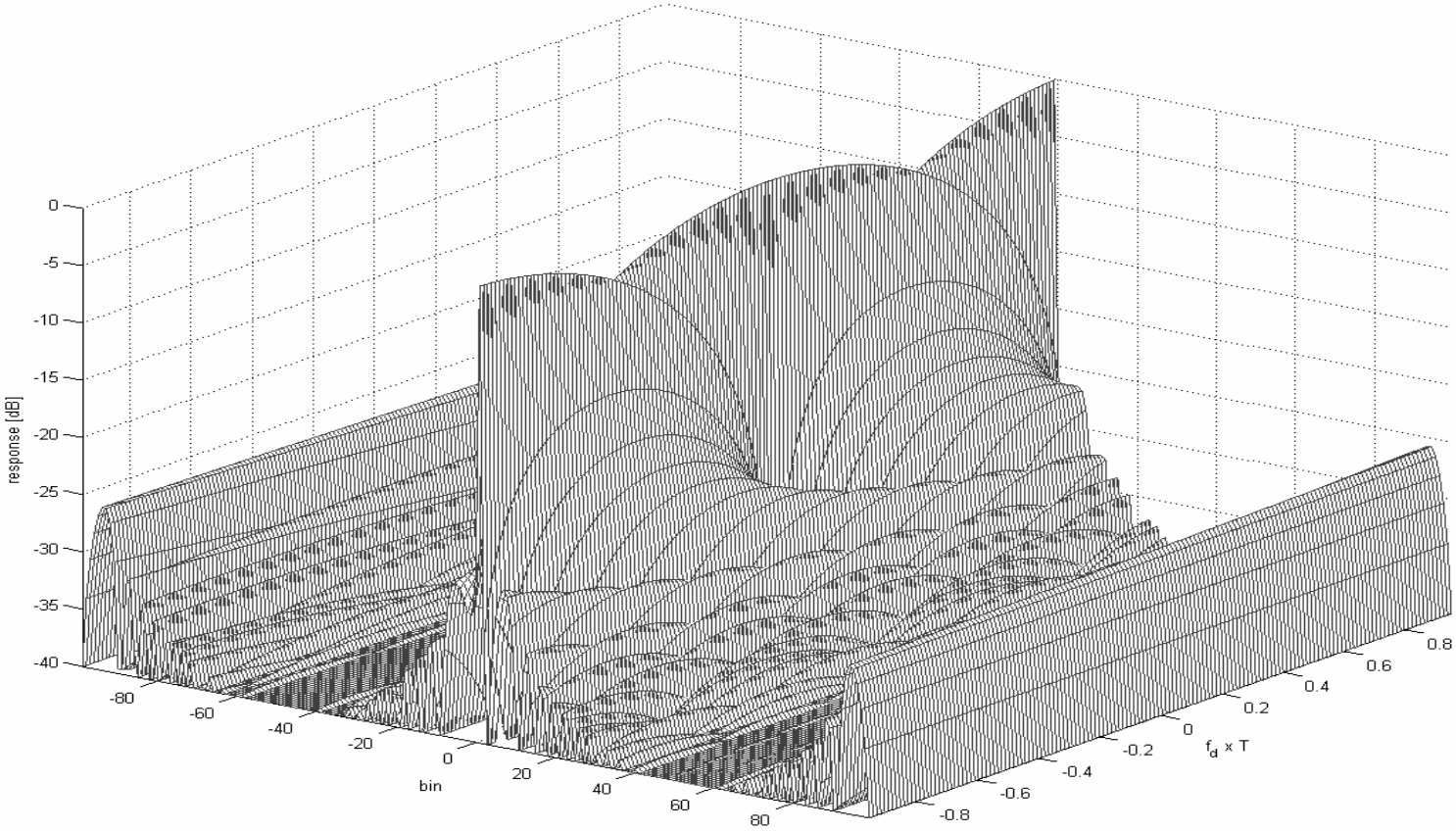

Figure 2.2: Ambiguity function of a 100 element P4 code

2.3. Pulse Compression

Pulse compression is a method for obtaining the resolution of a short pulse with the energy of a long pulse by internally modulating the phase or frequency of a long pulse so as to increase its bandwidth, and using a matched filter (also called a pulse compression filter) on reception to compress the pulse. It is used to obtain high range resolution when peak-power limited transmitters are used [1].

The concept of pulse compression was discovered during World War II. The matched filter concept developed in the 1940's revealed the theoretical performance of the pulsed radar systems independent of practical limitations of that time. The engineers were considering methods of improving the practical results that could be achieved with World War II radars. As the war progressed, the engineers understood that the major drawback of the radars was the power limitations of the transmitters being used. The problem in the transmitters used was two-fold. The peak power that could be provided to the transmitters was limited and even if this peak power was available many of the transmitter components could not have operated under such high power conditions. A straightforward solution could be the widening of pulse widths so that the power transmitted would be increased. However, this would decrease the range resolution so this method was not acceptable. The problem described above was solved by different people serving on both sides during the war. The method proposed a wide pulse be transmitted during which the carrier frequency was linearly swept. This was seen to yield a correlation between time and frequency that could be exploited in the radar receiver. The exploitation was proposed as a filter having a linear time delay versus frequency characteristics of such a sense that it would delay one end of the received pulse greater than the other end and by this way causing the signal compress in time and increase in peak amplitude [3].

By the pulse compression method, efficient use of the average power available at the radar transmitter and, in some cases, avoidance of peak power problems in the high power sections of the transmitter was accomplished. The resolution capabilities of the radars are also increased by pulse compression. In the range resolution case, the generation of fast rise-time, high peak power signals is bypassed when pulse compression techniques are used.

2.3.1. Range Resolution

Radars transmit electromagnetic waves into the space and receive echoes from any reflector in the path of the radiation from the radar. The time elapsed between transmission and echo repetition is used by the radar in order to determine the distance, or range, separating the target and the radar [12]. In this case,

$$R = \frac{c\Delta t}{2} \tag{2.12}$$

where c is the velocity of the electromagnetic wave propagation (i.e., speed of light) and Δt is the round trip transmit time of the electromagnetic wave transmitted.

The range resolution of a radar with a pulse of time duration of T_C can be given as,

$$\delta R = \frac{cT_C}{2} \tag{2.13}$$

where δR is the distance beyond which two targets must be separated so that their echoes can be seen by different pulses [12].

2.3.2. Doppler Shift

The radial velocity of the target in the radar radiation path causes a Doppler shift in the echo signal received by the radar. The Doppler shift phenomenon is used to discriminate real targets from the background clutter [2] and is given by,

$$f_D = \frac{2V_R}{c} f_0 \tag{2.14}$$

where V_R is the radial velocity of the target and f_0 is the carrier frequency of radar.

2.3.3. Discrete Coded Waveforms

The various types of modulation used in pulse compression are called codes [12]. Codes can be divided into two main groups as binary codes and polyphase codes. In the next two subsections the binary and polyphase codes are discussed briefly. The goodness of the given codes is determined based on the autocorrelation function since in the absence of noise; the output of the matched filter is proportional to the code autocorrelation.

The autocorrelation function of a discrete coded waveform can be given as:

$$\Phi(m) = \sum_{k=0}^{N-1} c_k c^*_{k+m} \tag{2.15}$$

where the integer index m steps over the domain $-(N-1) \leqslant m \leqslant (N-1)$ and $c_k = 0$ for $k < 0$ and $k > (N-1)$.

Two important parameters for radar performance analysis are the *peak sidelobe level* (PSL) and the *integrated sidelobe level* (ISL). PSL is a measure of the largest sidelobe as compared with the peak of the compression and ISL is a measure of the total power in the sidelobes as compared with the peak of the compression. For an N bit code [2]

$$PSL = 10 \log \frac{max\left|\Phi(i)\right|^2}{\left|\Phi(0)\right|^2} \tag{2.16}$$

$$ISL = 10 \log \sum_i \left|\frac{\Phi(i)}{\Phi(0)}\right|^2 \tag{2.17}$$

2.3.3.1. Binary Codes

Binary phase codes are obtained by dividing a relatively long pulse of width τ into N smaller subpulses each of width τ'. Then the phase of each subpulse is chosen as either 0 or π radians relative to an arbitrary reference. The code sequence c_n is obtained as:

$$c_n = e^{j\theta_n} \tag{2.18}$$

where $\theta_n = 0, \pi$. Since $\theta_n = 0, \pi$; it is seen that $c_n = \pm 1$.

One family of known binary codes is the Barker code. The Barker binary phase codes have maximum range-time sidelobes which are only one code element amplitude high. Thus they are also called optimum sequences. The match point peak to maximum sidelobe power ratio for an N element code is thus equal to N. The size of this family of codes is restricted and there exist no more than nine Barker sequences [9]. These codes are given in table 2.1 along with their autocorrelation ISL and PSL values.

Table 2.1: Barker Sequences

N	c_n	PSL, dB	ISL, dB
2	++	-6.0	-3.0
2	-+	-6.0	-3.0
3	++-	-9.5	-6.5
4	++-+	-12.0	-6.0
4	+++-	-12.0	-6.0
5	+++-+	-14.0	-8.0
7	+++--+-	-16.9	-9.1
11	+++---+--+-	-20.8	-10.8
13	+++++--++-+-+	-22.3	-11.5

The autocorrelation function of a Barker code with length 13 is given in Figure 2.3.

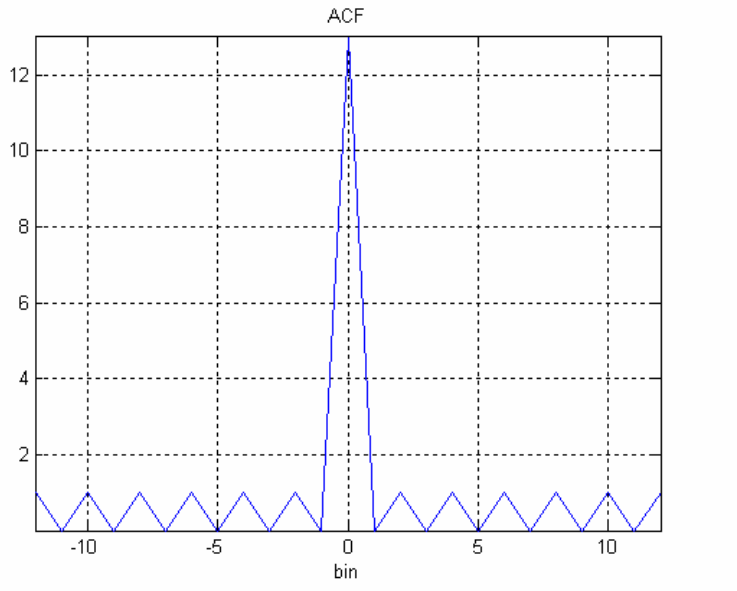

Figure 2.3: Autocorrelation of Barker code of length 13

Another class of codes that may be used for generating large pulse compression ratios are those whose sequence of plusses and minuses are chosen in an essentially randomly manner [2]. These codes are called pseudorandom codes (or maximal length sequences). A pseudorandom code is generated using a binary shift register circuitry with feedback.

The autocorrelation function of a pseudorandom code with length 15 is given in Figure 2.4.

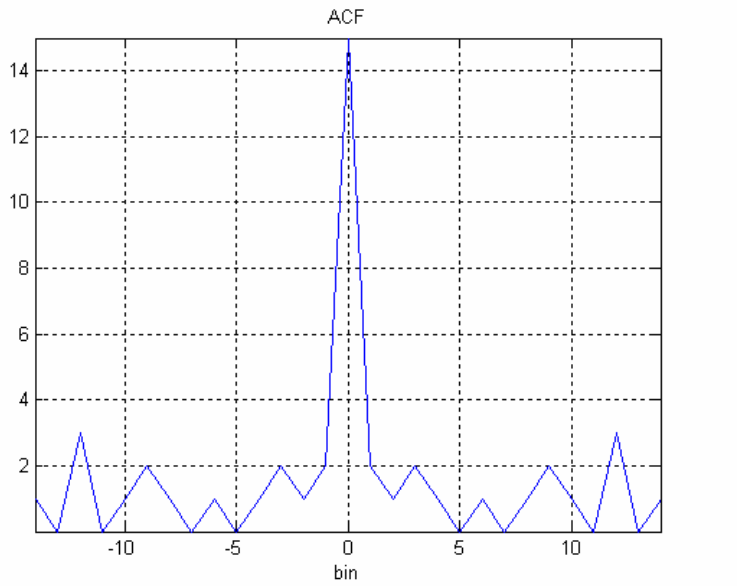

Figure 2.4: Autocorrelation of Pseudorandom code of length 15

While the pseudorandom codes are easy to generate and decode, the ratio of amplitude of the central peak to largest side peak remains close to $\sqrt{N}$. The maximal-length codes and the technique of combining codes can be used for creating codes of arbitrary long lengths. However, the technique of combining codes leads to relatively high sidelobes, and even when

mismatched filters are used to suppress these sidelobes, an SNR loss occurs because of the code-filter mismatch.

The ambiguity diagrams of the binary phase codes consist of single narrow pike surrounded by a plateau of time and Doppler frequency sidelobes. The match-point peak occurs over a very narrow range in time and in frequency. As a consequence, biphase codes have little Doppler shift tolerance, i.e., their performance is degraded by moving targets [12].

2.3.3.2. Polyphase Codes

Polyphase codes are obtained by dividing a relatively long pulse of width τ into N smaller subpulses each of width τ'. Then the phase of each subpulse is chosen from M discrete phases, where M is greater than 2. The code sequence c_n is obtained as:

$$c_n = e^{j\theta_n} \tag{2.19}$$

where θ_n takes values from M discrete phases.

The polyphase codes can be divided into three major groups according to their derivation technique [12]:

Step-frequency-derived (Frank and P1 codes)
Butler-matrix-derived (P2 code)
Linear-frequency-derived (P3 and P4 codes)

2.3.3.2.1. Frank Codes

The Frank polyphase code has been described by a matrix [13]:

0	0	0	.	.	.	0
0	1	2	.	.	.	(N'-1)
0	2	4	.	.	.	2(N'-1)
.						.
.						.
.						.
0	(N'-1)	2(N'-1)	.	.	.	$(N'-1)^2$

where the numbers represent the multiplying coefficients of a phase angle equal to $2\pi p / N'$ where p and N' are integers and p is relatively prime to N'. For this study it will be assumed that $p = 1$. The actual coded sequence is formed by placing the rows (or columns) side by side. This will yield a sequence containing $N = (N')^2$ elements. The Frank code sequences for $N' = 2, 3, 4 \text{ and } 5$ are given in Table 2.2.

Table 2.2: Frank Codes

N'	N	Code Sequence
2	4	(a)0,0/0,1 (b)0,0/1,0
3	9	0,0,0/0,1,2/0,2,1
4	16	0,0,0,0/0,1,2,3/0,2,0,2/0,3,2,1
5	25	0,0,0,0,0/0,1,2,3,4/0,2,4,1,3/0,3,1,4,2/0,4,3,2,1

The sequences for $N' = 2$ are also seen to be the Barker binary sequences. The elements of the sequences are presented $mod\, N'$ and that each of the N' groups starts with a zero element. The first group in the sequences corresponds to no phase shift; in the next group the coefficients progress in

steps of one; in the next group the coefficients progress in steps of two and so on. Because the phase progresses to the right in an orderly quadratic manner, the Frank polyphase coded waveforms formed from such sequences have also been described as quantized phase linear FM [9]. The total time duration of these waveforms is $N\tau'$ and they have an effective bandwidth of $1/\tau'$. The total time-bandwidth product is therefore N. Also, for large N' the peak-to-sidelobe ratio of the Frank codes asymptotically approaches $\pi N'$ [9].

The Frank code phases may be stated mathematically as follows [12]. The phase of the i^{th} code element in the j^{th} phase group is:

$$\theta_{i,j} = \frac{2\pi}{N'}(i-1)(j-1) \tag{2.20}$$

where the index i ranges from 1 to N' for each of the values of j ranging from 1 to N'.

The autocorrelation function of a Frank code with length 100 is given in Figure 2.5.

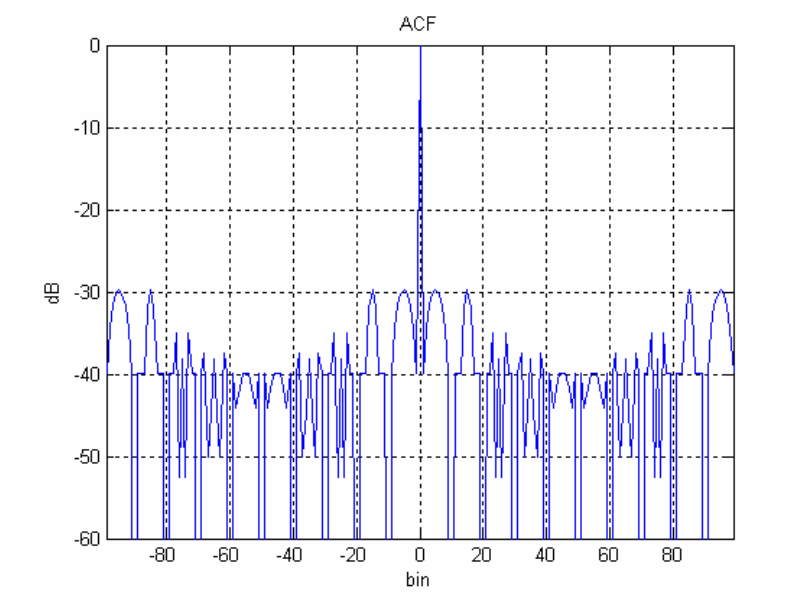

Figure 2.5: Autocorrelation of Frank code of length 100

Comparing the Frank polyphase code to binary phase codes, the Frank code has a PSL which is approximately 10 dB better than the best pseudorandom codes [2]. In the presence of Doppler shift, the autocorrelation function of Frank codes degrades at much slower rate that for binary codes, however the peak shifts in position rapidly and a range error occurs due to this shift.

2.3.3.2.2. P1 and P2 Codes

P1 and P2 codes are similar to Frank polyphase code in many respects. These similarities include low sidelobes, good Doppler tolerance and ease of implementation. The P1 code has an autocorrelation function magnitude which is identical to the Frank code for zero Doppler shift. While the peak sidelobes of the P2 code are the same as the Frank code for zero Doppler case, the mean square sidelobes of the P2 code are slightly less [14].

The significant advantage of the P1 and P2 codes over the Frank code is that they are more tolerant of receiver bandlimiting prior to pulse compression.

This bandlimiting is required to avoid out-of-band noise fold over caused by sampling in conversion to digital format. For the case of Frank code, the limited receiver bandwidth results in an unfavorable mismatch which causes degradation in the PSL of the compressed pulse. A similar degradation occurs for binary coded waveforms. By increasing the receiver bandwidth, sampling rate, and matching to this oversampled signal, the degradation can be reduced. However this requires faster circuitry and additional complexity. The reason for the degradation of the Frank coded waveforms is that the smoothing or averaging effect caused by bandlimiting has the least effect on the ends of the Frank code, where the phase changes between adjacent code elements are the smallest, and has the most effect in the middle of the code where the phase changes from code element to code element are the largest. That is, thinking of the phase groups as corresponding to the frequencies, bandlimiting has the effect of attenuating the center frequencies of the Frank coded waveform the most, which amounts to an inverse of the normal amplitude weighting employed to reduce sidelobes [14]. These considerations catalyzed the search for phase coded waveforms which have the largest phase increments at the ends of the waveform which represent the highest and lowest frequencies in the radar passband.

The P1 code can be thought of a rearranged Frank code with the zero frequency group in the middle. P1 code consists of $N = (N')^2$ elements and the phase of the i^{th} code element in the j^{th} phase group is:

$$\theta_{i,j} = -\frac{\pi}{N'}\left[N'-(2j-1)\right]\left[(j-1)N'+(i-1)\right] \qquad (2.21)$$

where i and j are integers ranging from 1 to N'.

The P2 code, which also has desired feature as the P1 code, is valid for N' even, and each group of the code is symmetric about 0 phase. For N' even, the P1 code has the same phase increments within each phase group as the

P2 code, except that the starting phases are different [14]. The i^{th} code element in the j^{th} group of the P2 code is given by:

$$\theta_{i,j} = \frac{\pi}{2N'}(N'+1-2i)(N'+1-2j) \qquad (2.22)$$

where i and j are integers ranging from 1 to N' as before. The requirement for N' to be even in this code stems from the desire of low autocorrelation sidelobes. An odd value of N' results in high autocorrelation sidelobes [14].

The ambiguity diagram of the P1 code for N' odd is identical to that of Frank code. For N' even, the ambiguity diagrams of the P1 and P2 codes are similar to each other and to that of Frank code.

The autocorrelation function of a P1 code with length 121 is given in Figure 2.6.

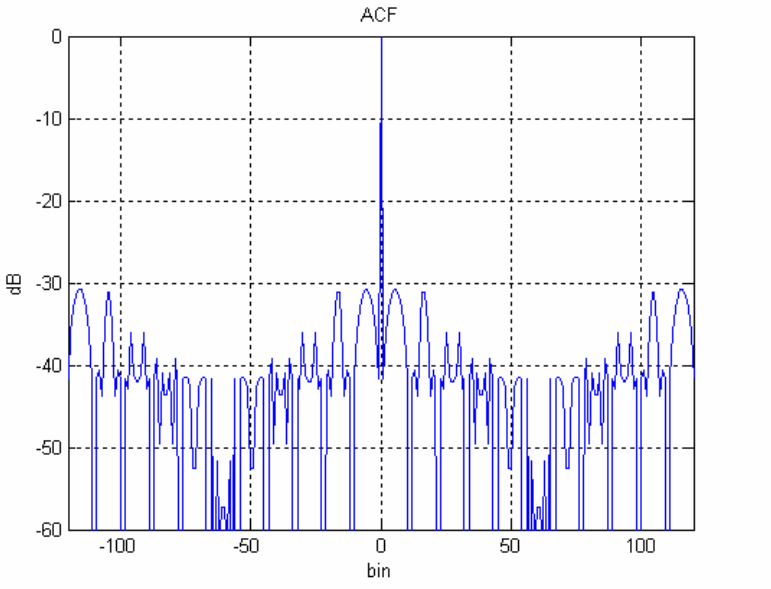

Figure 2.6: Autocorrelation of P1 code of length 121

The autocorrelation function of a P2 code with length 100 is given in Figure 2.7.

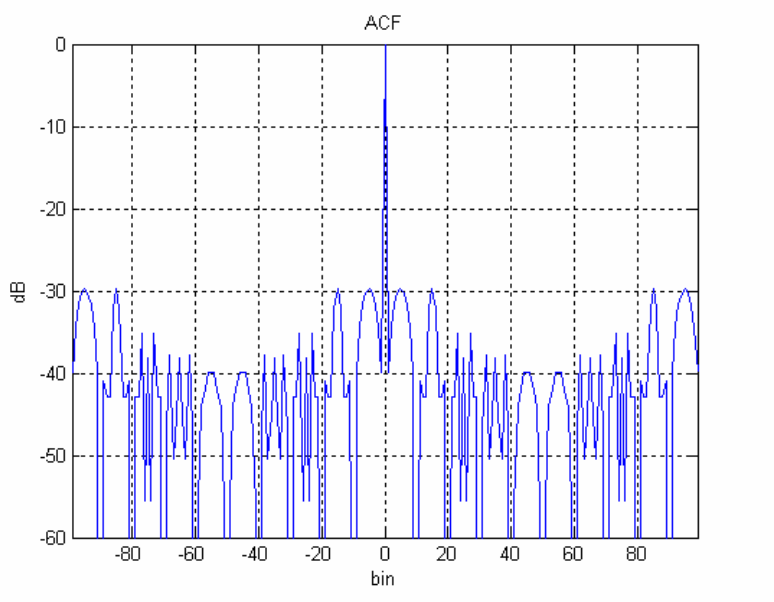

Figure 2.7: Autocorrelation of P2 code of length 100

2.3.3.2.3. P3 and P4 Codes

P3 and P4 codes are conceptually derived from a linear frequency modulation waveform (LFMW) and are more Doppler tolerant than other phase codes derived from a step approximation to a LFMW such as P1 or P2 codes. The P3 code is not precompression bandwidth limitation tolerant but is much more Doppler tolerant than the Frank or P1 and P2 codes. The P4 code is a rearranged P3 code with the same Doppler tolerance and with better precompression bandwidth limitation tolerant [15].

The P3 code is generated conceptually by converting a linear frequency modulation waveform to baseband using a local oscillator on one end of the

sweep and sampling the waveform at the Nyquist rate. The P3 code is given by [15]:

$$\theta_i = \frac{\pi}{N}(i-1)^2 \tag{2.23}$$

where i is an integer ranging from 1 to N.

The P4 code is conceptually derived from the same waveform as the P3 code. However, in this case, the local oscillator frequency is changed to overcome precompression bandwidth problem. The phase values of the P4 code is:

$$\theta_i = \frac{\pi}{N}(i-1)^2 - \pi(i-1) \tag{2.24}$$

where i is an integer ranging from 1 to N.

The largest phase increments from code element to code element are on the two ends of the P4 code but are in the middle of the P3 code. Thus the P4 code is more precompression bandwidth tolerant than the P3 code.

The phase values of P3 and P4 codes of lengths 100 are given in Figure 2.8.

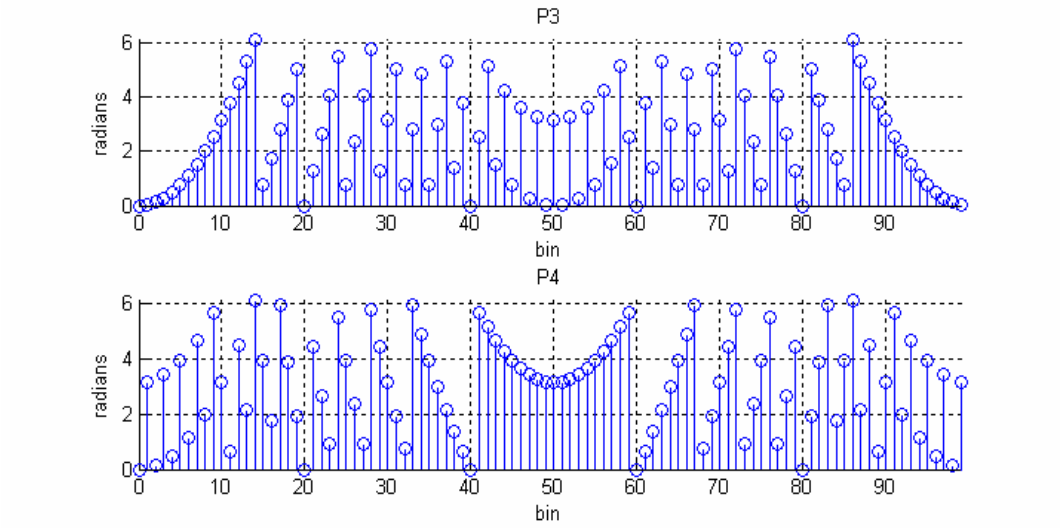

Figure 2.8: Phases of P3 and P4 codes of length 100

The autocorrelation function of a P4 code with length 100 is given in Figure 2.9.

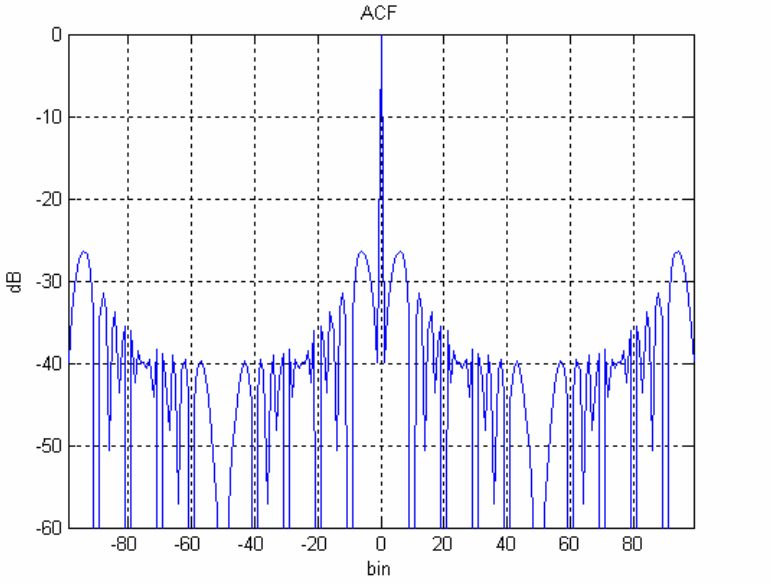

Figure 2.9: Autocorrelation of P4 code of length 100

CHAPTER 3

PARALLEL DOPPLER FILTERS FOR RADAR RECEIVER

3.1. The Need for Parallel Filters

Radars transmit electromagnetic waves into the space and receive echoes from targets within their volume of coverage. When the transmitted signal is reflected from a moving target such as a plane, the radial velocity of the target causes a Doppler shift in the echo signal. The Doppler shift in the echo signal leads to a mismatch between the received signal and the matched filter used in the receiver filter. This gives rise to an SNR loss in the radar system. Depending on the target radial velocity and the radar parameters this mismatch loss can be very significant.

In (2.14) the Doppler shift in the echo signal due to target radial velocity was given. In discrete-time system model this shift can be expressed as [16]:

$$w_D = 2\pi \frac{2V_R}{c} f_0 T_S \tag{3.1}$$

where c is the velocity of the electromagnetic wave propagation, V_R is the radial velocity of the target, f_0 is the carrier frequency of the radar and T_S is the sampling period.

Then, the output of the matched filter used in the receiver is:

$$\Phi(m) = \sum_{k=0}^{N-1} u_k v^*_{k+m} \tag{3.2}$$

where u_n and v_n are the transmitted and received signals respectively. Because of the Doppler shift, the received echo can be written as $v_n = u_n e^{jw_D n}$. For a discrete coded sequence of c_n the output of the receiver filter can be rewritten as:

$$\Phi(m) = \sum_{k=0}^{N-1} c_k c^*_{k+m}\, e^{-jw_D(k+m)} \tag{3.3}$$

where the integer index m steps over the domain $-(N-1) \leqslant m \leqslant (N-1)$ and $c_k = 0$ for $k < 0$ and $k > (N-1)$. If the output signal is sampled at the ideal position, i.e. at $m = 0$, then with a normalization of N the output of the receiver filter is:

$$\Phi(0) = \frac{1}{N} \sum_{k=0}^{N-1} e^{-jw_D k} \tag{3.4}$$

$\Phi(0)$ is the attenuation in the output of the receiver filter due to target radial velocity and the magnitude of this function can be written as:

$$|\Phi(0)| = |A(w_D)| = \frac{1}{N} \left| \frac{\sin(\frac{w_D N}{2})}{\sin(\frac{w_D}{2})} \right| \tag{3.5}$$

The attenuation function $|A(w_D)|$ for the following radar parameters is given in Figure 3.1:

$c = 3x10^8\, m/s$

$f_0 = 9.5GHz$

$\delta R = 15m$

$N = 100$

$T_S = T_c = \frac{2\delta R}{c} = 10^{-7}\, sec.$

For a target velocity of $V_R = 750\, m/s$ an attenuation of 3.5dB is obtained due to filter mismatch.

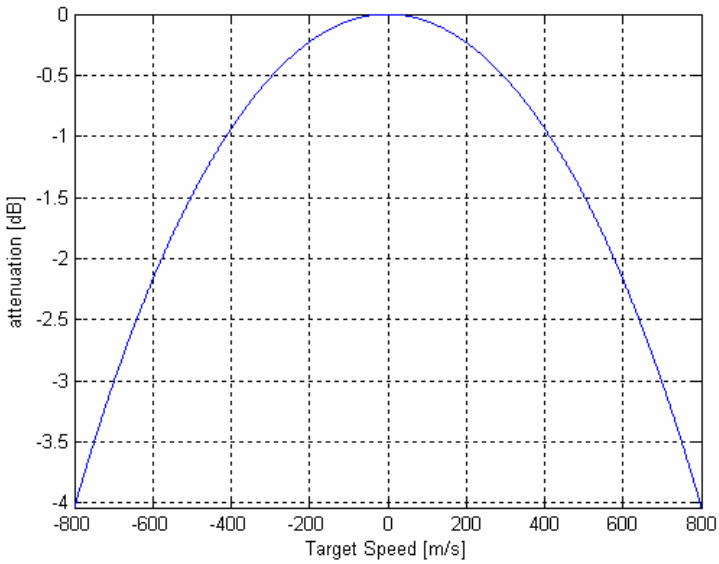

Figure 3.1: Attenuation function due to filter mismatch

The minimum target radial velocity for which the attenuation function is zero can be found as:

$$V_R\big|_{A(w_D)=0} = \frac{c}{2f_0 T_c N} \tag{3.6}$$

For the above parameters the minimum radial velocity making attenuation function zero is obtained at $V_R\big|_{A(w_D)=0} = 1579\, m/s$. The attenuation gets worse as the parameters in the denominator of (3.6) increases. An increase in radar center frequency f_0, code sequence length N or a decrease in radar's range resolution δR increases the attenuation function.

To overcome the mismatch loss given above, a parallel filter structure can be used as in Figure 3.2. The total number of filters, i.e. K, depends on the parameters given in (3.6) and the maximum radial target velocity.

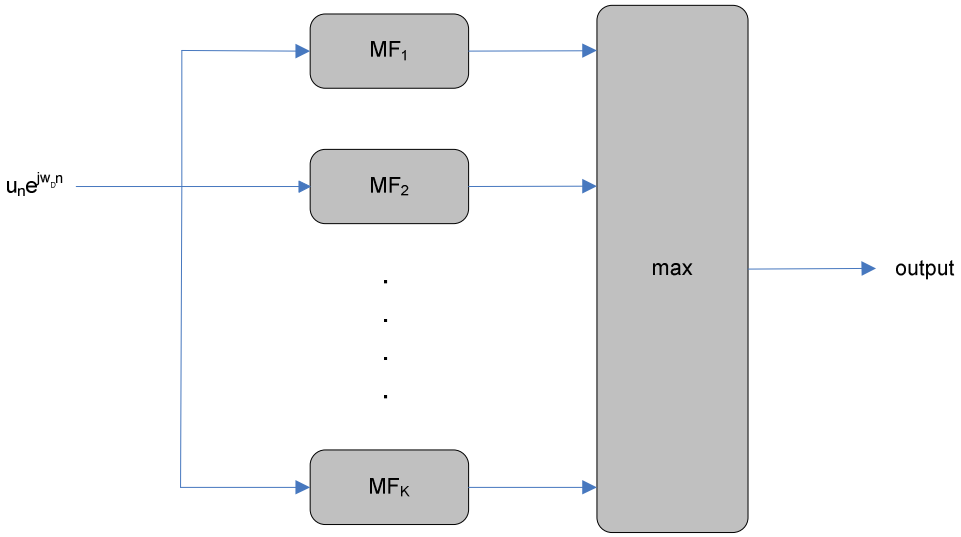

Figure 3.2: Parallel filter structure for the radar receiver

3.2. Proposed Parallel Filter Methods

The mismatch loss due to target Doppler shift in a radar receiver is presented in the previous subsection. This loss can be reduced by using parallel filters in the radar receiver each of which is matched to different target velocities.

The minimum number of filters needed depends on the maximum radial velocity of the target, radar center frequency, code sequence length and the range resolution of the radar.

For a desired maximum mismatch loss the parallel filter system can be designed in two ways. The total number of filters used determines this difference and can be chosen to be odd or even. In the following subsections these two filter structures are described. In this chapter, the term “odd case” is used where it is desired to mean that the total number of filters used is odd. If the total number of filters used is even this time the term “even case” is used.

3.2.1. Odd Number of Filters

For the odd case, the structure of the radar receiver is given in Figure 3.3.

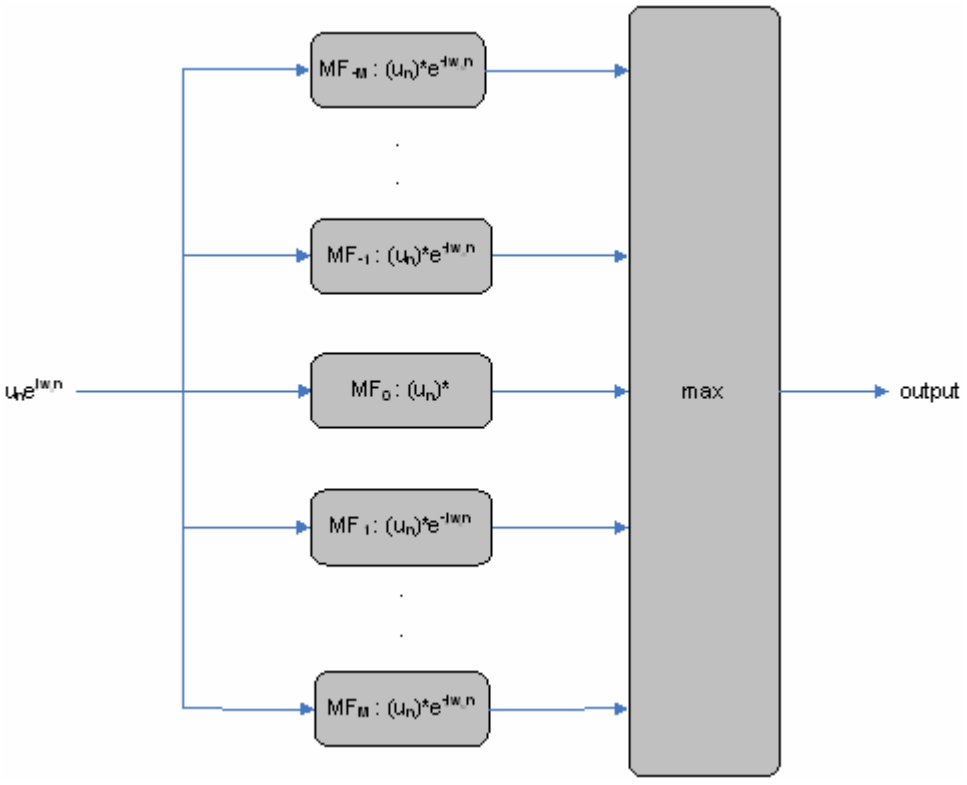

Figure 3.3: Parallel filter structure with odd number of filters

In the proposed system a total of K = 2M+1 parallel filters is used. MF_0 is the matched filter for zero Doppler shift, MF_1 is the matched filter for a Doppler shift of w_1 and MF_M is the matched filter for a Doppler shift of w_M. Since the direction of the target is not known a priori both the approaching and departing target velocities should be taken into account. Because of this, in the structure given above the matched filters are symmetric in Doppler frequency, i.e. there are filters for both w_k and w_{-k} for k = 1, 2,.., M.

The distribution of the filters in frequency axis versus the attenuation of each filter is shown in Figure 3.4. The filters are uniformly distributed over the frequency axis because there is no apriori information about the Doppler frequency of the target.

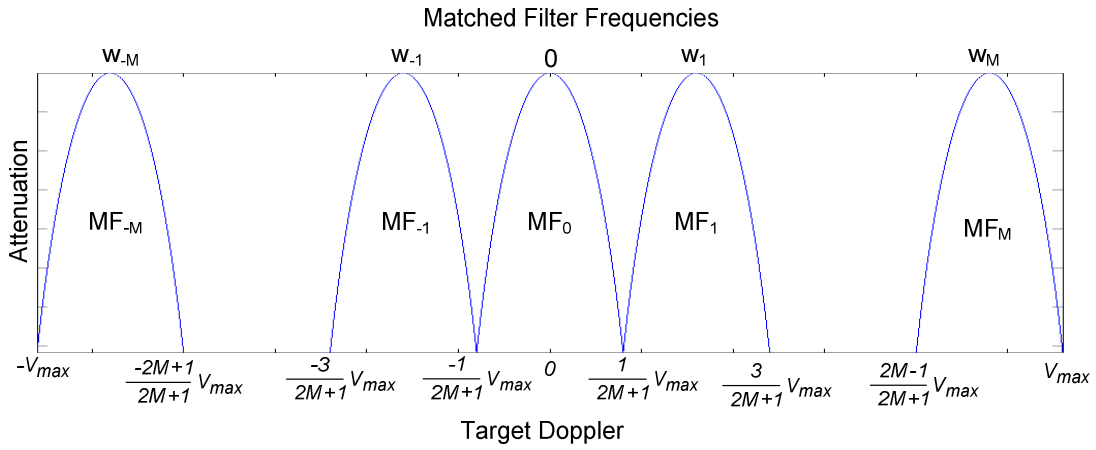

Figure 3.4: Parallel filter structure for the radar receiver for odd case

Because of the uniform distribution the intersection points of the matched filters over the Doppler axis is obtained as:

$$V_{int} = \frac{2i+1}{2M+1} V_{max} \tag{3.7}$$

where i = -M, .., -1, 0, 1, .., (M-1).

The maximum loss in the above system is obtained for the intersection points found above:

$$max.\ loss = \frac{1}{N}\left|\frac{sin(\frac{w_{int}N}{2})}{sin(\frac{w_{int}}{2})}\right| \tag{3.8}$$

where w_{int} is the Doppler of the intersection points and can be found as:

$$w_{int} = 2\pi\frac{2(\frac{1}{2M+1}V_{max})}{c}f_0T_S\,. \tag{3.9}$$

The procedure of obtaining the minimum required number of filters is as follows. The maximum loss of the filter structure is calculated starting with M = 0. If the calculated loss is smaller than the required loss than one filter is sufficient and a matched filter is used in the traditional way. Otherwise, M is increased until the loss of the parallel filter structure meets the requirements of the radar system.

The center Doppler frequencies of the filters are also obtained and can be expressed as:

$$V_i = \frac{2i}{2M+1}V_{max} \tag{3.10}$$

where i = -M, .., -1, 0, 1, .., M.

For the radar parameters below and a maximum desired mismatch loss of 0.5 dB the parallel filter structure is obtained as in Figure 3.5.

$V_{max} = 750\ m/s$

$c = 3x10^{8}\ m/s$

$f_0 = 9.5GHz$

$\delta R = 15m$

$N = 100$

$$T_S = T_C = \frac{2\delta R}{c} = 10^{-7}\ sec.$$

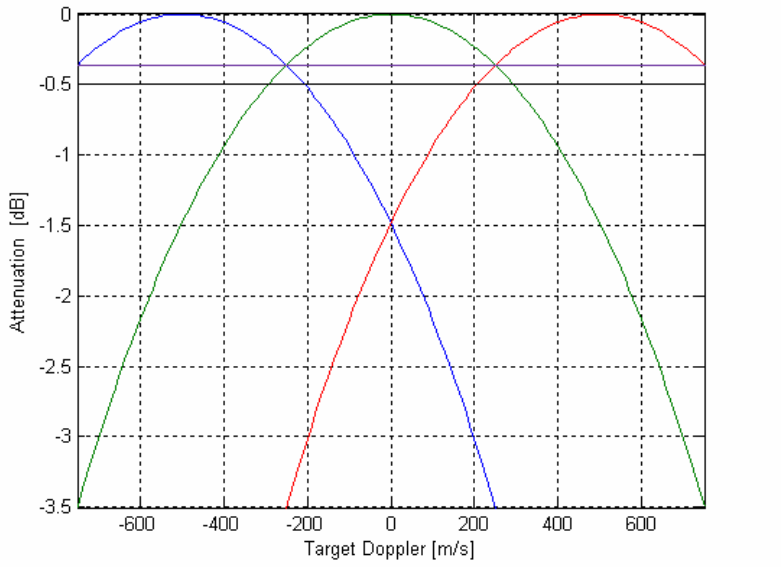

Figure 3.5: Attenuation in the output of parallel filter structure

As can be seen from Figure 3.5 the maximum loss is 0.36 dB and three parallel filters are required to obtain this worst case loss. The center Doppler frequencies of the filters are obtained as -500 m/s, 0 m/s and 500 m/s.

If the radar parameters are changed in a way of increasing the attenuation, i.e. for the radar parameters below changed while the others remain the

same and a desired maximum loss of 0.75 dB, the filter structure is obtained as in Figure 3.6.

$f_0 = 15.5GHz$

$N = 169$

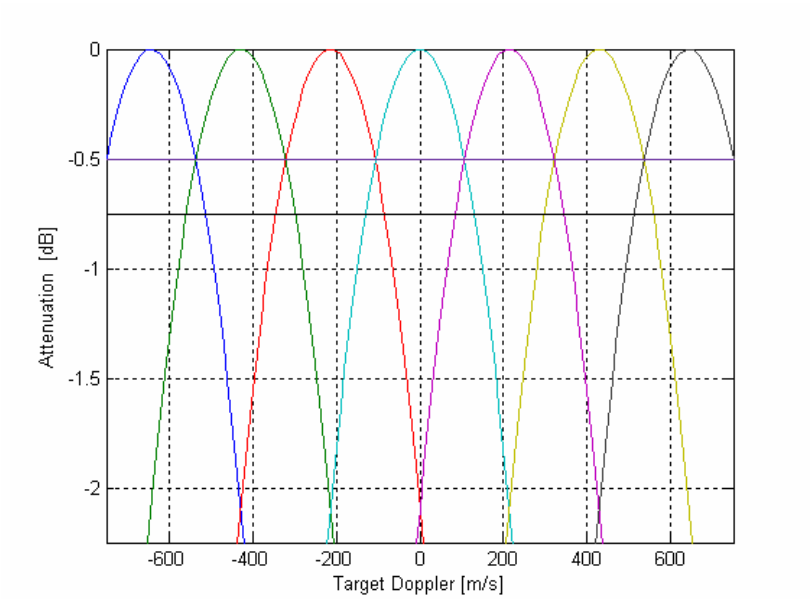

Figure 3.6: Attenuation in the output of parallel filter structure

For this case the maximum loss is 0.51 dB and seven parallel filters are required to obtain this worst case loss. The center Doppler frequencies of the filters is obtained as -642 m/s, -428 m/s, -214 m/s, 0 m/s, 214 m/s, 428 m/s and 642 m/s.

3.2.2. Even Number of Filters

For the even case the structure of the radar receiver is given in Figure 3.7.

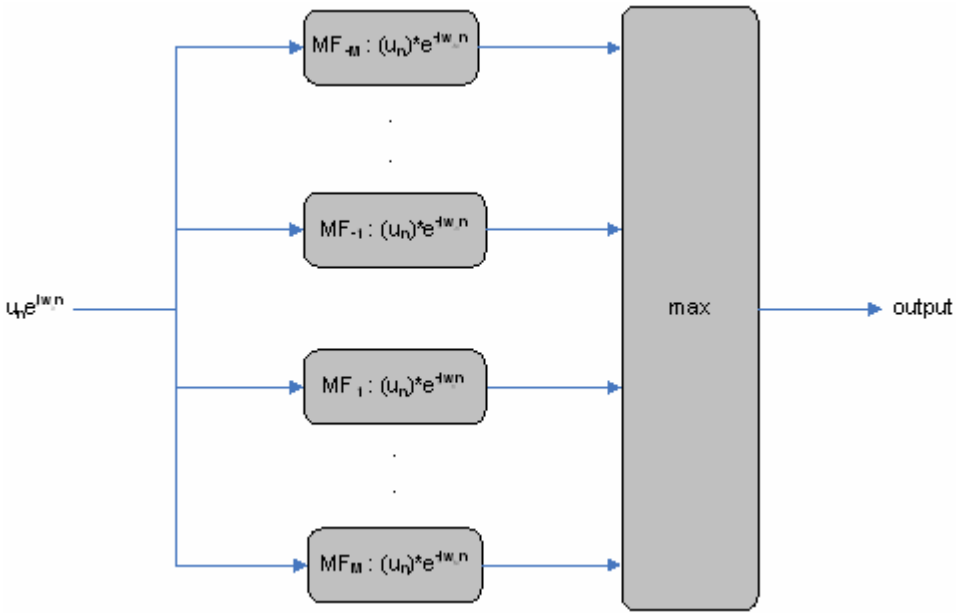

Figure 3.7: Parallel filter structure with even number of filters

In this case a total of K = 2M parallel filters is used. MF_1 is the matched filter for a Doppler shift of w_1 and MF_M is the matched filter for a Doppler shift of w_M as before. Again, since the direction of the target is not known apriori both the approaching and departing target velocities should be taken into account.

The distribution of the filters in Doppler axis versus the attenuation of each filter is given in Figure 3.8. The filters are uniformly distributed over the Doppler axis as in the odd case.

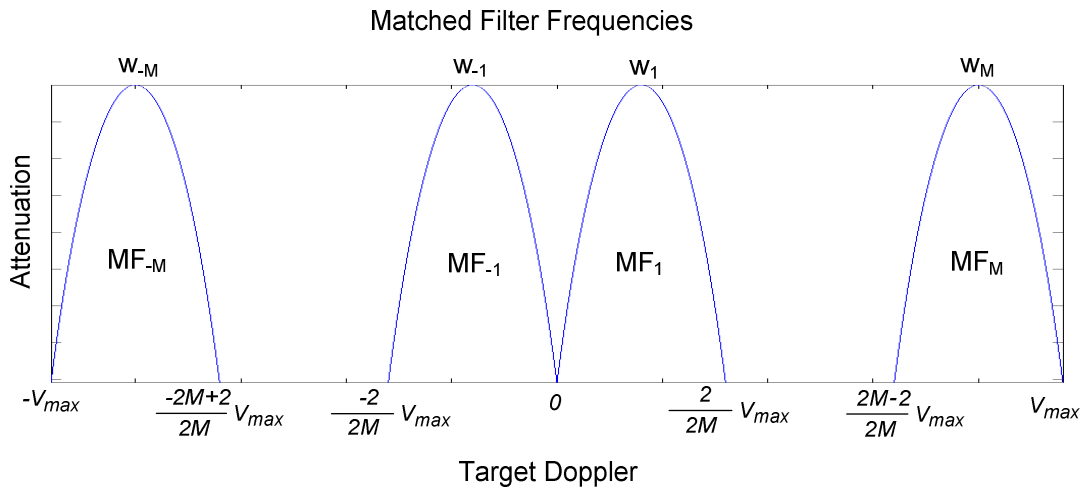

Figure 3.8: Parallel filter structure for the radar receiver for even case

Because of the uniform distribution the intersection points of the matched filters over the Doppler axis is obtained as:

$$V_{int} = \frac{2i}{2M} V_{max} \tag{3.11}$$

where i = -(M-1), .., -1, 0, 1, .., (M-1).

The maximum loss in the above system is obtained for the intersection points found above. It can again be written as:

$$max.\ loss = \frac{1}{N}\left|\frac{sin(\frac{w_{int}N}{2})}{sin(\frac{w_{int}}{2})}\right| \tag{3.12}$$

where w_{int} is the Doppler of the intersection points and can be written as:

$$w_{int} = 2\pi \frac{2(\frac{1}{2M} V_{max})}{c} f_0 T_S \tag{3.13}$$

The procedure of obtaining the minimum required number of filters is the same as in the odd number of filters case. The maximum loss of the filter structure is calculated starting with M = 1. If the calculated loss is smaller than the required loss than a two filter structure is sufficient and two matched filters located on the middle of the positive and negative Doppler axis are used. Else M is increased until the loss of the parallel filter structure meets the requirements of the radar system.

The center Doppler frequencies of the filters are also obtained and can be given as:

$$V_i = \frac{2i - 1}{2M} V_{max} \tag{3.14}$$

where i = -(M-1), .., -1, 0, 1, .., M.

For the radar parameters below and a maximum desired mismatch loss of 0.5 dB the parallel filter structure is obtained as in Figure 3.9.

$V_{max} = 750\ m/s$

$c = 3x10^8\ m/s$

$f_0 = 9.5GHz$

$\delta R = 15m$

$N = 100$

$T_S = T_C = \frac{2\delta R}{c} = 10^{-7}\ sec.$

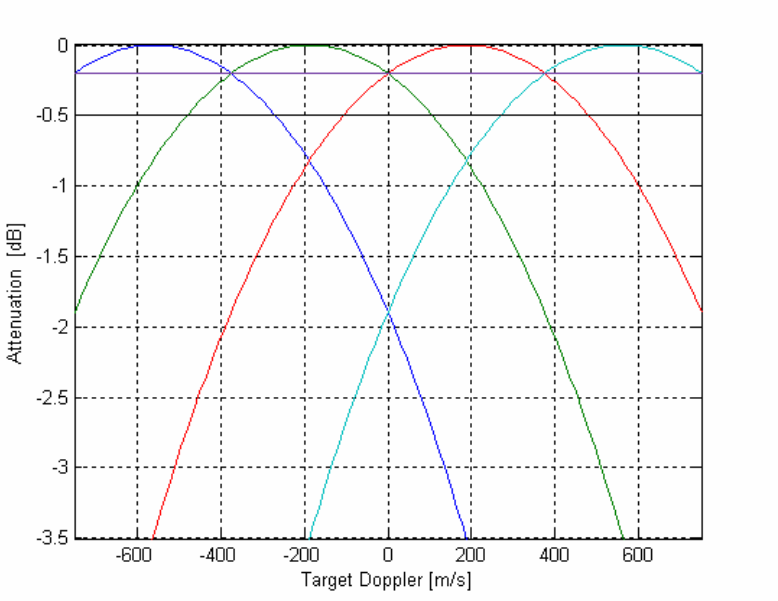

Figure 3.9: Attenuation in the output of parallel filter structure

As can be seen from Figure 3.9 the maximum loss is 0.2 dB and four parallel filters are required to obtain this worst case loss. The center Doppler's of the filters is obtained as -562.5 m/s, -187.5 m/s, 187.5 m/s and 562.5 m/s.

If the radar parameters is changed in a way of increasing the attenuation, i.e. for the below radar parameters changed while the others remain the same and a desired maximum loss of 0.75 dB the filter structure is obtained as in Figure 3.10.

$f_0 = 15.5GHz$

$N = 169$

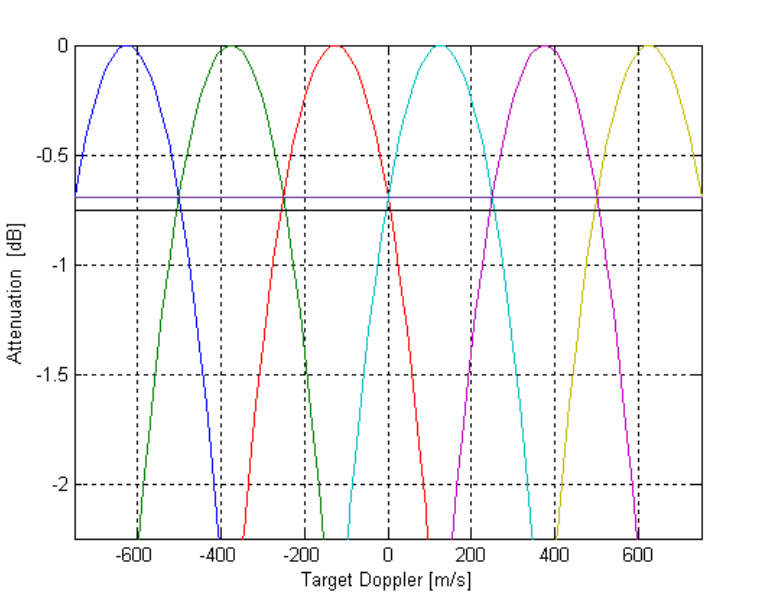

Figure 3.10: Attenuation in the output of parallel filter structure

For this case the maximum loss is 0.69 dB and six parallel filters are required to obtain this worst case loss. The center Doppler frequencies of the filters is obtained as -625 m/s, -375 m/s, -125 m/s, 125 m/s, 375 m/s and 625 m/s.

3.2.3. MATLAB Functions for Parallel Filter Method

Two Matlab functions have been written as a design aid for the parallel filter method, doppler_filter1.m and doppler_filter2.m. The first program calculates the maximum loss due to Doppler mismatch with the total filter number for given radar parameters and desired mismatch loss with a choice of odd/even case. The second one calculates the maximum loss for the minimum number of filters that satisfies the desired loss. Both programs also determine the center frequencies of the filters. The MATLAB codes of the programs are included in a CD attached.

CHAPTER 4

WEIGHTING TECHNIQUES FOR SIDELOBE SUPPRESSION

4.1. Introduction

The successful application of pulse-compression matched filter techniques described in Chapter 2 depends quite critically on producing at the output of the matched filter a compressed-pulse waveform having a low level of range sidelobes. Low level of range sidelobes are desired because in a multiple-target radar environment, the range sidelobes of one large target may appear as a smaller target at another range, or the integrated sidelobes from targets or clutter may mask all the information of another target.

Different solutions for the reduction of range sidelobes of ACF exist. In this chapter, the amplitude weighting in the receive filter is discussed. In this method, the receiver filter (i.e. matched filter) coefficients are windowed with a weighting function. Although weighting windows used both on transmit and receive provides better results, in this thesis only weighting on receive is discussed because weighting on transmit leads to a power loss since the available transmit power can not be fully utilized.

Along with the windowing method, the two sample sliding window averaging [18, 19] (or difference for some codes) is also considered and the results of

this method are also obtained. Most of the window functions used for computations are chosen from the window library of MATLAB. Some of them are shown in Figure 4.1. The effect of windowing methods on PSL, ISL, SNR loss and main lobe broadening (MLB) are obtained for P4, P3, P2, P1 and Frank codes for different code lengths. Results of P4 and Frank codes are provided in detail. Also, for the window functions that have variable parameters (such as sidelobe attenuation for Chebyshev window) the variation of PSL, ISL, SNR loss and MLB are obtained for the variation in that parameter.

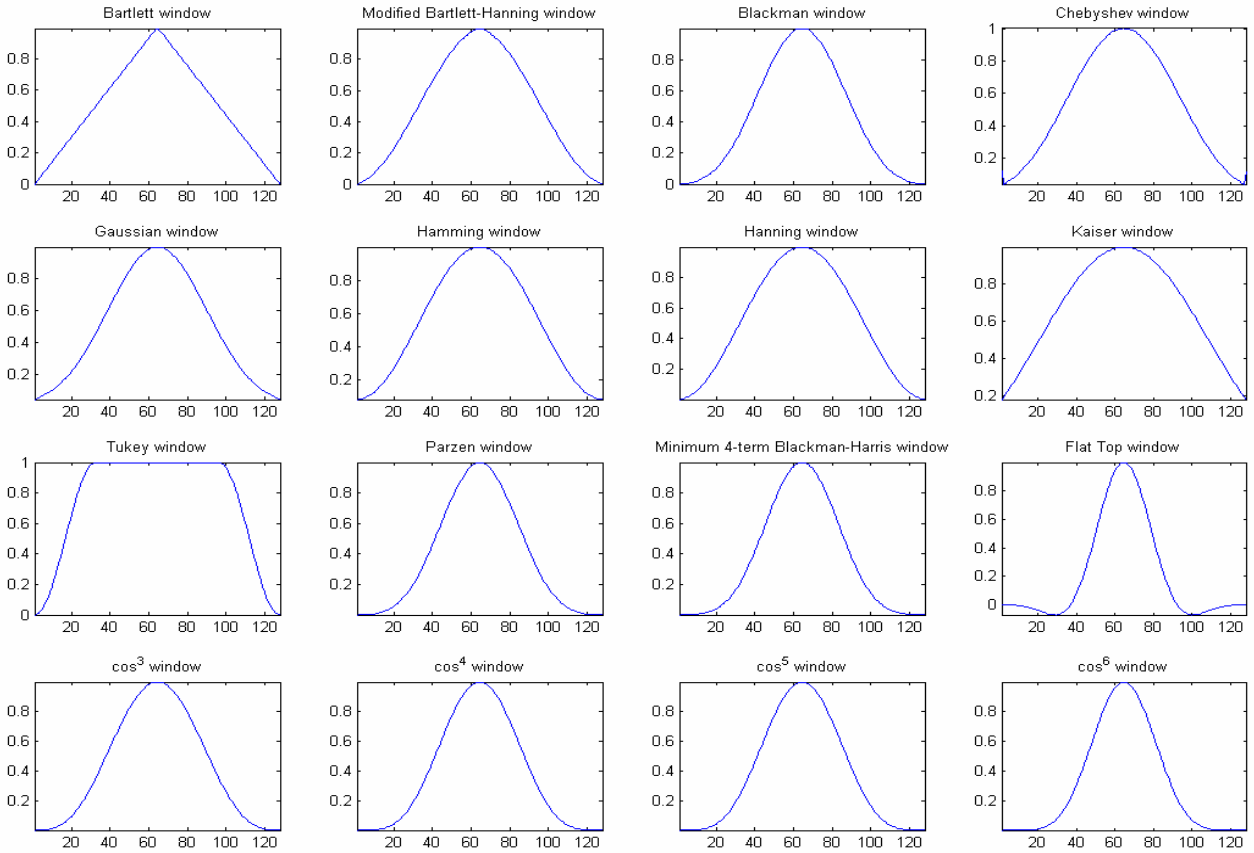

Figure 4.1: Some of the window functions used in computations

4.2. Basic Definitions

Figure 4.2 shows a simple model of the radar system. The system is assumed to be working in a clutter and noise free environment and a point target is assumed. For this system; u_n, h_n, y_n are the transmitted signal, receiver filter and output signal, respectively.

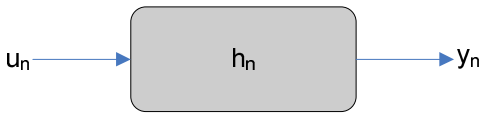

Figure 4.2: Radar receiver

The receiver filter, h_n , with weighting can be expressed as:

$$h_n = u^*_{N-n} x\, w_n \tag{4.1}$$

where u_n is the transmitted waveform, w_n is the weighting function, n is an integer ranging from 0 to $(N-1)$ and N is the code length.

If instead of a weighting window a two sample sliding window averager (TSSWA) or two sample sliding window differencer (TSSWD) is used then the receiver filter can be given as:

$$h_n = \sum_{k=0}^{1} g_k u^*_{N-(n-k)} \tag{4.2}$$

where g_n is the TSSWA ([1 1]) or TSSWD ([1 -1]).

The output of the receiver filter is:

$$y_n = \sum_{k=0}^{N-1} h_k u_{n-k} \tag{4.3}$$

where h_n is the receiver filter and u_n is the transmitted code. A weighting function at the receiver filter gives an output of length $(2N-1)$ while a TSSWA/TSSWD gives an output of length $2N$.This is because the TSSWA/TSSWD increases the length of h_n to $(N+1)$. For the general case if h_n is of length M then we get the output y_n of length $(N+M-1)$.

If the output signal y_n is sampled at the ideal position, assume for the general case $n = L$, then the output SNR of the receiver is:

$$SNR_o = \frac{|y_L|^2}{\sigma^2 \sum_{k=0}^{M-1} |h_k|^2} \tag{4.4}$$

where σ is the variance of the additive white Gaussian noise (WGN).

The SNR loss is defined relative to the matched filter output SNR (i.e. weighting filter has all the coefficients equal to unity). The output SNR of MF can be written as:

$$SNR_{o,MF} = \frac{N}{\sigma^2} \tag{4.5}$$

Combining (4.4) and (4.5) the SNR loss for the general case is:

$$SNR_{loss} = \frac{|y_L|^2}{N\sum_{k=0}^{M-1}|h_k|^2} \tag{4.6}$$

where SNR $loss_{dB} \leq 0$ dB.

For the windowing method the SNR loss can be simplified because both L and M are equal to N. The simplification can be written as:

$$SNR_{loss} = \frac{\left|\sum_{k=0}^{N-1} u_{N-k} u_{N-k}^{*} w_k\right|^2}{N\sum_{k=0}^{N-1}|h_k|^2} = \frac{\left|\sum_{k=0}^{N-1} w_k\right|^2}{N\sum_{k=0}^{N-1}|h_k|^2} \tag{4.7}$$

The definitions of PSL and ISL are as given in (2.16) and (2.17).

$$PSL = 10\log\frac{max|\Phi(i)|^2}{|\Phi(0)|^2} \tag{4.8}$$

$$ISL = 10\log\sum_i\left|\frac{\Phi(i)}{\Phi(0)}\right|^2 \tag{4.9}$$

In [19] main lobe broadening (MLB) is defined as ±2.5 times inverse bandwidth (ibw) from the mainlobe peak of receiver filter output, where *ibw* is equal to chip duration for binary and binary-based codes. The main lobe region is also chosen to contain all points above -6 dB relative to mainlobe peak.

4.3. P4 Code Weighting on Receive

A window function reduces the PSL and ISL values at the expense of an SNR loss and main lobe broadening due to filter mismatch. Generally, a window is preferred that reduces the sidelobes to a desired level while bringing a small SNR loss and a low MLB value.

Figure 4.3 shows the ACF function of P4 code of length 128. It is given for comparison with the other figures obtained with windowing the P4 code.

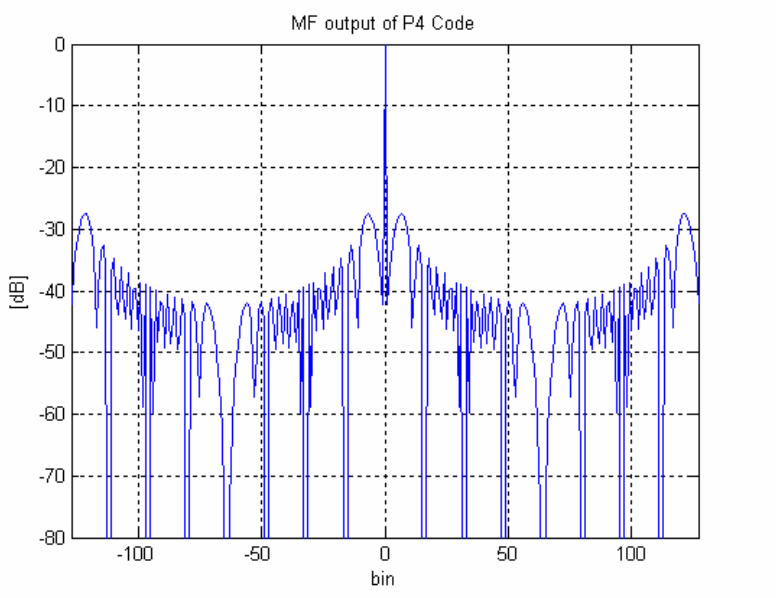

Figure 4.3: Autocorrelation of P4 code of length 128

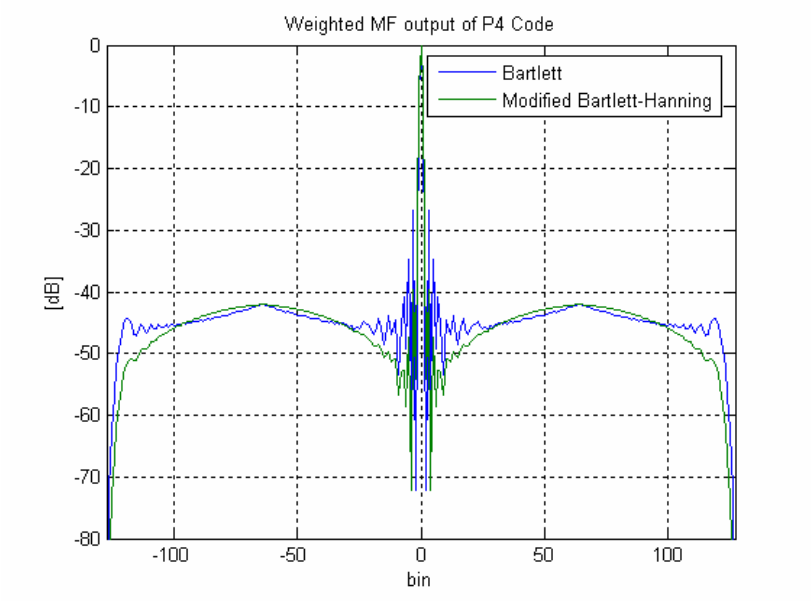

Figure 4.4: Receiver output for Bartlett and Modified Bartlett-Hanning windows

Figure 4.4 shows the receiver filter output for Bartlett and modified Bartlett-Hanning windows. As seen in Figure 4.1 the Bartlett window is similar to a triangular window. The Bartlett window of length 128 causes an SNR loss of 1.28 dB, and a MLB of 1.34. Both of these values are acceptable values but the PSL of Bartlett window is worse than the rectangular window, i.e. no window case. Bartlett window has a PSL value of -26.67 dB whereas rectangular window has a PSL of -27.41 dB. The ISL of Bartlett window is -20.01 dB and if compared to -12.67 dB which is the ISL of rectangular window, it is again an acceptable value. Modified Bartlett-Hanning window has a mainlobe at the origin and asymptotically decaying sidelobes on both sides like Bartlett window. It is a linear combination of weighted Bartlett and Hann windows with near sidelobes lower than both Bartlett and Hann and with far sidelobes lower than both Bartlett and Hamming windows [20]. The modified Bartlett-Hanning window of length 128 has an SNR loss of 1.67 dB, MLB of 1.47, PSL of -39.65 dB and an ISL of -22.60 dB. This window has worse SNR loss and MLB values and better ISL and PSL with respect to

Bartlett window. So, if one has to choose one of them, Bartlett-Hanning window is a better choice.

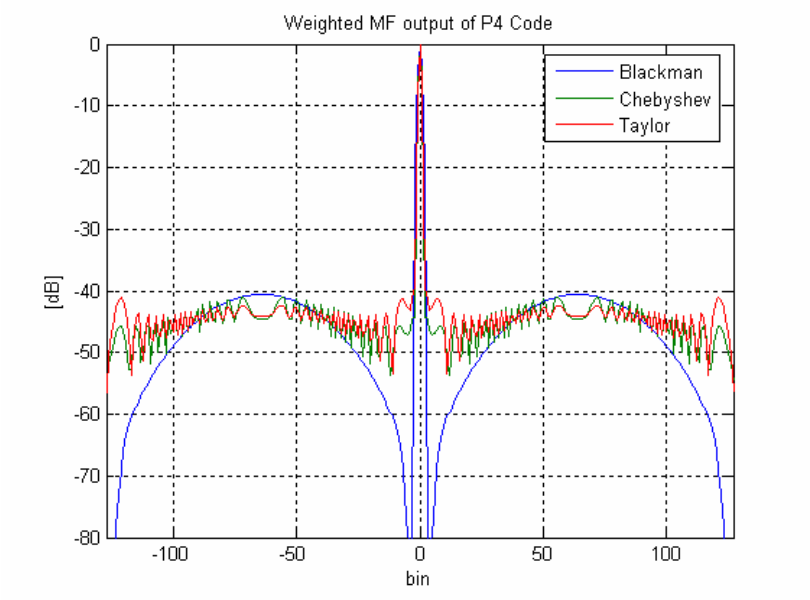

Figure 4.5: Receiver output for Blackman, Chebyshev and Taylor windows

Figure 4.5 shows the receiver filter output for Blackman, Chebyshev and Taylor windows. Blackman window is in the form of:

$$a_0 + a_1 \cos(w) + a_2 \cos(2w) + a_3 \cos(3w) \qquad (4.10)$$

with $a_0 = 0.42$, $a_1 = 0.5$, $a_2 = 0.08$ and $a_3 = 0$ where $-\frac{\pi}{2} < w < \frac{\pi}{2}$.

Blackman window has slightly wider central lobes and less sideband leakage than equivalent length Hamming and Hann windows [20]. It has an SNR loss of 2.40 dB, MLB of 1.74, PSL of -40.56 dB and ISL of -23.31 dB. Chebyshev window has a variable parameter, R, which defines the Fourier transform

sidelobe magnitude with respect to the mainlobe magnitude. For this computation it is taken as 50 dB. Chebyshev window with 50 dB relative sidelobe level has an SNR loss of 1.47 dB, MLB of 1.40, PSL of -41.01 dB and ISL of -22.27 dB. Taylor window with n_{bar}=6 and 40 dB sidelobe level is used together with the window functions above. Taylor window is not present in the window library of MATLAB and the coefficients of Taylor window is obtained from [21]. It has an SNR loss of 1.17 dB, MLB of 1.31, PSL of -41.14 dB and ISL of -21.54 dB. If these three window functions are compared among each other Taylor window comes out to be the best one. The second window would be Chebyshev window with 50 dB sidelobe level.

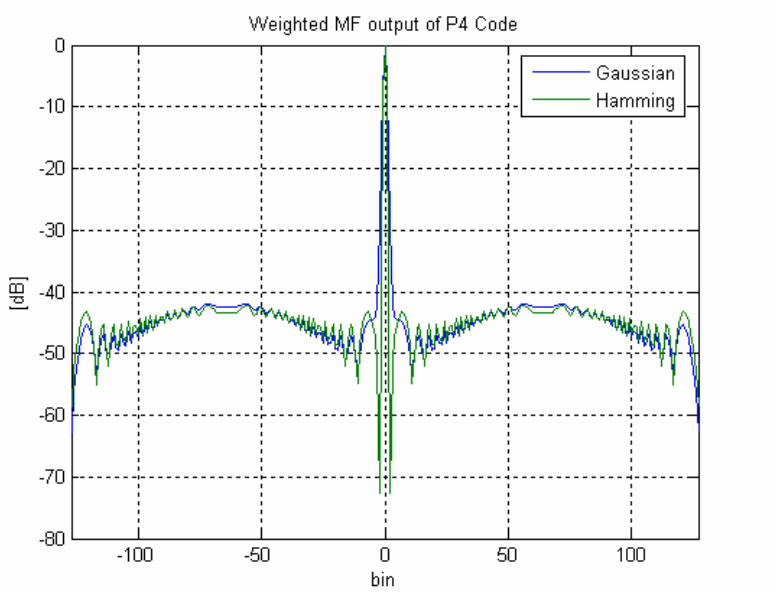

Figure 4.6: Receiver output for Gaussian and Hamming windows

Figure 4.6 shows the receiver filter output for Gaussian and Hamming windows. Gaussian window has a parameter α which is the inverse of the standard deviation. The width of the window is inversely related to the value of α; larger values of α produces a narrower window [20]. In this computation

α is taken as 2.5. Gaussian window gives an SNR loss of 1.60 dB, MLB of 1.45, PSL of -41.92 and ISL of -22.68 dB. Hamming window has the form given in (4.10) with $a_0 = 0.54$, $a_1 = 0$, $a_2 = 0.46$ and $a_3 = 0$. It has an SNR loss of 1.37 dB, MLB of 1.37 and has PSL and ISL values of -42.21 dB and -22.08 dB respectively. The results for Hamming window are better than results of Gaussian window. If all the window functions mentioned until here are compared to each other, the Hamming and the Taylor windows come out to be the ones with lowest sidelobe levels; least SNR loss and MLB.

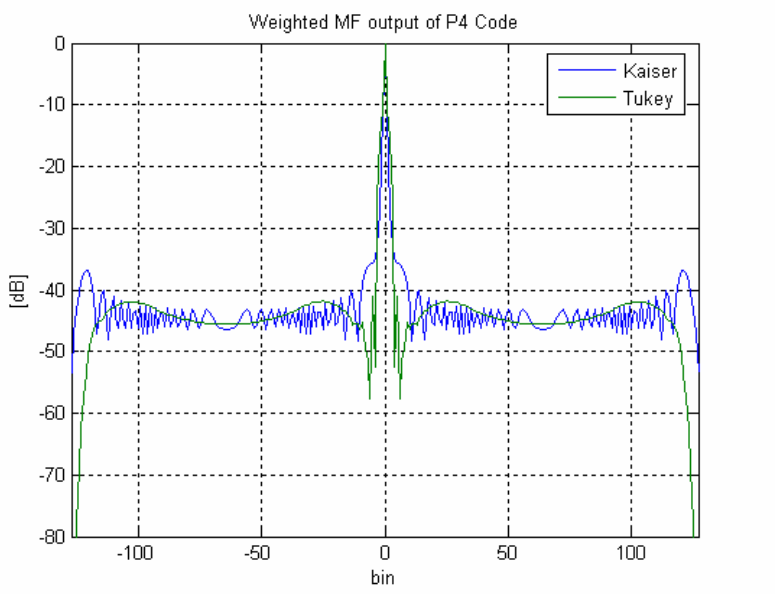

Figure 4.7: Receiver output for Kaiser and Tukey windows

Figure 4.7 shows the receiver filter output for Kaiser and Tukey windows. Kaiser window has a parameter β that affects the sidelobe attenuation of the Fourier transform of the window. For the computation it is taken as π. Kaiser window of length 128 has an SNR loss of 0.63 dB, MLB of 1.16, PSL and ISL of -36.73 dB and -20.48 dB respectively. Its SNR loss and MLB values are the best among the window functions given. However, its sidelobe levels are

not as good as Hamming or Taylor windows. Tukey window is a cosine-tapered window. It has a parameter , r, which is the ratio of taper to constant sections and takes values between 0 and 1 [20]. r is taken as 0.5 for the computation. Tukey window has an SNR loss of 0.91 dB, MLB of 1.23, PSL of -41.03 dB and ISL of -21.17 dB. Tukey window is between Kaiser and Hamming / Taylor windows because its SNR loss, MLB are worse than Kaiser but better than Hamming / Taylor. Also it has sidelobe levels close to Hamming window which is better than Kaiser window sidelobe levels.

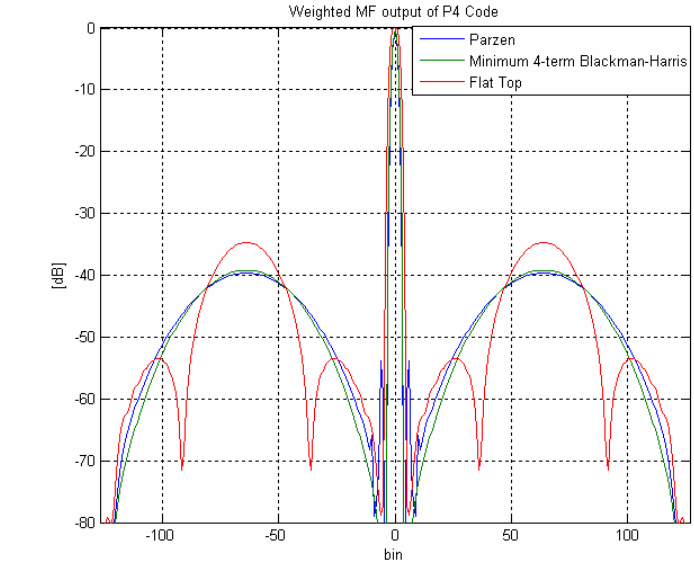

Figure 4.8: Receiver output for Parzen, Flat-top and Blackman-Harris windows

Figure 4.8 shows the receiver filter output for Parzen, Flat-top and Minimum 4-term Blackman-Harris windows. Parzen windows are piecewise cubic approximations of Gaussian windows [20]. Parzen window of length 128 has an SNR loss of 2.83 dB, MLB of 1.92, PSL and ISL of -39.64 dB and -23.48 dB respectively. Minimum 4-term Blackman-Harris window is minimum in the sense that its maximum sidelobes are minimized [20]. It is in the form of (4.9)

with $a_0 = 0.35875$, $a_1 = 0.48829$, $a_2 = 0.14128$ and $a_3 = 0.01168$. The performance of Minimum 4-term Blackman-Harris window is close to Parzen window. It has an SNR loss of 3.05 dB, MLB of 2.02, PSL and ISL values of -39.17 dB and -23.57 dB respectively. The Flat Top window has very low passband ripple (< 0.01 dB) and is used primarily for calibration purposes. Its bandwidth is approximately 2.5 times wider than a Hann window [20]. In this triple group flat top window has the worst performance. Its SNR loss is 5.80 dB, it has a MLB of 3.80, PSL and ISL of -34.77 dB and -23.84 dB. This group has the worst values among the window functions mentioned till here. A careful designer does never use these window functions.

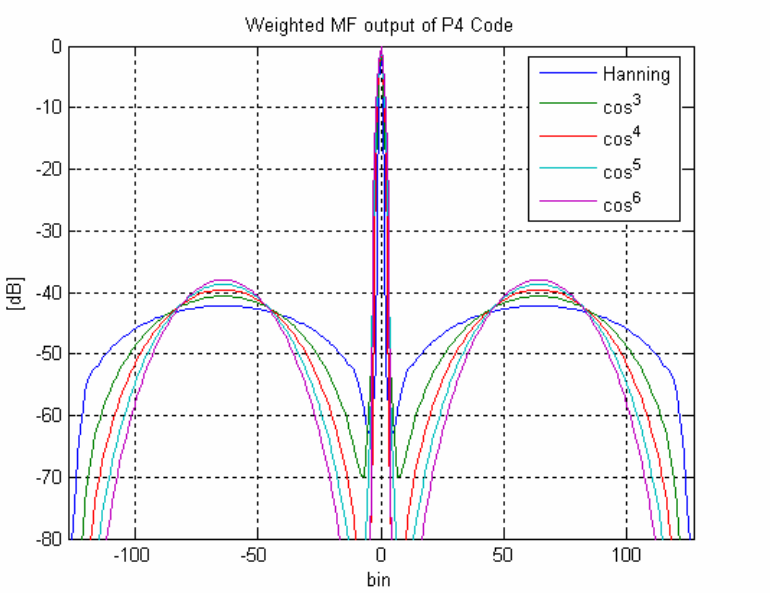

Figure 4.9: Receiver output for $\cos^2$, $\cos^3$, $\cos^4$, $\cos^5$ and $\cos^6$ windows

In Figure 4.9 $\cos^n$ windows for n = 2, 3, 4, 5 and 6 are given. $\cos^2$ window is also called Hann or Hanning window. Best performance in the group is obtained using Hanning window. It has SNR loss of 1.73 dB, MLB of 1.49, PSL and ISL of -42.21 dB and -22.81 dB. Its performance is the best in $\cos^n$ group but not as good as Taylor or Hamming windows.

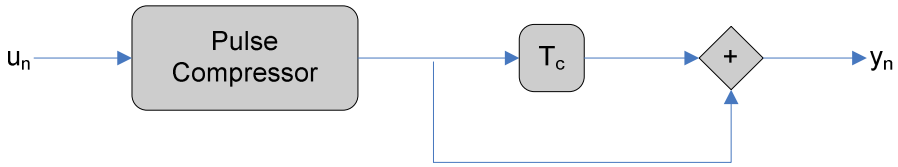

Figure 4.10: Pulse compressor followed by a TSSWA in radar receiver

TSSWA structure in the radar receiver is given in Figure 4.10. Each chip of the compressed pulse is delayed by one chip duration and added to the previous chip. This system acts as a sliding window two-sample adder.

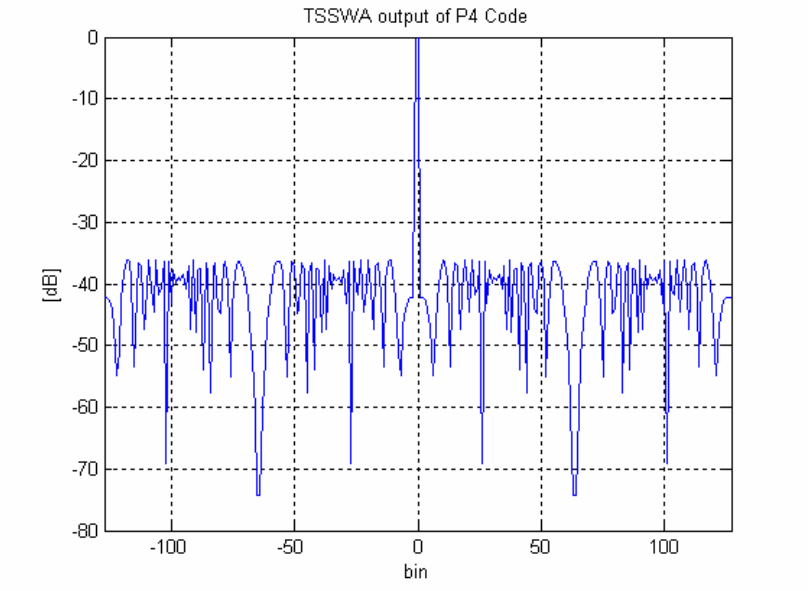

Figure 4.11: Receiver output for TSSWA

In Figure 4.11, the receiver output of P4 code using a two sample sliding window averager is given. TSSWA causes an SNR loss of 3.01 dB. This is

because the TSSWA doubles the noise power without changing the signal power. In [17] it is given that a detector would have two chances to detect the signal in two adjacent time cells containing different noise values. And the consequence of this is given as an SNR loss on the order of 1 dB. The MLB of TSSWA is 2.03 which decrease the resolution by a factor of two because of addition. It gives a PSL of -36.12 dB and an ISL value of -18.77 dB.

The MLB, SNR loss, PSL and ISL values of the window functions given above are listed in Table 4.1.

Table 4.1: Performance of Window Functions for P4 Code of Length 128

window	SNR loss [dB]	MLB [cells]	PSL [dB]	ISL [dB]
Rectangular	0	1	-27.41	-12.67
Bartlett	1.28	1.34	-26.67	-20.01
Bartlett - Hann	1.67	1.47	-39.65	-22.60
Blackman	2.40	1.74	-40.56	-23.31
Chebyshev (50 dB sidelobe)	1.47	1.40	-41.01	-22.27
Gaussian ($\sigma = 0.4$)	1.60	1.45	-41.92	-22.68
Hamming (n = 2, k = 0.08)	1.37	1.37	-42.21	-22.08
Taylor ($n_{bar} = 6$, 40dB)	1.17	1.31	-41.14	-21.54
Kaiser ($\beta = \pi$)	0.63	1.16	-36.73	-20.48
Tukey (r = 0.5)	0.91	1.23	-41.03	-21.17
Parzen	2.83	1.92	-39.64	-23.48
Blackman - Harris	3.05	2.02	-39.19	-23.57
Flat top	5.80	3.80	-34.77	-23.84
Hanning	1.73	1.49	-42.21	-22.81
$\cos^3$	2.43	1.75	-40.65	-23.31
$\cos^4$	2.92	1.96	-39.56	-23.51
$\cos^5$	3.33	2.15	-38.71	-23.63
$\cos^6$	3.67	2.33	-37.99	-23.71
TSSWA	3.01	2.03	-36.18	-18.77

In the next six figures the double groups obtained from SNR loss, MLB, PSL and ISL of the window functions used above are given. Some extra window functions are also added and some window functions exist twice or more with different parameters. Figure 4.12 shows SNR loss versus PSL. The window functions located in the upper-left corner of Figure 4.12 are better from the point of SNR loss and PSL. Figure 4.13 shows SNR loss versus ISL. Similarly the window functions at upper-left side are better. Hamming, Tukey with r = 0.5 and 0.6, Taylor, Kaiser with β = 5 windows are at the upper left corner in both figures. So they are good choice in the sense of SNR loss, PSL and ISL. In Figure 4.14, SNR loss versus MLB is given. Again the upper-left corner located window functions are better. However, one has to consider Figure 4.14 on one hand and Figure 4.17 (PSL versus ISL) on the other hand. Each windowing function has to be controlled in both figures not to conclude in a wrong decision. MLB versus PSL is given in Figure 4.15. The better window functions are at the lower left corner of the figure. As in the SNR loss versus PSL and SNR loss versus ISL cases the Hamming, Tukey with r = 0.5 and 0.6, Taylor, Kaiser with β = 5 windows are the best choices. In Figure 4.16 MLB versus ISL is shown. Again the same windowing functions as before which reside in the lower left corner give better results. PSL versus ISL is given in Figure 4.17. Window functions located at the lower-left corner are better. Tukey window with r = 0.6, Hamming, Hanning and Kaiser window with β = 5 are convenient in the sense of PSL and ISL. For the selection of a window function such a method can be also applied: The designer defines a cost function with the parameters SNR loss, MLB, ISL and PSL. Then, the window that minimizes the cost function for that application is the optimum one. On the overall; Hamming, Tukey with r = 0.5 and 0.6, Taylor n_{bar} = 6, Kaiser with β = 5 windows give adequate performance. If the radar designer has a primary concern, for example PSL, then he should use Tukey window with r = 0.6. This window will provide adequate SNR loss, ISL and MLB while maintaining a low level of PSL.

In the following subsections the window functions that have a variable parameter are studied.

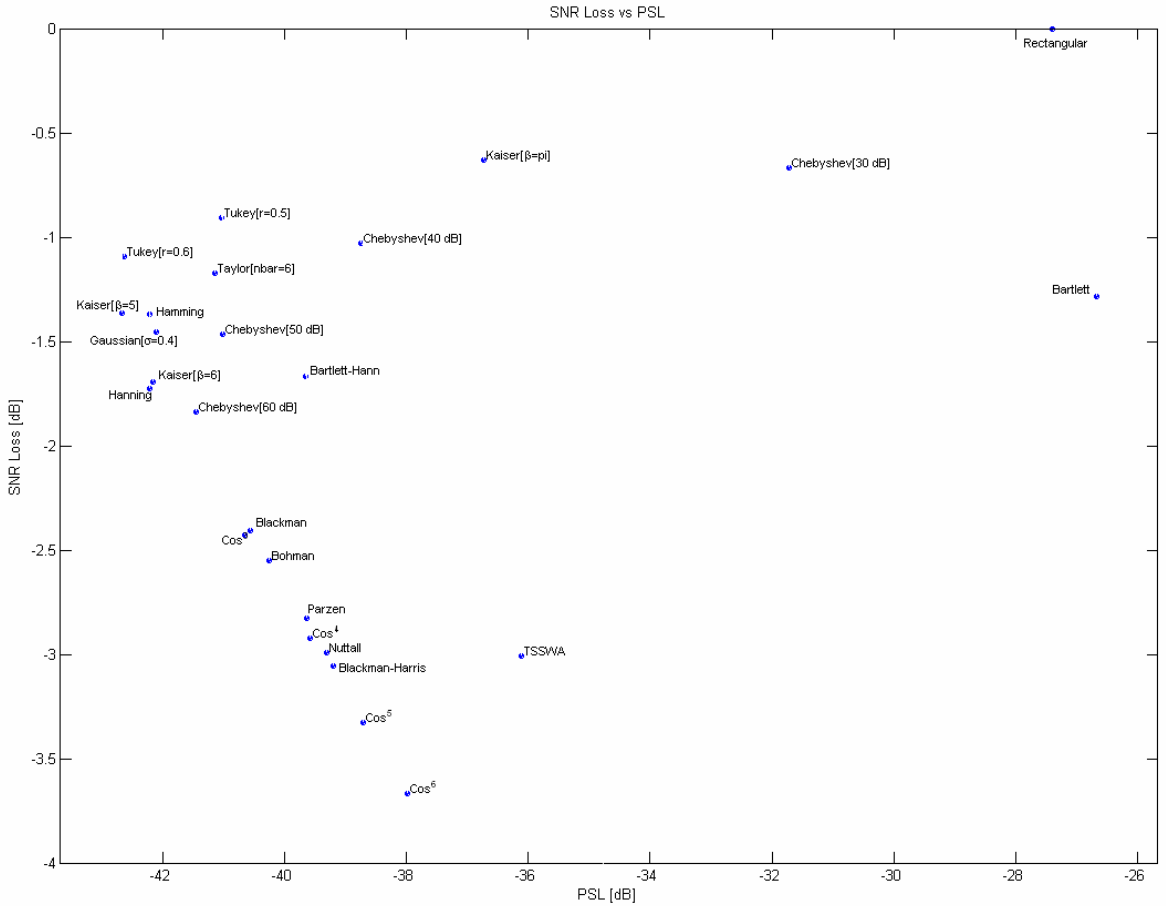

Figure 4.12: SNR loss versus PSL

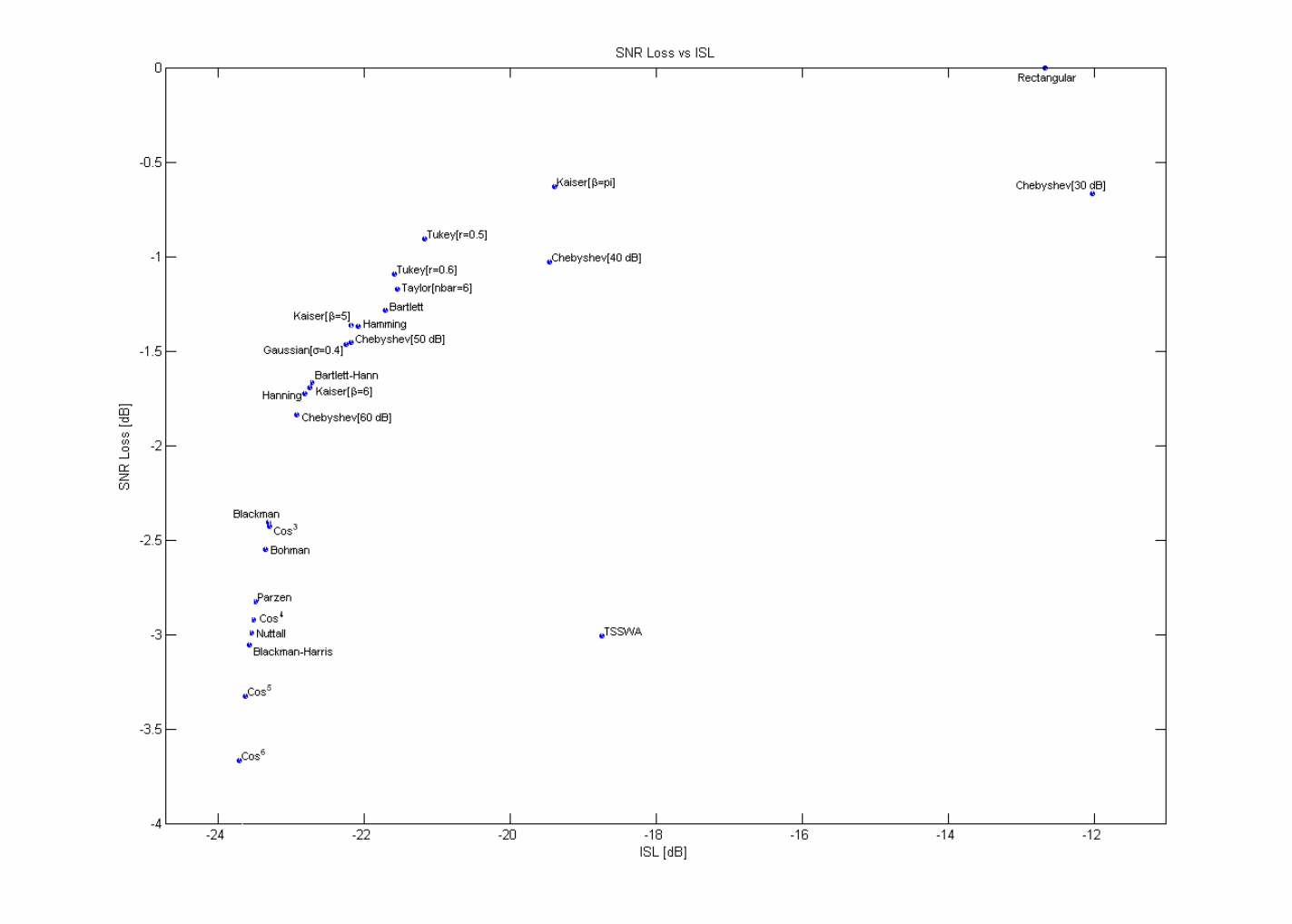

Figure 4.13: SNR loss versus ISL

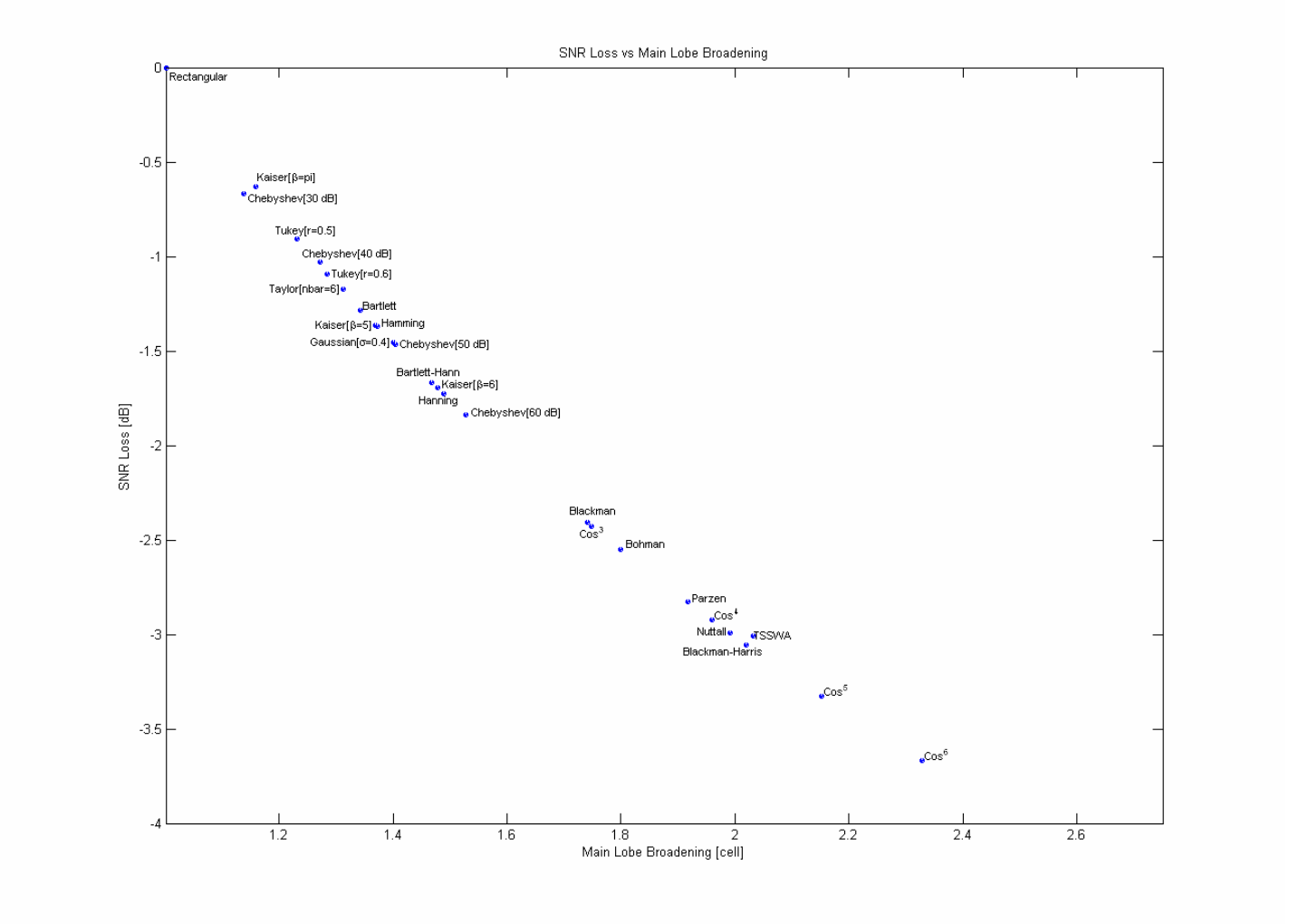

Figure 4.14: SNR loss versus MLB

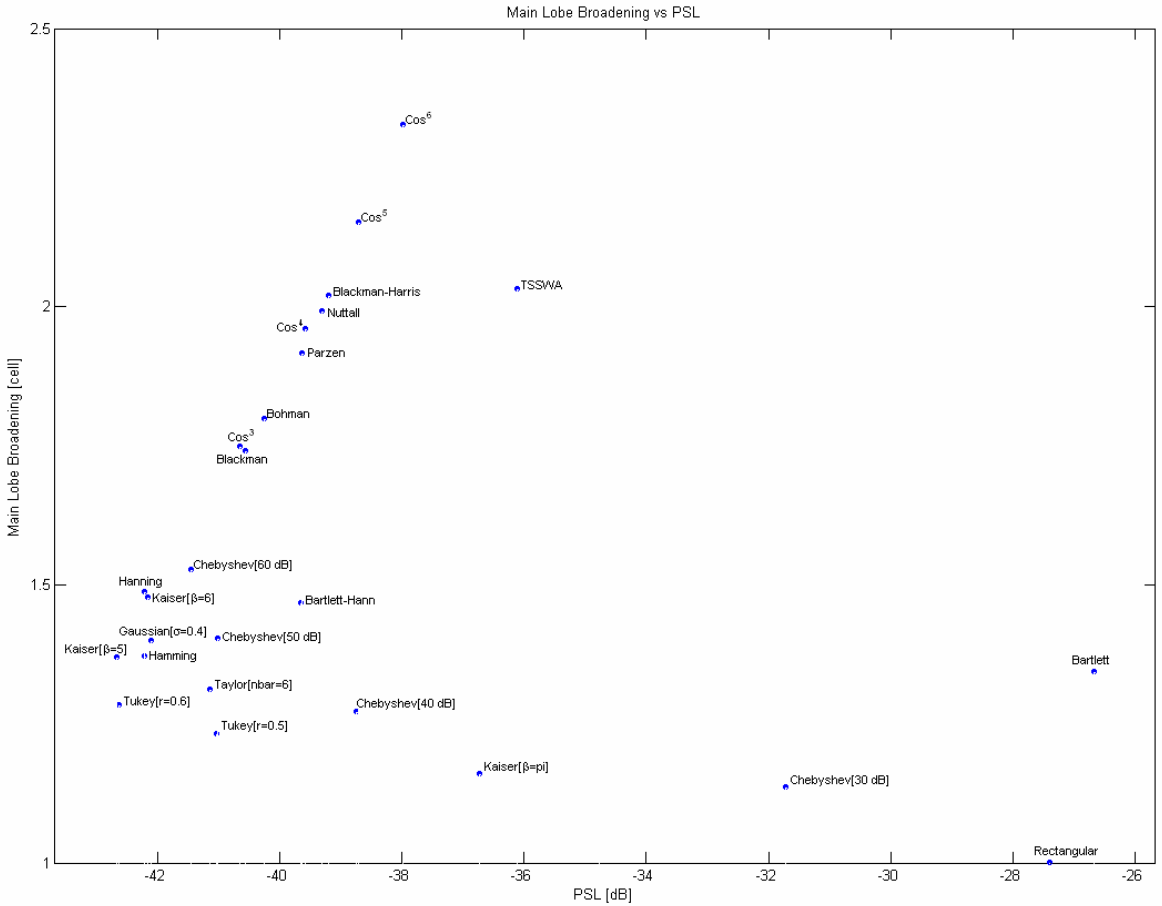

Figure 4.15: MLB versus PSL

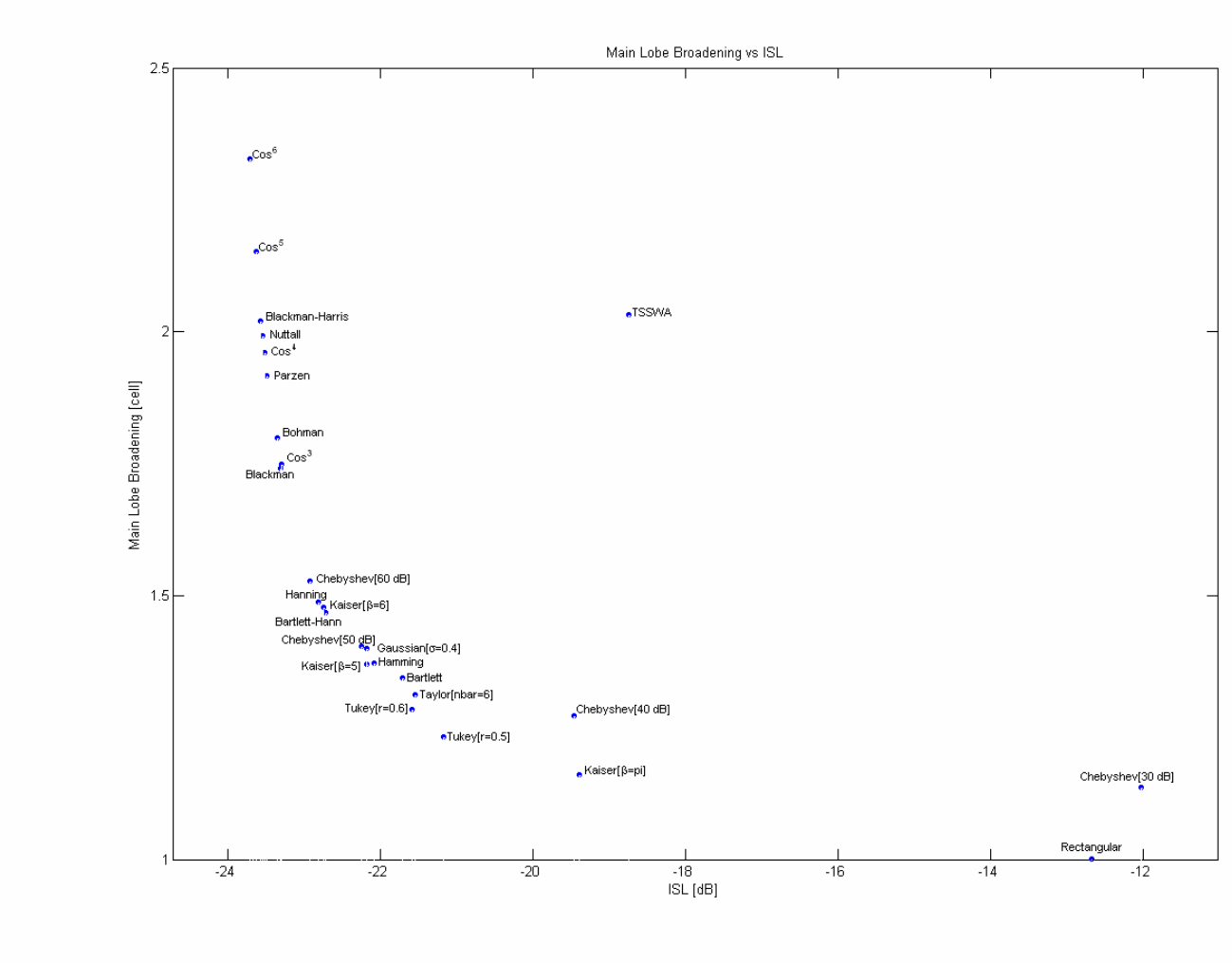

Figure 4.16: MLB versus ISL

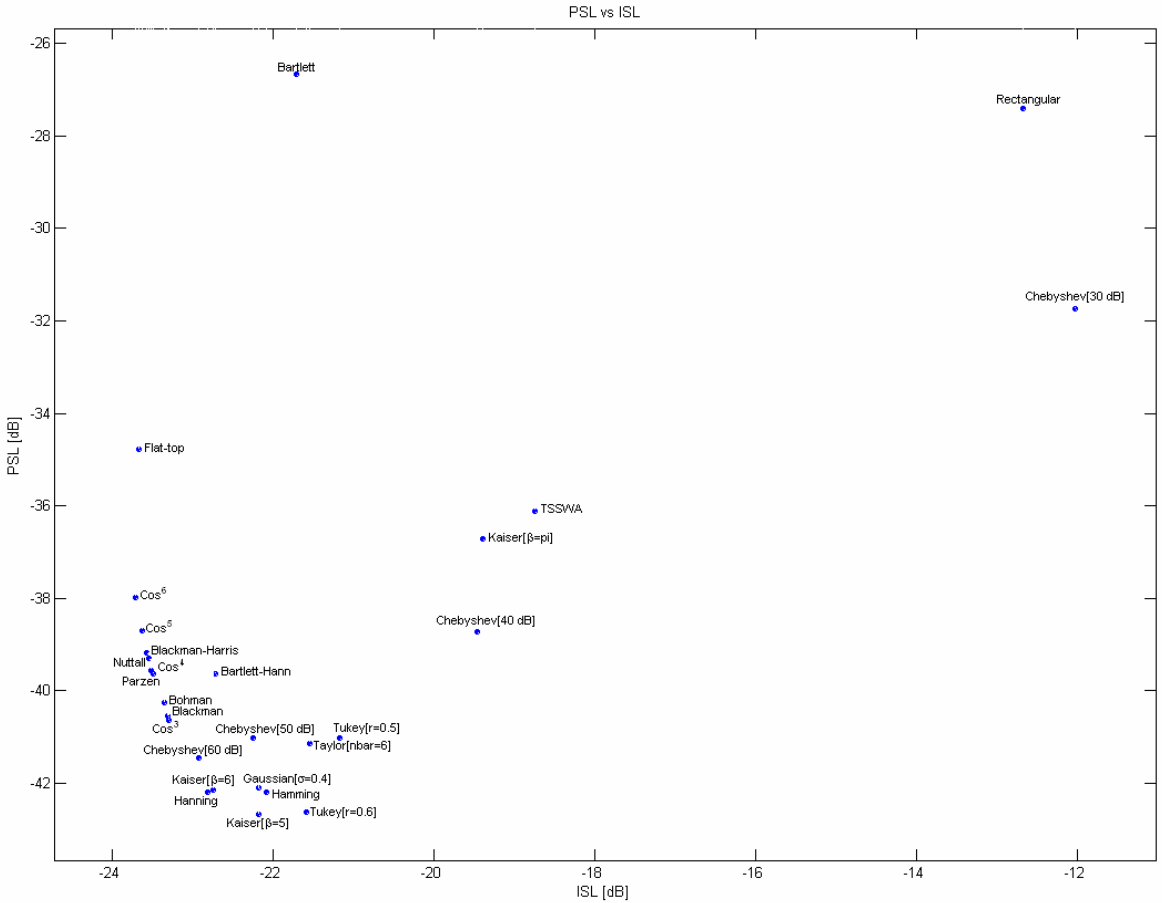

Figure 4.17: PSL versus ISL

The computations in the next subsections are obtained with a P4 code of length 128.

4.3.1. $\cos^n$ on pedestal k window

$\cos^n$ on pedestal k window is in the form of:

$$k + (1 - k)\cos(w)^n \tag{4.11}$$

where k is the pedestal height between 0 and 1 and n is the order of cosine with $-\frac{\pi}{2} < w < \frac{\pi}{2}$.

Figures 4.18-4.21 plot the data associated with the $\cos^n$ on pedestal k weighting functions. Figure 4.18 shows the effect of pedestal height on SNR loss for different integer values of n. As seen in Figure 4.18 SNR loss increases as the order of cosine increases.

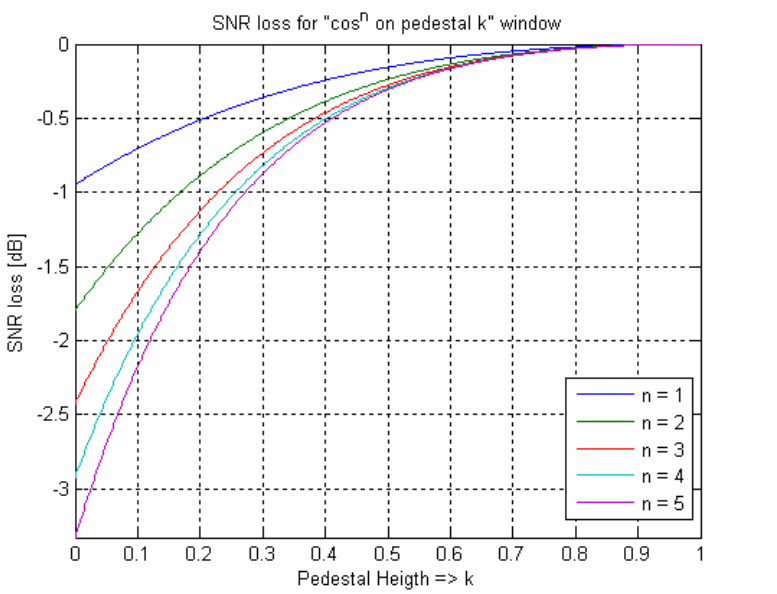

Figure 4.18: SNR loss versus pedestal height for n = 1, 2, 3, 4 and 5

In Figure 4.19 the pulse widening versus pedestal height is given. Like SNR loss, as n increases MLB gets worse.

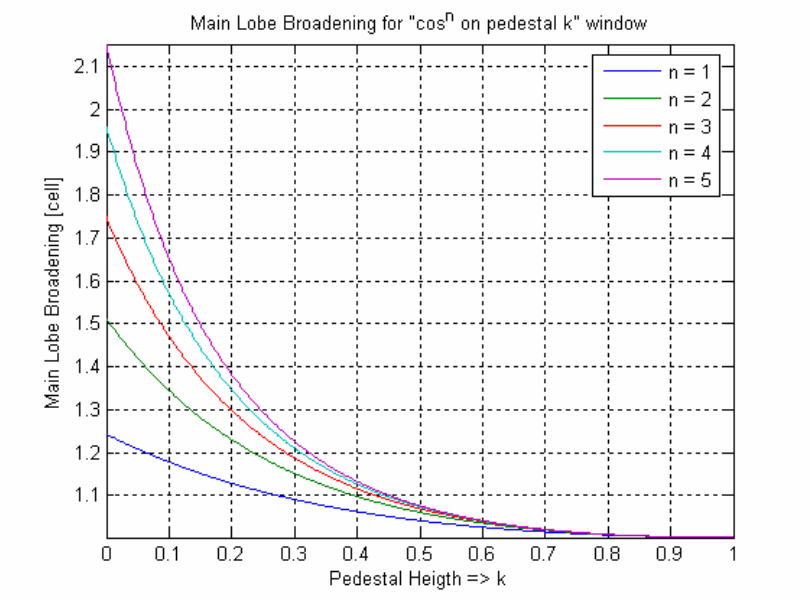

Figure 4.19: MLB versus pedestal height for n = 1, 2, 3, 4 and 5

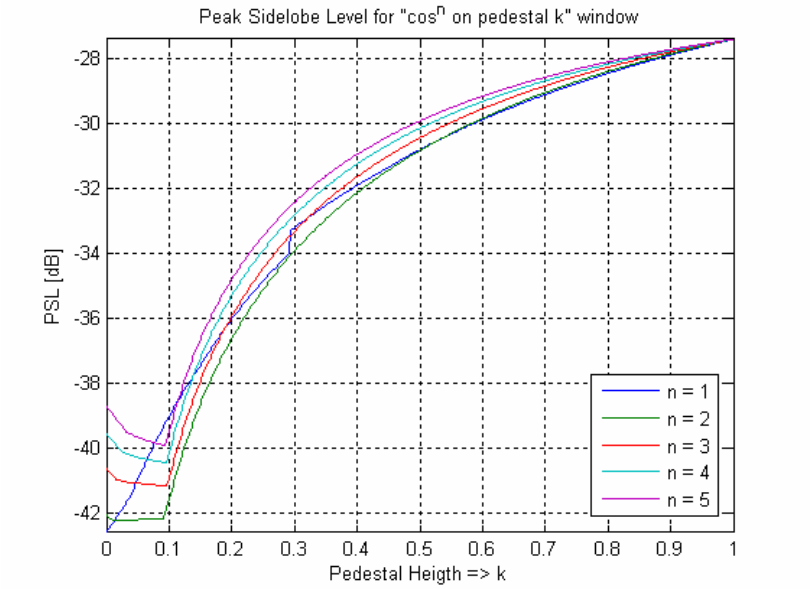

Figure 4.20: PSL versus pedestal height for n = 1, 2, 3, 4, and 5

The variation of PSL with respect to pedestal height for different n values is given in Figure 4.20.

Variation of PSL does not resemble the previous results. Lowest PSL values are obtained for n = 2. For low pedestal heights n = 1 gives the worst PSL values and as pedestal height increases its PSL values approach that of n = 2. The lowest PSL value is obtained with n = 2 and k = 0.08 which is the Hamming window indeed. In [9] it is also given that the Hamming function (k = 0.08, n = 2) represents the optimum for this family of weighted pulse shapes. The sudden jump in $\cos^1$ for k = 0.292 is due to the increase of the closest sidelobe to the mainlobe. For k between 0 and 0.292 the highest sidelobe is at the end of the receiver output. As k increases, the sidelobe close to the mainlobe increases especially for $\cos^1$ window. This increase depends on the shape of the $\cos^1$ window. It is much wider in the center compared other $\cos^n$ windows and is always concave whereas the other $\cos^n$ windows are convex in some part and concave in the other parts.

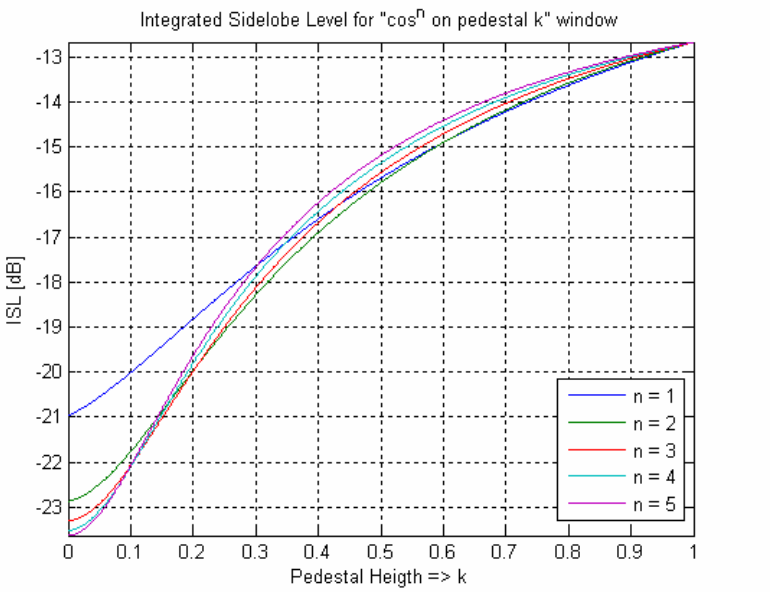

Figure 4.21: ISL versus pedestal height for n = 1, 2, 3, 4, and 5

In Figure 4.21 ISL versus pedestal height is depicted. The lowest ISL value at k = 0.08 is obtained for n = 5. But as k increases n = 5 gives worst ISL values. The behavior of $\cos^1$ is similar to PSL case. It is worse for low pedestal heights and approach best as pedestal height increases.

On the overall the SNR loss and MLB are lower for pedestal height close to 1 whereas PSL and ISL take lowest values for pedestal height between 0 and 0.1. Especially PSL quickly increases as pedestal height passes 0.1. Therefore, the best choice for $\cos^n$ on pedestal k window as stated in [9] is the Hamming window with k = 0.08 and n = 2.

4.3.2. Chebyshev window

As stated previously, Chebyshev window has a variable parameter, r, which defines the Fourier transform sidelobe magnitude with respect to the mainlobe magnitude. Preceding results were obtained with r = 50 [dB]. In the following plots, the Fourier transform sidelobe magnitude is varied between 20 dB and 200 dB.

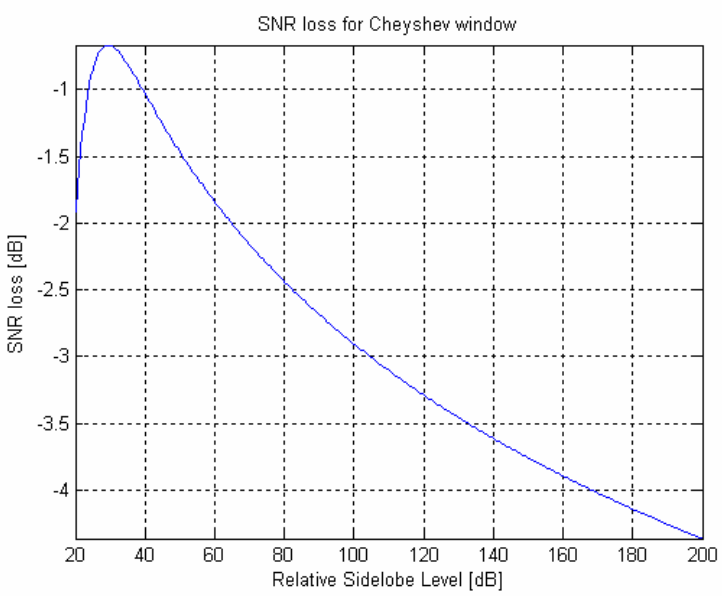

Figure 4.22: SNR loss versus relative sidelobe level

Figure 4.22 shows the SNR loss versus relative sidelobe level. Minimum level of SNR loss is obtained for 30 dB relative sidelobe level. For the relative sidelobe between 20 and 30 dB SRN loss decreases and after 30 dB it increases quickly.

The variation of main lobe broadening versus relative sidelobe level is given in Figure 4.23. MLB increases constantly with the decrease in the relative sidelobe level of Chebyshev window.

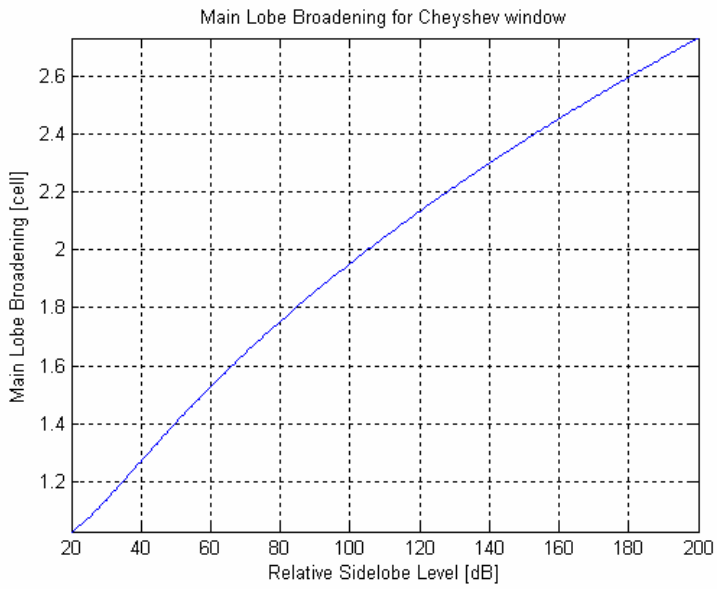

Figure 4.23: MLB versus relative sidelobe level

In Figure 4.24 PSL versus relative sidelobe level is given for the Chebyshev window. PSL takes the lowest value for 60 dB relative sidelobe level. At 60 dB sidelobe level PSL makes a notch. Before 60 dB PSL decreases and after 60 dB PSL increases.

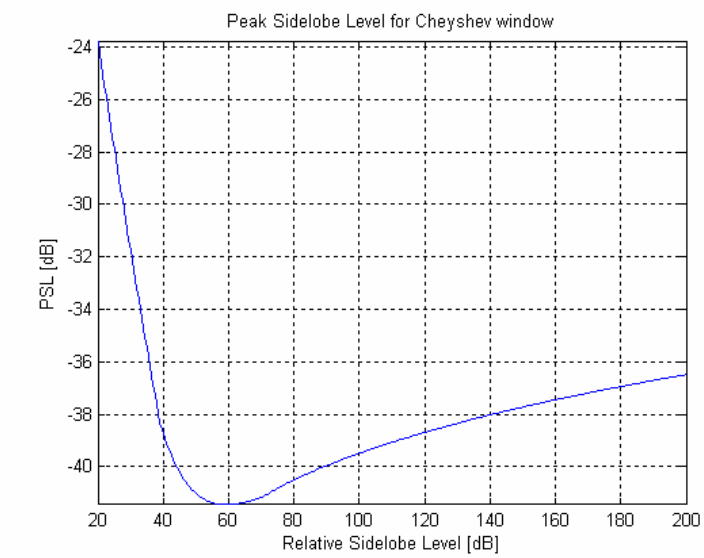

Figure 4.24: PSL versus relative sidelobe level

Figure 4.25 shows ISL versus relative sidelobe level. ISL decreases quickly as relative sidelobe level increases from 20 dB to 50 dB. Between 50 dB and 160 dB ISL decreases more slowly. After 160 dB of relative sidelobe level ISL starts to increase slowly.

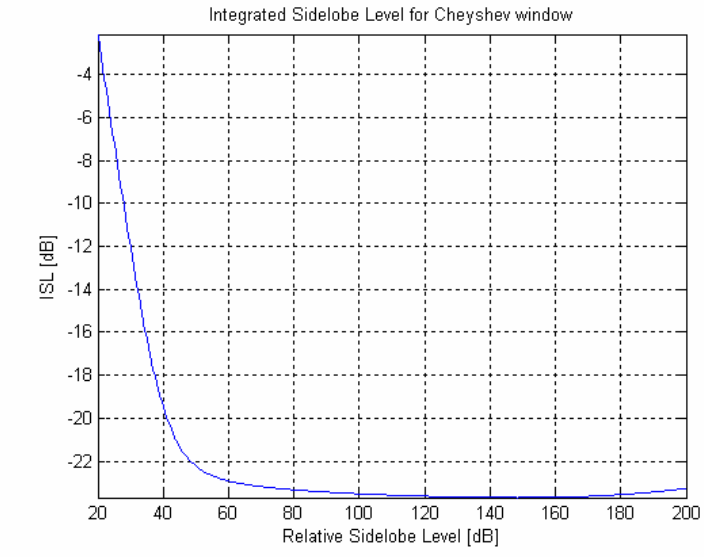

Figure 4.25: ISL versus relative sidelobe level

SNR loss and MLB take lower values for lower relative sidelobe levels for the Chebyshev window. SNR loss is minimum for relative sidelobe level between 20 dB and 60 dB. PSL and ISL take acceptable values when the relative sidelobe level is between 50 dB and 70 dB. So, the designer has to choose the window according to his priorities. For example, if PSL has the highest priority then the designer should choose a Chebyshev window with relative sidelobe level of 60 dB.

4.3.3. Gaussian window

As given previously, Gaussian window has a parameter α which is the inverse of the standard deviation. The width of the Gaussian window is inversely related to α, i.e. higher α values result in a narrower window. In the previous computation α taken as 2.5. In the following plots α is varied between 0.2 and 10.

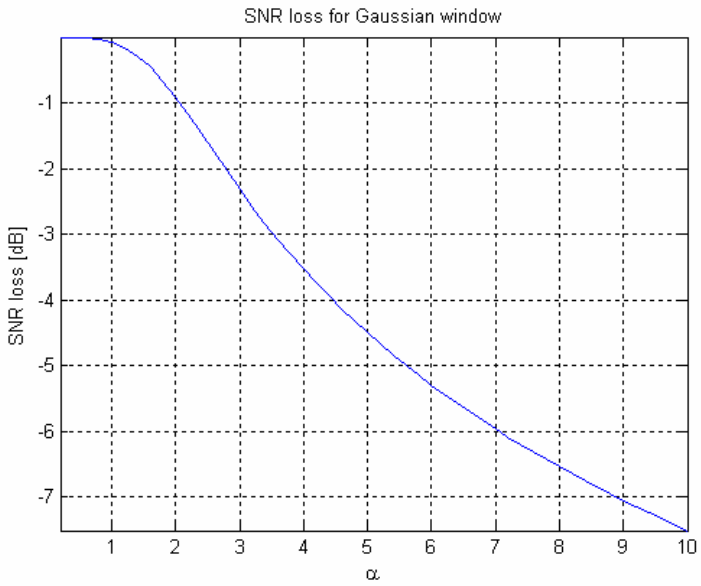

Figure 4.26: SNR loss versus α

Figure 4.26 shows SNR loss versus α. As the Gaussian window gets narrower, the SNR loss increases.

Figure 4.27: MLB versus α

Main lobe broadening versus α is given in Figure 4.27. Similar to SNR loss narrower Gaussian windows worsen the result, i.e. increases the MLB.

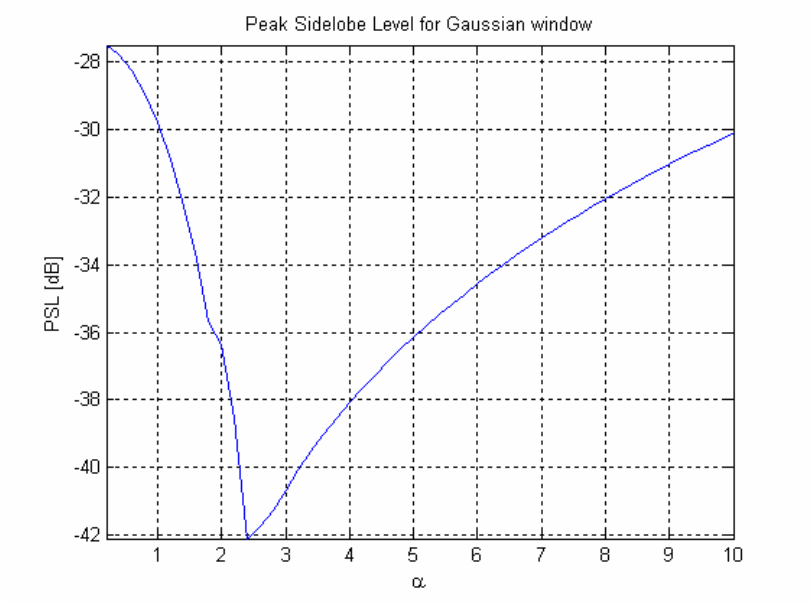

Figure 4.28: PSL versus α

In Figure 4.28 PSL versus α is given for the Gaussian window. PSL takes the lowest value for α = 2.4 which gives a standard deviation close to 0.42. Around α = 2.4 a notch is present in the plot and lowest PSL values are obtained.

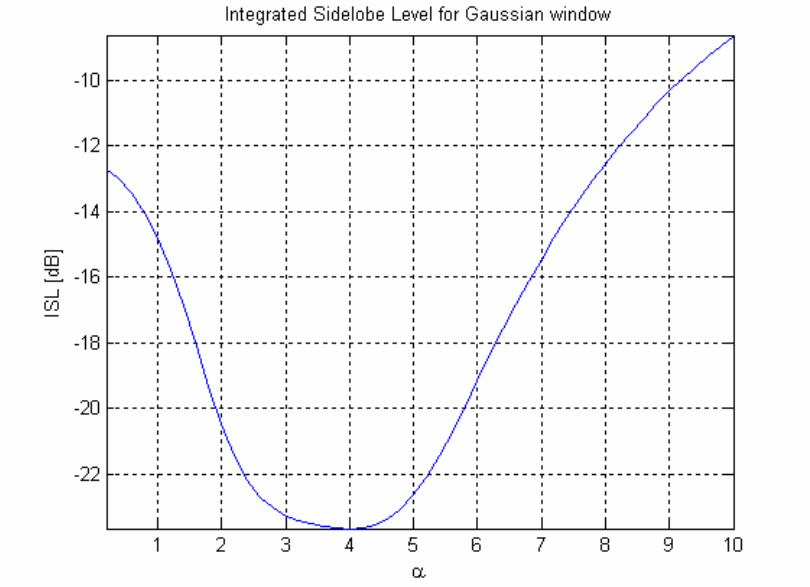

Figure 4.29: ISL versus α

The variation of ISL with respect to α is given in Figure 4.29. Similar to PSL a notch is present for the ISL case but this time around α = 4.

Similar to previously examined window functions, both SNR loss and MLB are lower for lower α values for the Gaussian window. For the PSL and ISL notches occur at different α values. It is reasonable to select Gaussian window with α = 2.4 because it gives the lowest PSL value, moderate ISL and acceptable SNR loss and MLB values. If α is chosen as 4 then ISL gets its lowest value but this time the SNR loss, PSL and MLB get higher values with respect to α = 2.4 case. Therefore, the designer could choose α = 2.4 if he wants to use a Gaussian window.

4.3.4. Kaiser window

Similar to Chebyshev window, Kaiser window has a parameter, β, that affects the sidelobe attenuation of the Fourier transform of the window. For the previous computation it is taken as π. In the following plots β is varied between 0 and 30.

The variation of SNR loss with respect to β is given in Figure 4.30. As β increases the SNR loss increases uniformly for Kaiser window.

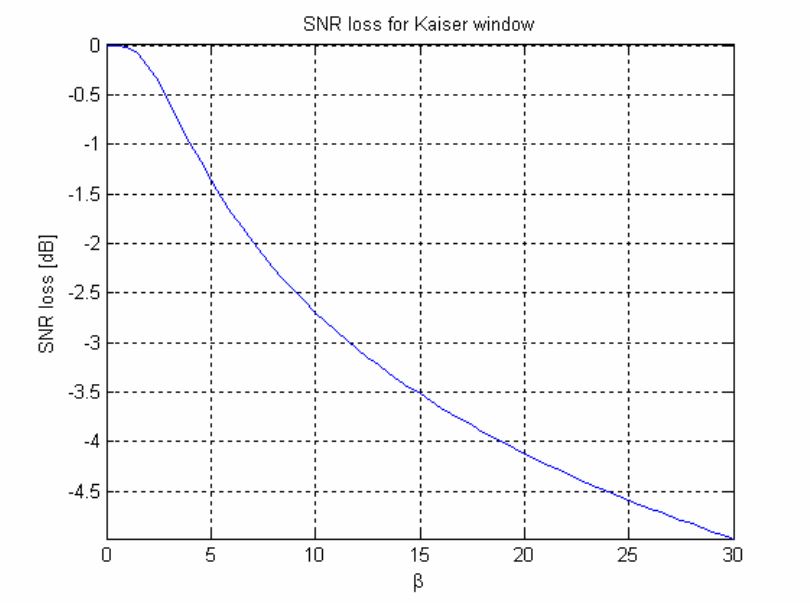

Figure 4.30: SNR loss versus β

In Figure 4.31 main lobe broadening versus β is given for the Kaiser window. Similar to SNR loss case, MLB increases with increasing β values.

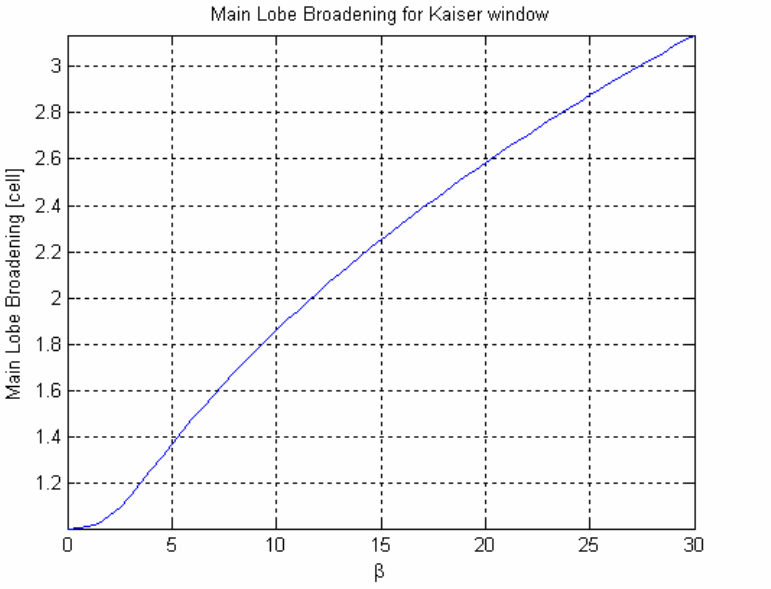

Figure 4.31: MLB versus β

PSL versus β is given in Figure 4.32. Similar to previous window functions investigated a notch is present around β = 4.5. PSL decreases to its lowest value quickly when β increases from 0 to 4.5. After 4.5 PSL increases but not as quick like β is between 0 and 4.5.

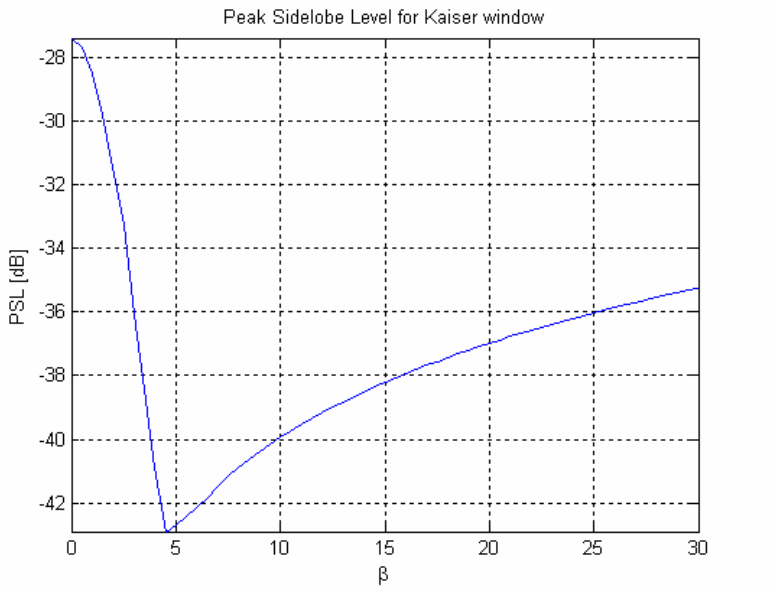

Figure 4.32: PSL versus β

The variation of ISL versus β is given in Figure 4.33. Similar to PSL case and previous cases the ISL versus β has a notch around β = 17. The width of the notch is much higher than the PSL case.

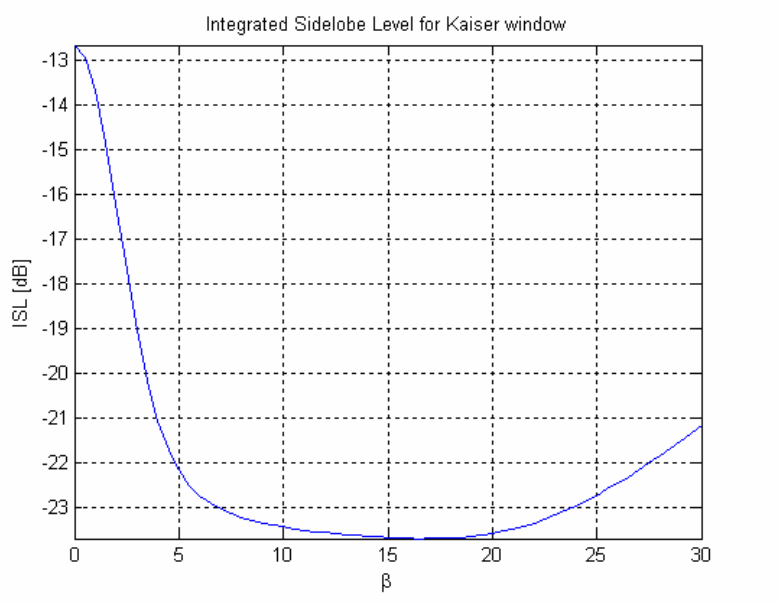

Figure 4.33: ISL versus β

The results of Kaiser window are very similar to the results of Gaussian window. For lower values of β, SNR loss and MLB take lower values. Again the minimum point notches of PSL and ISL are at different β values. Selecting the β around 4.5 gives the lowest PSL and SNR loss values and acceptable ISL value.

4.3.5. Effect of code length

In the previous subsections the results were obtained for P4 code of length 128. In this subsection the code length is varied with Hamming window (which is the optimum in $\cos^n$ on pedestal k group). The results are obtained with the code length changed from 16 to 512.

Figure 4.34 shows the variation of SNR loss with code length. SNR loss has a rapid decrease when the code length increases from 16 to 100. As the code length is increased above 100 the decrease in SNR loss gets slower.

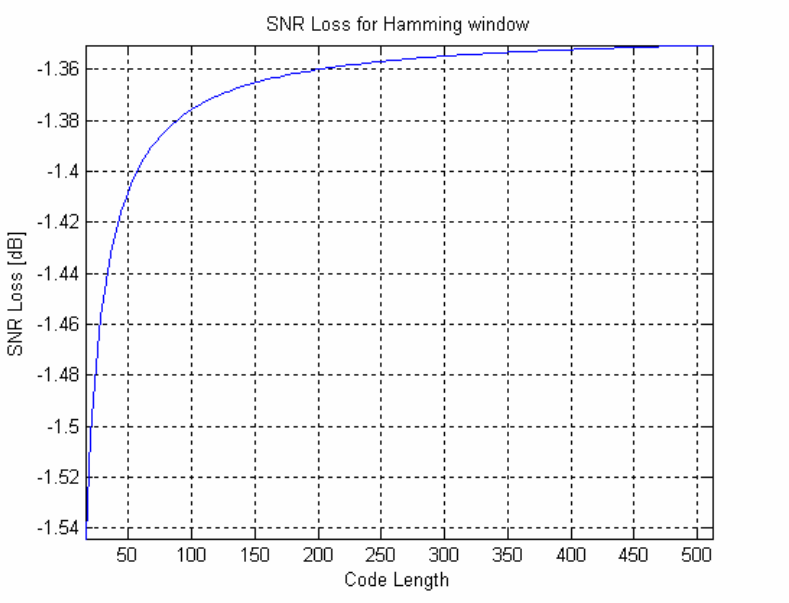

Figure 4.34: SNR loss versus code length

In Figure 4.35 MLB versus code length is given. MLB decreases as code length increases. Similar to SNR loss MLB does not vary much after code length of 100.

PSL versus code length is given in Figure 4.36. As code length is increased the PSL decreases as expected. However the decrease is much faster for lower values of code length especially between 16 and 144.

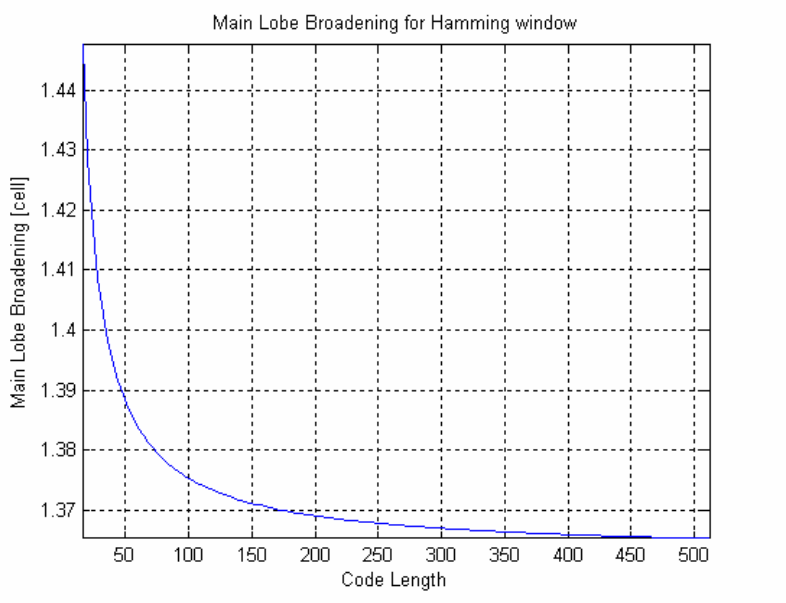

Figure 4.35: MLB versus code length

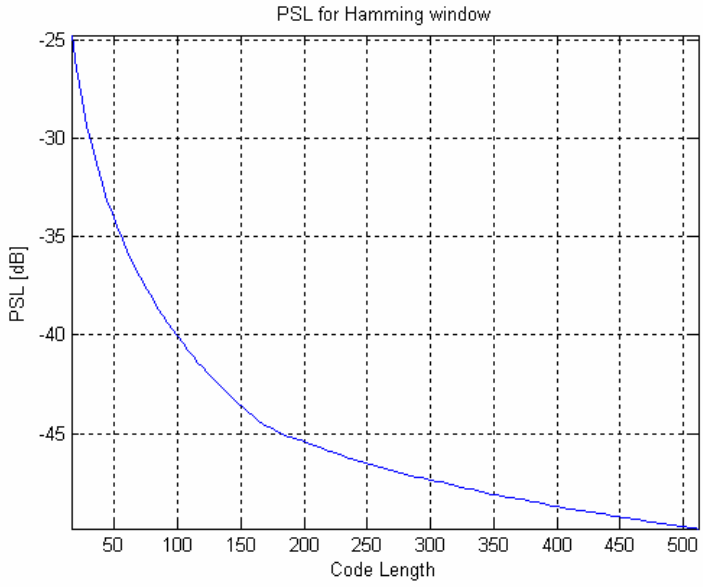

Figure 4.36: PSL versus code length

Figure 4.37 depicts ISL versus code length for Hamming windowed P4 code. The behavior of ISL is very similar to that of PSL.

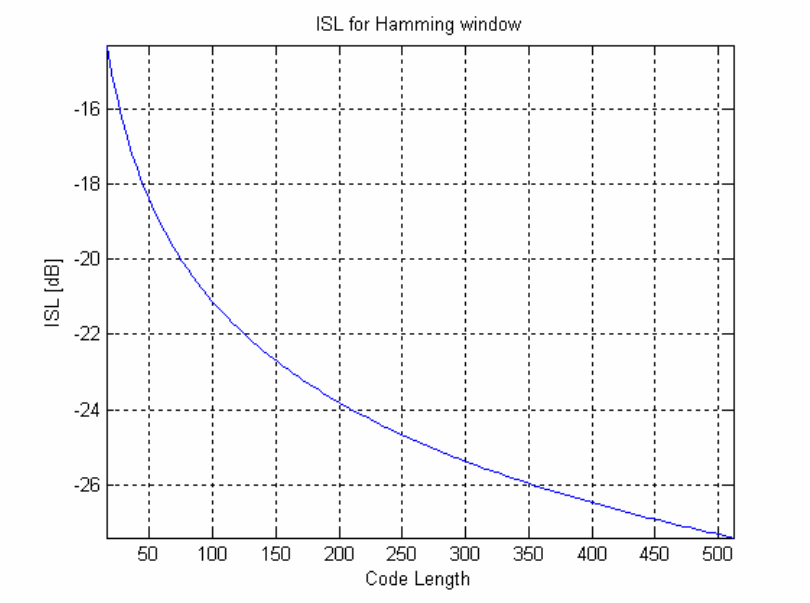

Figure 4.37: ISL versus code length

In the next subsection the effects of weighting on Frank code is obtained.

4.4. Frank Code Weighting on Receive

Weighting windows used with Frank code gives unacceptable results especially in PSL. Most of the window functions increases the value of PSL above from the no window case. Because of this only the table below is given in this thesis. The MLB, SNR loss, PSL and ISL values of the window functions for Frank code is given in Table 4.2.

Table 4.2: Performance of Window Functions for Frank Code of Length 121

window	SNR loss [dB]	MLB [cells]	PSL [dB]	ISL [dB]
Rectangular	0	1	-30.74	-14.19
Bartlett	1.28	1.33	-27.29	-16.58
Bartlett - Hann	1.67	1.46	-26.71	-16.95
Blackman	2.41	1.72	-24.58	-15.42
Chebyshev (50 dB sidelobe)	1.47	1.39	-27.22	-17.46
Gaussian ($\sigma = 0.4$)	1.60	1.44	-26.98	-17.10
Hamming (n = 2, k = 0.08)	1.37	1.36	-27.76	-17.56
Taylor ($n_{bar} = 6$, 40dB)	1.17	1.31	-28.66	-17.96
Kaiser ($\beta = \pi$)	0.63	1.16	-32.54	-18.57
Tukey	0.91	1.22	-30.23	-17.36
Parzen	2.83	1.89	-23.73	-14.48
Blackman - Harris	3.06	1.99	-23.34	-13.94
Flat top	5.80	3.67	-18.06	-8.42
Hanning	1.73	1.47	-26.52	-16.89
$\cos^3$	2.43	1.73	-24.48	-15.41
$\cos^4$	2.92	1.93	-23.51	-14.28
$\cos^5$	3.33	2.12	-22.90	-13.34
$\cos^6$	3.67	2.28	-22.48	-12.54
TSSWD	3.01	2.03	-35.57	-16.23

4.5. Other Codes

Weighting windows are also tested with other polyphase codes. P3 code gives the same results with the P4 code. But instead of a TSSWA, a TSSWD is used for P3 code [18]. P1 and P2 codes act similar to Frank code of similar length. Because of similar outputs obtained the results of P1, P2 and P3 codes are not given in this study.

4.6. Doppler Properties of Weighting Techniques

The Doppler response performance of P4 code with various windowing functions is investigated in this subsection. The main performance criteria are again SNR loss, main lobe broadening, PSL and ISL. The results are obtained with the windowing functions that gave the best performance with zero Doppler; i.e. Hamming, Tukey with r = 0.5, Taylor with n_{bar} = 6, Kaiser with β = 5 windows and also with TSSWA for comparison. P4 code is of length 128 and the target Doppler is varied between 0 m/s and 1500 m/s with the given radar parameters below:

$c = 3x10^{8}\, m/s$

$f_0 = 9.5GHz$

$\delta R = 15m$

$T_S = T_C = \frac{2\delta R}{c} = 10^{-7}\, sec.$

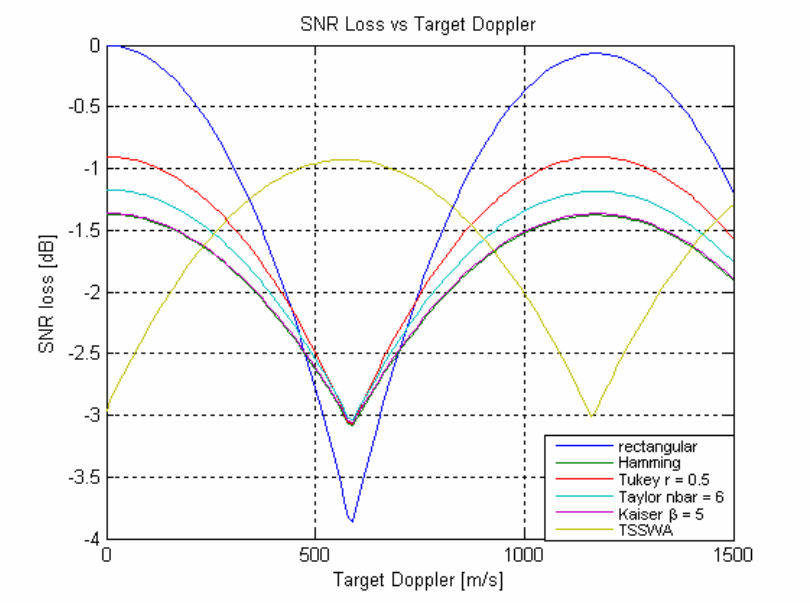

Figure 4.38: SNR loss versus target Doppler shift

Figure 4.38 illustrates the variation of SNR loss with Doppler shift under four different window functions and sliding window averager. Windowing functions react to Doppler shifts almost the same. Starting with their zero Doppler PSL values; Hamming, Tukey, Taylor and Kaiser windows give notch at 620 m/s and give an SNR loss of 3.05 dB at that Doppler. This Doppler value is half of the minimum target radial velocity for which the attenuation function given in (3.6) is zero. P4 code with no window also gives a notch for that Doppler but its SNR loss increases to 3.88 dB. This loss is due to the mismatch of the Doppler shifted echo signal and the matched filter. After 620 m/s Doppler shift the SNR loss decreases again and approaches its zero Doppler shift value for the windowing functions. At 1240 m/s (twice the Doppler of notch and first null of attenuation function given in (3.6)) the SNR loss reaches its maximum value and starts decreasing again. This peak is due to the *range-doppler coupling* [3] and the receiver gives the output with one range resolution error. In the TSSWA case behavior of SNR loss is the opposite of window function cases. At 620 m/s SNR loss reaches its peak value of 0.93 dB and at 1240 m/s approaches its zero Doppler value which is 3.01 dB.

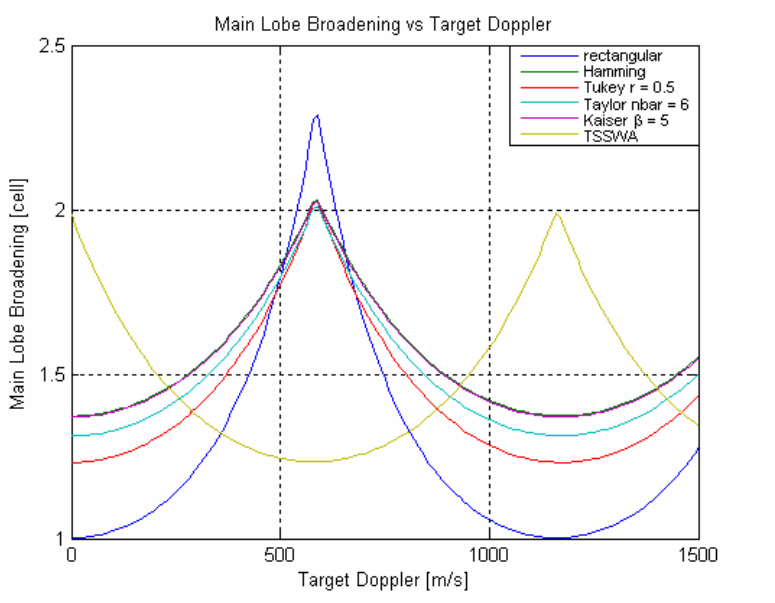

Figure 4.39: MLB versus target Doppler shift

Main lobe broadening versus target Doppler is given in Figure 4.39. The behavior of MLB is very similar to SNR loss. The window functions begin with their zero Doppler values and increase until 620 m/s. Then turn back to their zero Doppler values at 1240 m/s. TSSWA act in the opposite way as previously.

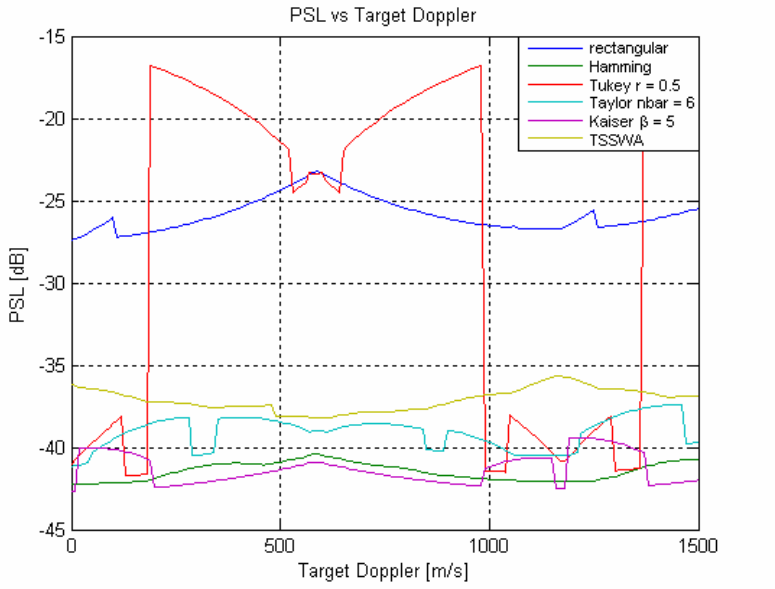

Figure 4.40: PSL versus target Doppler shift

Figure 4.40 depicts the variation in PSL due to target Doppler. Because of Doppler the peak sidelobes of the windowed code can act independently, i.e. one sidelobe can increase and one other sidelobe can decrease while the target Doppler increases. These two sidelobes can increase / decrease with different ratios due to target Doppler shift, and this is one of the reasons of the sudden jumps in PSL. Sometimes a sidelobe can appear / disappear in the mainlobe again causing sudden changes in PSL. Most windowing functions and TSSWA give nearly constant PSL over the Doppler range. Tukey window does not act like the other window functions. It makes a sudden jump at 180 m/s with a PSL change of close to 25 dB. This is due to the sidelobe formed from the mainlobe at that Doppler. With that instability Tukey window is not a good choice. Taylor window spans a 3.7 dB PSL interval over the Doppler range. This is the widest interval in the group apart from the Tukey window. Hamming window is the most stable window in the sense of PSL. It has a dynamic range of 1.8 dB over the whole Doppler range, and is the best choice from the viewpoint of PSL.

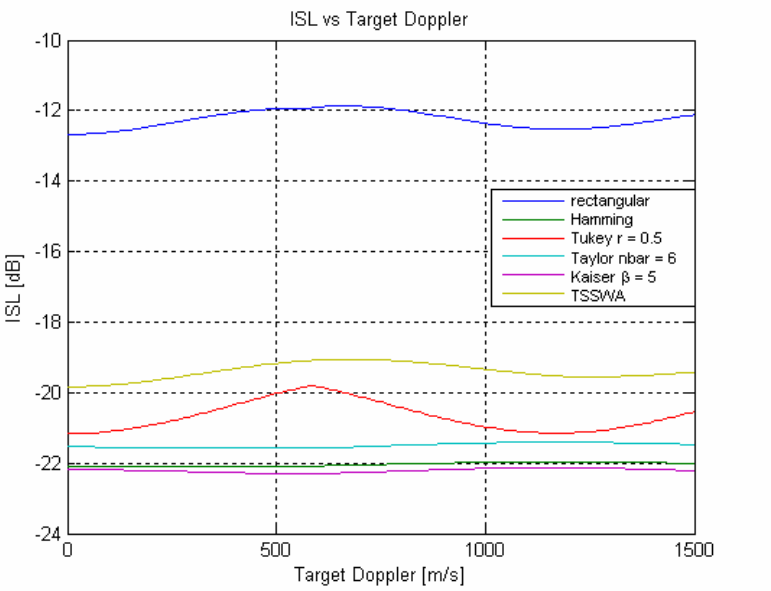

Figure 4.41: ISL versus target Doppler shift

Variation of ISL versus target Doppler for window functions is given in Figure 4.41. The change of ISL is similar to PSL. But since ISL is the sum of the sidelobe energy there is no sudden jump in ISL. Again, Tukey window has the widest dynamic range and Hamming window has the narrowest. Hamming window has a nearly constant ISL about -22 dB over the Doppler axis.

The corresponding properties of P3 code under different window functions weighting are almost the same as P4 code [22]. Because of that the result of P3 code is not given here. Frank, P1 and P2 codes have yielded unacceptable results for no Doppler case and because of that they are not examined here.

CHAPTER 5

INVERSE FILTER FOR SIDELOBE SUPPRESSION

5.1. Introduction

Previous chapter dealt with the reduction of range sidelobes of matched filter output based on windowing functions and sliding windows. In this chapter the sidelobe suppression problem is approached from a different viewpoint: The method discussed in this chapter is inverse filtering.

A large amount of work on this area has been done by geophysicists that is directly relevant to this problem [25, 26]. The application of inverse filtering to radar range sidelobe reduction is first discussed in [23]. The results of the proposed method are illustrated with Barker code of length 13 and the results are compared with matched filter results. The suggested method minimizes the energy of the difference between the actual and the ideal MF response sequences. This is actually an optimization procedure which minimizes the ISL. A similar method is also developed in [24] for the minimization of peak sidelobe level in the correlation of a biphase code.

The method employed in this chapter minimizes the integrated sidelobe energy. In the next subsection it is shown that this minimization procedure results in the solution given in [23]. The inverse filter method given in [23] is

applied to P4 code with various filter lengths. The variation of SNR loss, MLB, PSL and ISL are obtained with respect to inverse filter length. The effect of Doppler shifts on inverse and filter performance is also obtained. Finally, the results of sidelobe suppression methods are compared.

5.2. Inverse Filtering

The output of the receiver filter of radar can be expressed by:

$$y_n = \sum_{k=0}^{M-1} h_k u_{n-k} \tag{5.1}$$

where h_n is the receiver filter of length M and u_n is the received code sequence of length N.

When one is concerned basically about sidelobe levels, ideally, the desired response of an inverse filter is a sequence of elements except one is all zero. This filter is indeed the inverse of the code sequence. The position of the nonzero element, L, is immaterial at this point. If the code sequence is (u_0, u_1, u_2,.., u_{N-1}) then the desired inverse filter has a Z transform of:

$$H(z) = \frac{z^{-L}}{u_0 + u_1 z^{-1} + u_2 z^{-2} + .. + u_{N-1} z^{-N+1}}. \tag{5.2}$$

Obviously, H(z) can not be realized with a finite impulse response (FIR) filter. So a realizable method is the minimization of the energy of the sidelobes of y_n:

$$E = \sum_{n=0}^{N+M-1} [y_n - \delta_{n-L}]^2 \tag{5.3}$$

The energy of sidelobes, whish is indeed ISL, can also be given as:

$$E = \sum_{n=0}^{N+M-1} \left(\sum_{k=0}^{M-1} h_k u_{n-k} - \delta_{n-L} \right)^2 \tag{5.4}$$

To find the inverse filter which gives the minimum ISL, the derivative of E is taken with respect to h_m for $0 \leqslant m \leqslant (M-1)$.

$$\frac{\partial E}{\partial h_m} = \sum_{n=0}^{N+M-1} 2 \sum_{k=0}^{M-1} \left[h_k u_{n-k} - \delta_{n-L} \right] u_{n-m} = 0 \tag{5.5}$$

$$\sum_{k=0}^{M-1} h_k \sum_{n=0}^{N+M-1} \left[u_{n-k} u_{n-m} \right] = u_{L-m} \tag{5.6}$$

The equation in (5.6) should be solved for $0 \leqslant m \leqslant (M-1)$.

m = 0:

$$\sum_{k=0}^{M-1} h_k \sum_{n=0}^{N+M-1} \left[u_{n-k} u_n \right] = u_L \tag{5.7}$$

$$\sum_{k=0}^{M-1} h_k \left[u_0 u_{-k} + u_1 u_{1-k} + u_2 u_{2-k} + .. + u_{N-1} u_{(N-1)-k} \right] = u_L \tag{5.8}$$

$$\begin{aligned} & h_0 (u_0 u_0 + u_1 u_1 + u_2 u_2 + .. + u_{N-1} u_{N-1}) + \\ & h_1 (u_0 u_1 + u_1 u_2 + u_2 u_3 + .. + u_{N-2} u_{N-1}) + \\ & h_2 (u_0 u_2 + u_1 u_3 + u_2 u_4 + .. + u_{N-3} u_{N-1}) + .. + \\ & h_{M-1} (u_0 u_{M-1} + u_1 u_M + u_2 u_{M+1} + .. + u_{N-M} u_{N-1}) = u_L \end{aligned} \tag{5.9}$$

m = 1:

$$\sum_{k=0}^{M-1} h_k \left[\sum_{n=0}^{N+M-1} \left[u_{n-k} u_{n-1} \right] \right] = u_{L-1} \tag{5.10}$$

$$\sum_{k=0}^{M-1} h_k \left[u_0 u_{1-k} + u_1 u_{2-k} + u_2 u_{3-k} + .. + u_{N-1} u_{N-k} \right] = u_{L-1} \tag{5.11}$$

$$\begin{aligned} & h_0 (u_0 u_1 + u_1 u_2 + u_2 u_3 + .. + u_{N-2} u_{N-1}) + \\ & h_1 (u_0 u_0 + u_1 u_1 + u_2 u_2 + .. + u_{N-1} u_{N-1}) + \\ & h_2 (u_0 u_1 + u_1 u_2 + u_2 u_3 + .. + u_{N-2} u_{N-1}) + .. + \\ & h_{M-1} (u_0 u_{M-2} + u_1 u_{M-1} + u_2 u_{M+1} + .. + u_{N-M} u_{N-1}) = u_{L-1} \end{aligned} \tag{5.12}$$

.

.

.

.

m = M - 1:

$$\sum_{k=0}^{M-1} h_k \left[\sum_{n=0}^{N+M-1} \left[u_{n-k} u_{n-(M-1)} \right] \right] = u_{L-(M-1)} \tag{5.13}$$

$$\sum_{k=0}^{M-1} h_k \left[u_0 u_{M-1-k} + u_1 u_{M-k} + u_2 u_{M+1-k} + .. + u_{N-1} u_{N+M-2-k} \right] = u_{L-(M-1)} \tag{5.14}$$

$$\begin{aligned} & h_0 (u_0 u_{M-1} + u_1 u_M + u_2 u_{M+1} + .. + u_{N-M} u_{N-1}) + \\ & h_1 (u_0 u_{M-2} + u_1 u_{M-1} + u_2 u_M + .. + u_{N-(M-1)} u_{N-1}) + \\ & h_2 (u_0 u_{M-3} + u_1 u_{M-2} + u_2 u_{M-1} + .. + u_{N-(M-2)} u_{N-1}) + .. + \\ & h_{M-1} (u_0 u_0 + u_1 u_1 + u_2 u_2 + .. + u_{N-1} u_{N-1}) = u_{L-(M-1)} \end{aligned} \tag{5.15}$$

After obtaining the equations given above, one can solve these equations to get h_m. These equations can be put into matrix/vector form:

$$\underline{\underline{A}}\,\underline{h} = \underline{r} \tag{5.16}$$

where $\underline{h}$ is a column vector whose elements are the elements of the weighting sequence that is to be calculated (i.e. h_m's) and $\underline{r}$ is a vector containing the discrete cross-correlation function of the input sequence (u_0, u_1, u_2,.., u_{N-1}) and the desired output sequence. $\underline{\underline{A}}$ is a matrix each row of which consists of a shifted version of the autocorrelation of the input sequence. Then, the inverse filter coefficient vector $\underline{h}$ is:

$$\underline{h} = \underline{\underline{A}}^{-1}\,\underline{r}\,. \tag{5.17}$$

5.3. IF on Receive

For the study of inverse filtering on receive, P4 code is used due to its previous success on windowing and Doppler shifts. The ACF function of P4 code of length 128 was given in Figure 4.3. Figure 5.1 depicts the response of IF (Inverse Filter) to the P4 code obtained with the solution of (5.17).

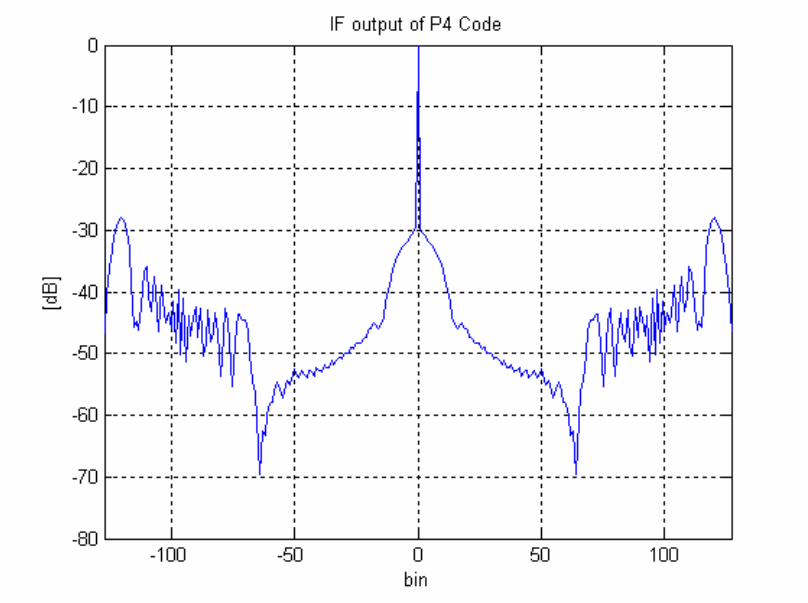

Figure 5.1: P4 code of length 128 filtered with IF of length 128

In the case of IF, the filter length can be chosen arbitrarily; i.e. filter length does not have to be equal to the code length. Also, the desired location of the output peak does not have to be at the middle of the IF output. But the performance of the computations show that the IF length at least has to be equal to or greater than the input code sequence length. The optimum location of the output peak is found to be the middle point of the output sequence which has a length of (N+M-1). If these two requirements are not met, the sidelobes increase too much approaching the main peak which forms a contradiction with the main purpose of inverse filtering.

P4 code of length 128 with inverse filtering of length 128 applied has an ISL value of -15.15 dB which is about 2.48 dB lower than the matched filter output. While trying to minimize ISL, the inverse filter also lowers the PSL. Inverse filtered P4 has a PSL value of -28.00 dB which is about 0.6 dB lower than MF case. One difference about PSL of MF and IF is the location of the peak sidelobe of the output. In the MF case the peak sidelobe is close to the main peak while in the IF case it is close to the end. One advantage of this

difference is that two close targets in space can be distinguished better using IF. The drawback of inverse filtering is an SNR loss due to filter mismatch and in this case a mismatch loss of 0.08 dB occurs. The pulse widening due to inverse filtering is negligible with a value of 1.01.

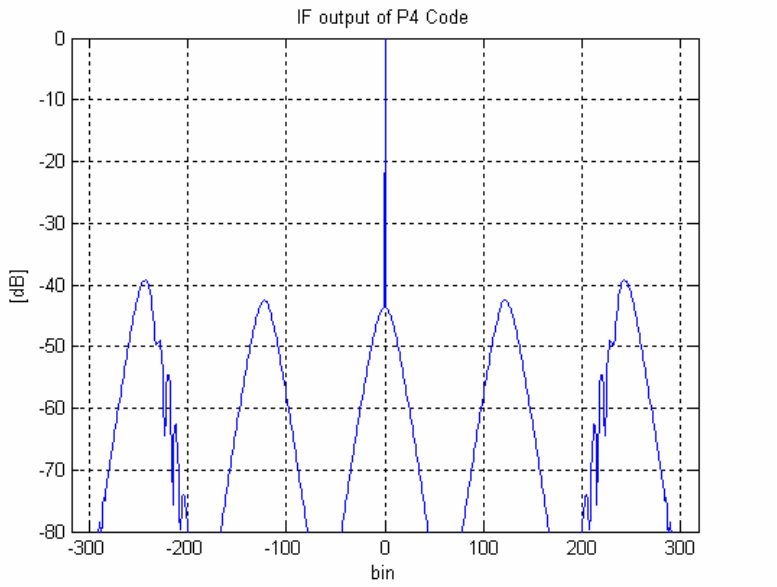

Figure 5.2: P4 code of length 128 filtered with IF of length 512

As stated previously, the filter length in inverse filtering case can be variable. Figure 5.2 shows the response of an inverse filter of length 512 to a P4 code of length 128. For this case the ISL value is lowered to -21.94 dB, 9.27 dB lower than MF ISL value. The PSL is -39.23 dB which is 11.42 dB lower than MF PSL. But as the filter length increases the SNR loss due to mismatch also increases and the resultant loss of this IF is 0.34 dB. The MLB value of inverse filter is obtained as 1.00.

In the following figures the variation of SNR loss, main lobe broadening, PSL and ISL are given with respect to inverse filter length (M) for a P4 code of

length 128. Figure 5.3 shows the effect of filter length on SNR loss. The filter length is varied between 128 and 640. As seen in Figure 5.3 SNR loss increases as the filter length increases. There is a sharp jump in the SNR loss as the filter length varies between 350 and 400. Another jump occurs when the filter length exceeds 600. To make a better comparison with MF case the upper limit of the plot is taken to 0 dB.

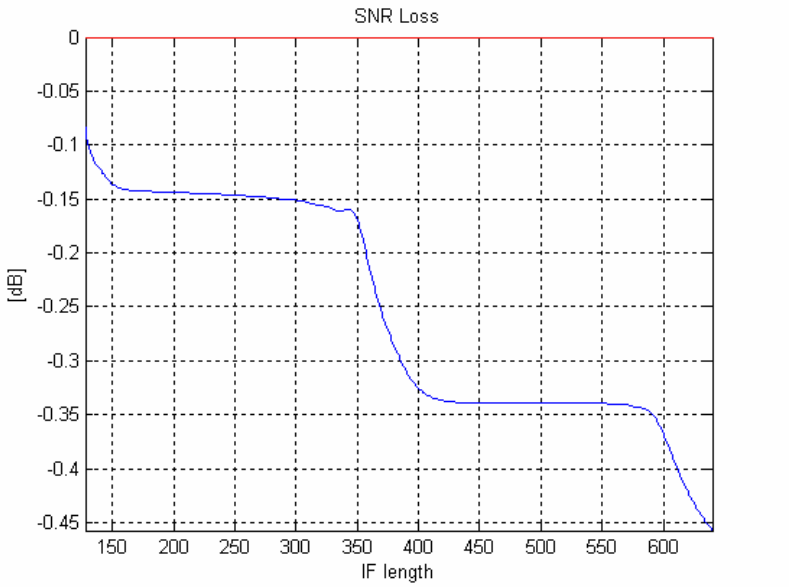

Figure 5.3: SNR loss versus IF length

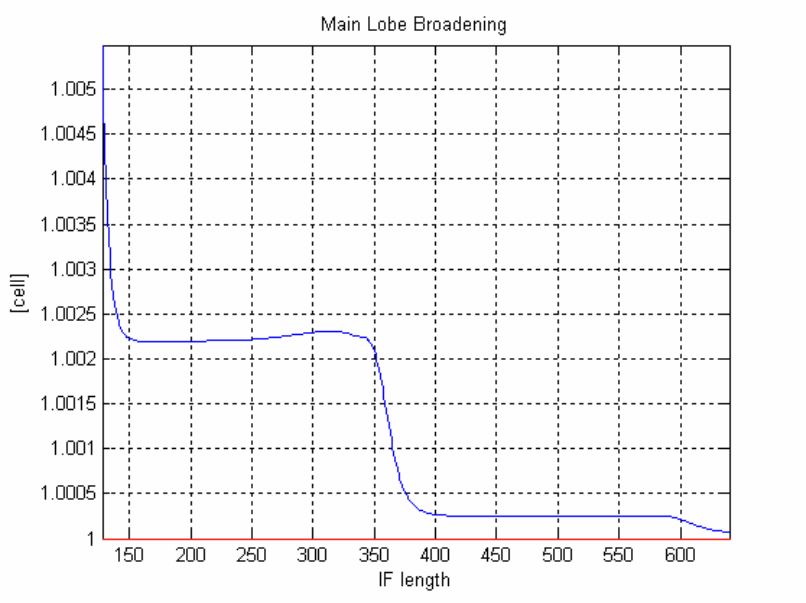

Figure 5.4: MLB versus IF length

Main lobe broadening versus inverse filter length is given in Figure 5.4. On the contrary of windowing case the main lobe of the filter output does not widen in the IF case. As the filter length is varied between 128 and 640 the MLB varies between 1.0055 and 1.0001. Similar to SNR loss a jump occurs in MLB when the filter length varies between 350 and 400.

The variation of PSL with respect to inverse filter length is given in Figure 5.5. The PSL of MF output is also given on the plot. Similar to previous plots the PSL has a sudden jump as the filter length passes between 350 and 400. This difference is about 9.1 dB. So, if the designer can use an inverse filter with length not necessarily equal to the code length and if PSL is the primary concern in the design then the designer should choose the filter length greater than 400. After a code length of 400 the PSL remains approximately constant till the code length reaches 600. So, varying filter length between 400 and 600 does not bring the designer any benefit. As the filter length is increased the realization of the theory in practice gets harder so it seems reasonable to choose a filter length around 400.

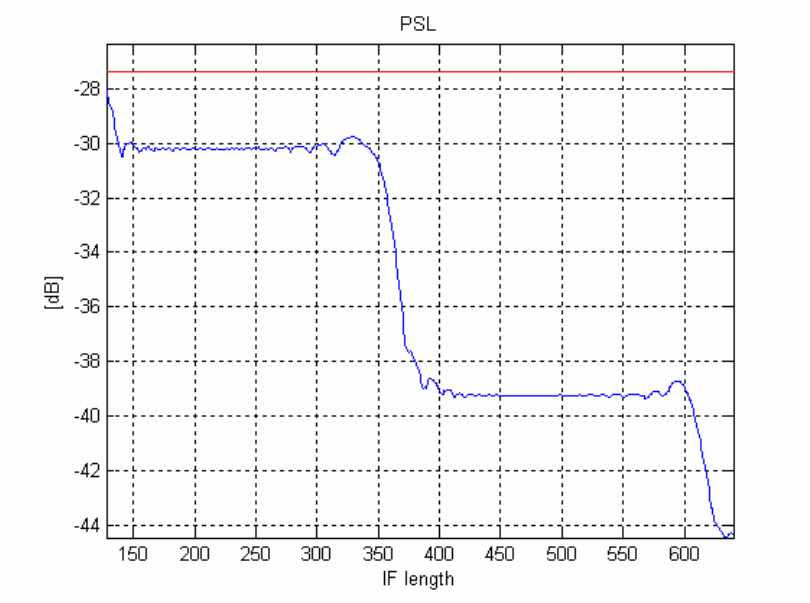

Figure 5.5: PSL versus IF length

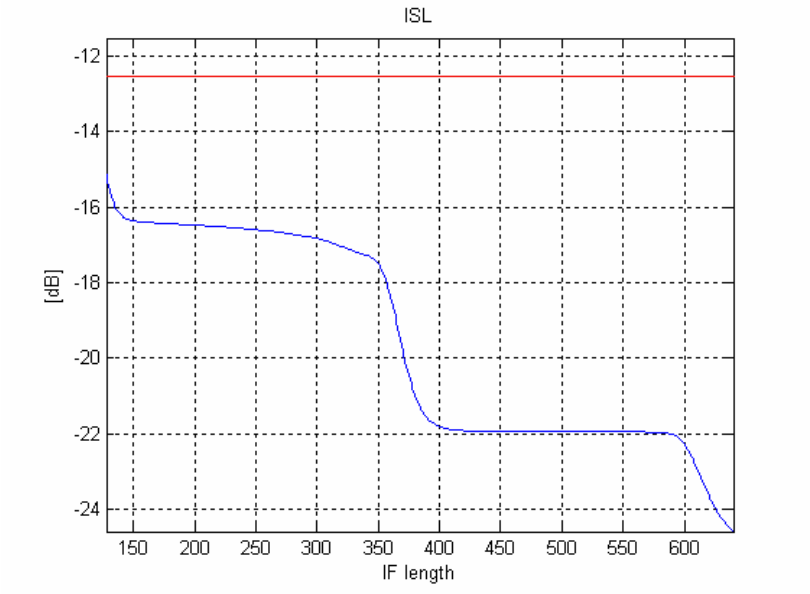

Figure 5.6: ISL versus IF length

ISL versus inverse filter length is given in Figure 5.6. ISL value of the MF output is also given in the plot. As in the previous three plots, the ISL has a jump when the filter length changes between 350 and 400 and there is a second jump at 600. The difference of ISL when the filter length changes

from 350 to 400 is about 4.6 dB. Similar to PSL case the filter length can be selected as 400 if ISL is the primary or secondary concern.

In the next subsection Doppler response of the IF method is given.

5.4. Doppler Performance of IF Technique

The Doppler response of inverse filtered P4 code is investigated in this subsection. The main performance criteria are again SNR loss, main lobe broadening, PSL and ISL as before.

First the Doppler performance of Taylor window is obtained. For this purpose a P4 code of length 128 is used with the radar parameters below. Target radial velocity is selected as 750 m/s.

$$c = 3x10^{8}\, m/s$$
$$f_0 = 9.5GHz$$
$$\delta R = 15m$$
$$T_S = T_C = \frac{2\delta R}{c} = 10^{-7}\, sec.$$

Figure 5.7 through 5.12 show the plots of the response of filters to P4 code. Figures on the left show the no Doppler case and the figures on the right show the response of the filter on the left to a Doppler shifted input sequence. Inverse filter length is equal to the code sequence length. The peak levels of the filter responses to Doppler shifted inputs are also shown on the plots. The values of the peak points are equal to the SNR loss due to target Doppler shift mismatch only. There is also an SNR loss due to filter mismatch. These values were given in Table 4.1. Table 5.1 gives the performance of the cases given in Figures 5.7-5.12. WMF refer to windowed MF.

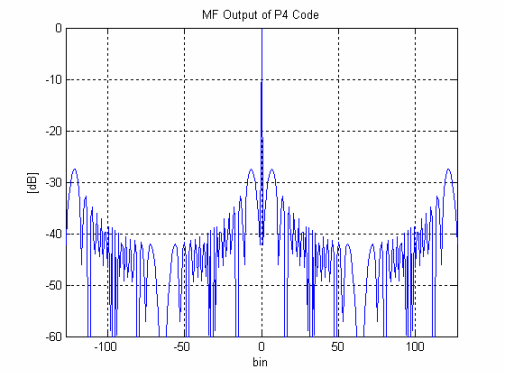

Figure 5.7: MF output of P4 code

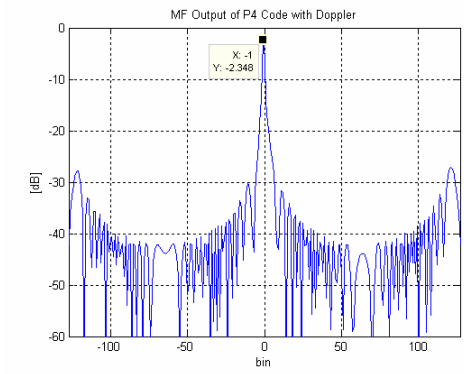

Figure 5.8: MF output of P4 code with Doppler shift

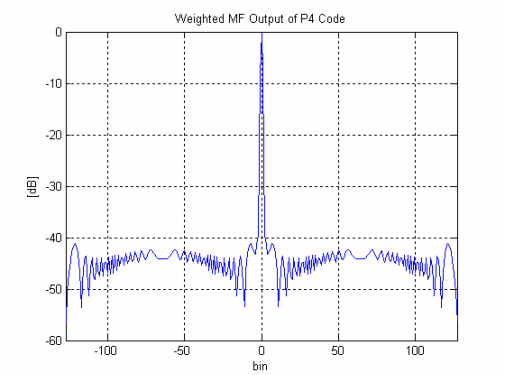

Figure 5.9: WMF output of P4 code

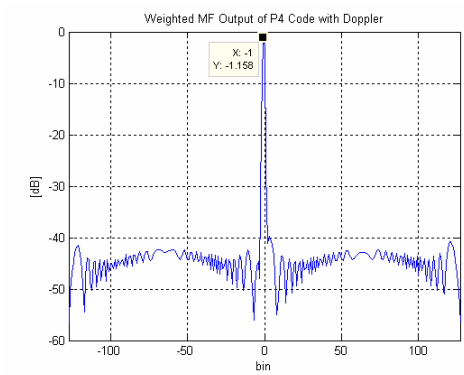

Figure 5.10: WMF output of P4 code with Doppler shift

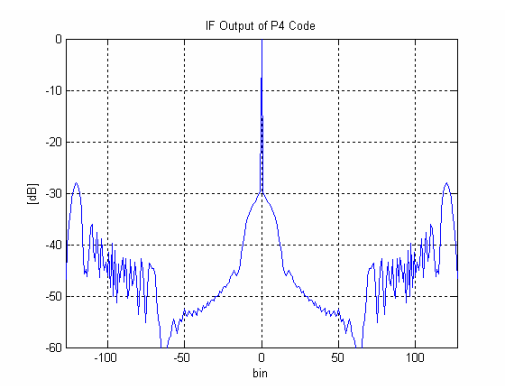

Figure 5.11: IF output of P4 code

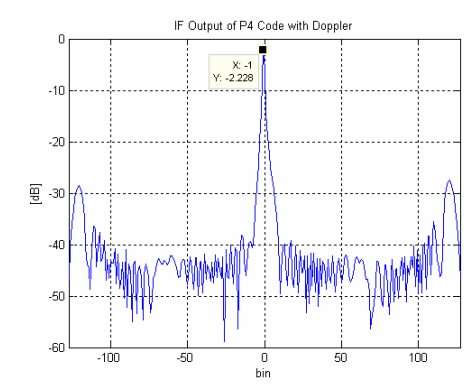

Figure 5.12: IF output of P4 code with Doppler shift

Table 5.1: Performance of Filtering Methods for P4 Code and Taylor Weight

Filter type	PSL [dB]	ISL [dB]	MLB [cells]	Mismatch Loss (Doppler) [dB]	Mismatch Loss (Filter) [dB]	Mismatch Loss (Total) [dB]
MF	-27.41	-12.67	1	NA	0	0
MF & Doppler	-24.68	-11.89	1.61	2.35	0	2.35
WMF	-41.14	-21.54	1.31	NA	1.17	1.17
WMF & Doppler	-38.57	-21.52	1.71	1.16	1.17	2.33
IF	-28.00	-15.15	1.01	NA	0.08	0.08
IF & Doppler	-25.25	-13.51	1.61	2.23	0.08	2.31

First, third and fifth and rows are obtained in the previous chapters or sections. They are repeated here again to give a reference point. The responses of the filters given in these rows to Doppler shifted input code sequence are given in the second, fourth and sixth rows. If the receiver is IF only a mismatch loss of 2.23 dB occurs due to Doppler. Due to filter mismatch there exists a 0.08 dB loss also. Total is 2.31 dB mismatch loss in the IF only case. MF results in a 2.35 dB mismatch loss due to Doppler. Comparing these two conditions IF is a better choice also with its lower MLB, PSL and ISL values. If IF only case is compared with WMF then WMF can be a better choice with lower PSL and ISL values. Mismatch loss of WMF is 2.33 dB and is only 0.02 dB higher than IF mismatch loss. These results are only

valid for a target radial velocity of 750 m/s. So a better understanding can be gained if the IF case is investigated over the whole Doppler space.

Figure 5.13 plots the variation of mismatch loss versus inverse filter length for the radar and target parameters used above.

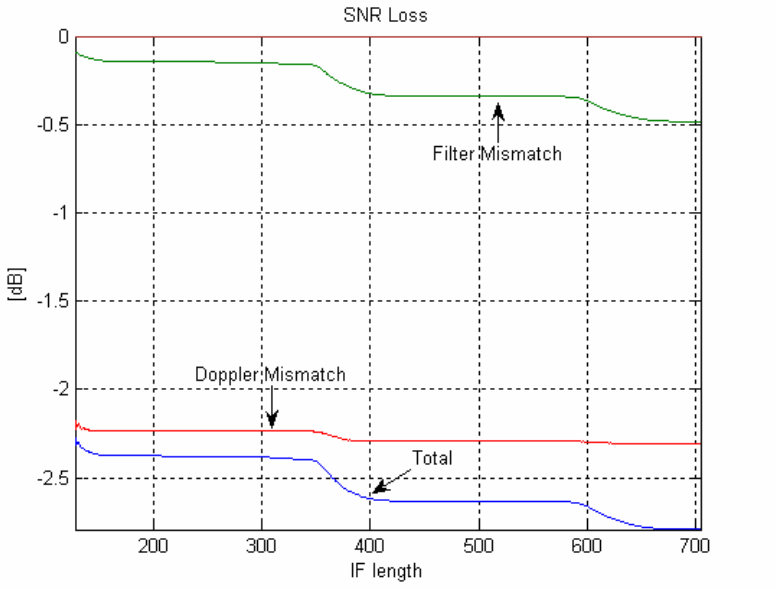

Figure 5.13: SNR loss versus inverse filter length

The variation of mismatch loss versus inverse filter length with no Doppler on target echo was given in Figure 5.3. Figure 5.13 gives the mismatch loss of an inverse filter due to filter mismatch only, which was given in Figure 5.3, target Doppler only and the total of both losses. Here, target radial velocity is again taken as 750 m/s. All the mismatch losses make a step down when the IF length is between 350 and 400. The jump of Doppler mismatch is not very sharp. Therefore, the step in the total loss is mainly due to filter mismatch. Except that little step down the Doppler mismatch remains nearly constant through the whole filter lengths.

Figure 5.14 gives the SNR loss versus target Doppler frequency variation of IF method. The response of IF is almost the same as the response of MF or WMF methods. Similar to MF case the loss in SNR makes a notch at 620 m/s with a value of 3.78. This loss was 3.88 dB for MF. Thus, the inverse filter response has less loss compared with matched filter response at the same target Doppler frequency. After the notch point SNR loss decreases again and approaches its zero Doppler value as in MF case.

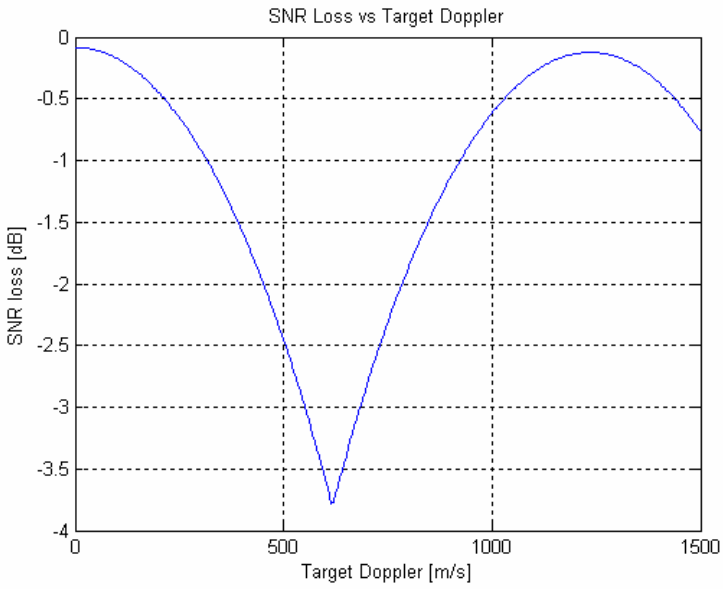

Figure 5.14: SNR loss versus Doppler shift

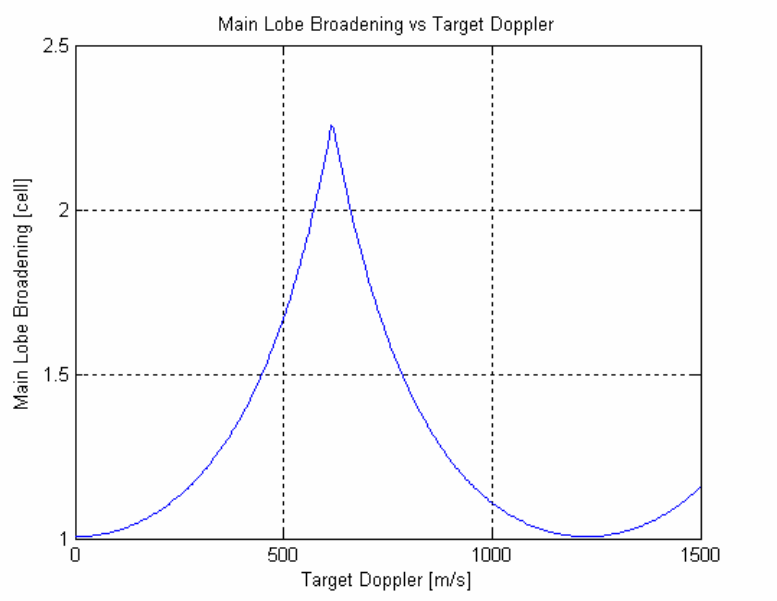

Figure 5.15: MLB versus Doppler shift

Response of IF to target radial velocity in the case of MLB is similar to the variation of SNR loss. MLB first increases to its peak value as the target Doppler reaches 620 m/s and then decreases and approaches its zero Doppler value as radial velocity goes to 1240 m/s. Figure 5.15 and 4.39 are almost the same. This can also be seen in Table 5.1. The MLB values of MF and IF are very close to each other.

Figure 5.16 depicts the variation in PSL with radial target velocity. The PSL increases with increasing radial velocity and reaches its peak value at the 620 m/s target velocity. After that point the PSL starts decreasing with increasing target Doppler. As the radial velocity reaches 1240 m/s the PSL makes a notch, but the PSL value at that point is not as low as zero Doppler shift PSL value.

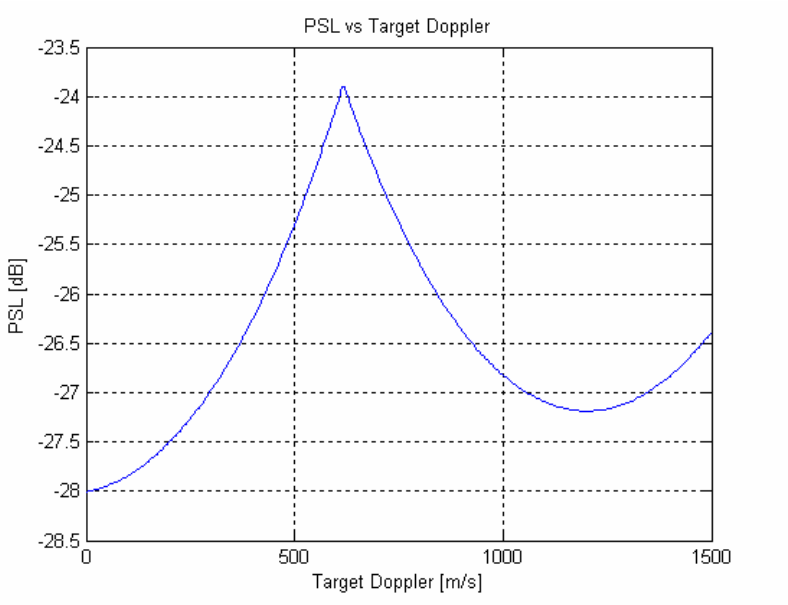

Figure 5.16: PSL versus Doppler shift

Variation of ISL versus target Doppler shift is given in Figure 5.17. The change of ISL is similar to PSL. ISL makes the peak at 620 m/s radial velocity and decreases as velocity reaches 1240 m/s and makes a notch at that target Doppler shift. Then after that point ISL starts increasing again.

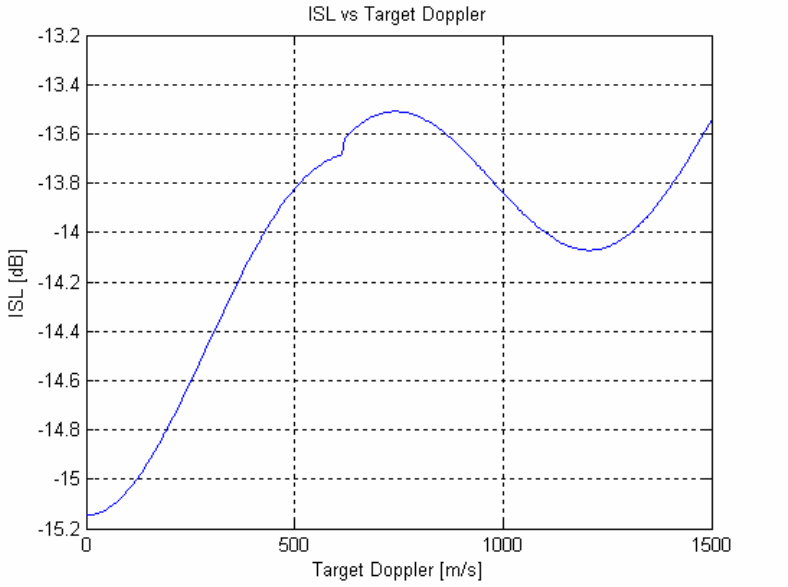

Figure 5.17: ISL versus Doppler shift

CHAPTER 6

QUANTIZATION EFFECTS

6.1. Introduction

In modern radars, A/D converters are used in different parts of the system. When the incoming echo signal is converted from analog to digital, quantization errors occur due to the finite bit length of the A/D converters. In addition, the coefficients used in the receiver system are represented by a finite number of bits.

The finite bit representation of the receiver filter coefficients and quantization of the analog input signal increase the sidelobes of the ACF, decrease the probability of detection (P_D) and / or increase the probability of false alarm (P_{FA}) of the radar, depending on the quantization levels used.

In this chapter, the effect of quantization on radar performance is examined. The variation of sidelobe levels with the number of bits used is studied in Section 6.2. The results are obtained and compared for different receiver filters (matched, inverse) and different weighting windows.

Section 6.3 investigates the extra input SNR required for a desired P_D and P_{FA} for different receiver filters and for different levels of quantization.

6.2. Quantization Effects on Sidelobes

Figure 6.1 shows a simple radar receiver model with quantization effects taken into account.

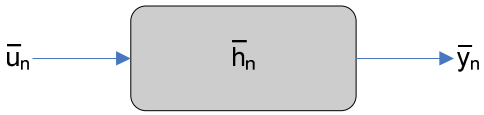

Figure 6.1: Radar receiver with quantization

$\bar{u}_n$ is the transmitted signal with q_1 levels of quantization and can be given as:

$$\bar{u}_n = Q_1(u_n) \tag{6.1}$$

where Q_1 is the quantizer function with q_1 levels.

Similarly $\bar{h}_n$ is the receiver filter with q_2 levels of quantization and can be given as:

$$\bar{h}_n = Q_2(h_n) \tag{6.2}$$

where Q_2 is the quantizer function with q_2 levels and $\bar{y}_n$ is the output.

A quantizer function with 4 bits of quantization is plotted in Figure 6.2. The input signal is assumed to be within the dynamic range of the quantizer. The maximum value of the input signal is taken as α times the maximum value of

the quantizer. The value of α is taken as 0.9 in the computations and q_1 and q_2 are used with equal values.

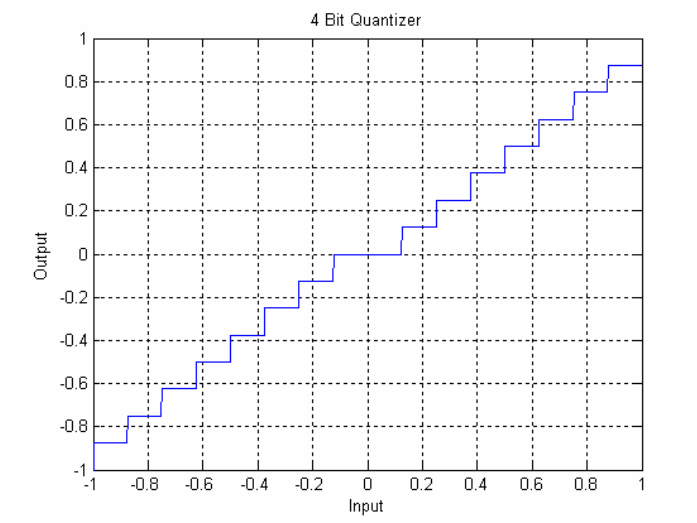

Figure 6.2: 4 bit quantizer

In the computations performed, the effect of saturation is not taken into account. Gray and Zeoli [27] have investigated the effect of quantization and saturation with an input signal that has an assumed Gaussian probability density function. They have found an optimum value (k_{opt}) that relates the input signal rms value and the quantizer dynamic range. They have shown that, for all the quantization levels used (3, 4,..,10) a ±10 percent change in k results in a very small change in total noise power. In their study the noise power is broken into two parts, one due to quantization and one due to saturation. They have also shown that at optimum k, the quantization noise is several times larger than saturation noise. In [12] computations are performed to quantify the effects of quantization on Frank code. Compression ratios of 36 and 144 are considered in computations. The general conclusion reached is that the polyphase code is relatively insensitive to the number of bits beyond a certain number. That certain number is 8 bits at worst case.

The computations in this chapter are performed with P4 code of length 128 as before. The MF output of a P4 code with 4 bits of quantization is given in Figure 6.3. As stated before, both the incoming signal and the MF coefficients are quantized with the quantizer given in Figure 6.2, i.e. $q_1=q_2=q$. As compared with Figure 4.3, the sidelobe level of MF output has increased.

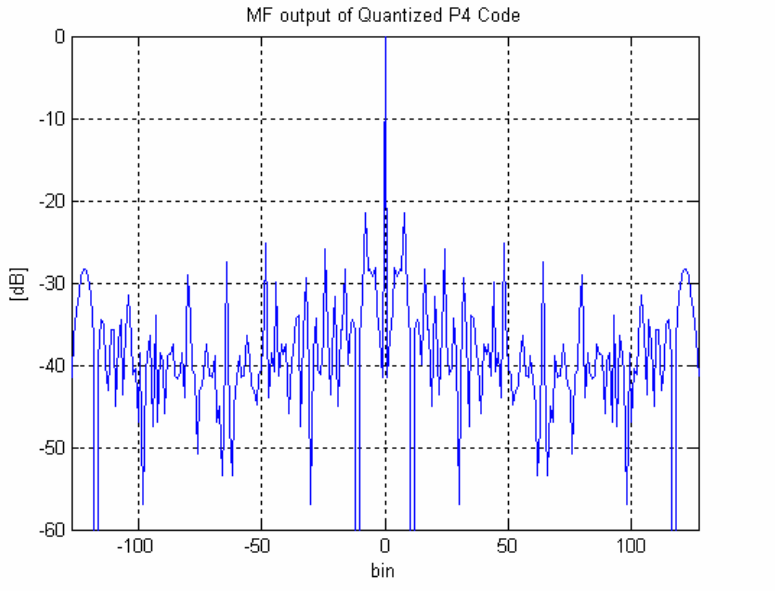

Figure 6.3: MF output of 4 bit quantized P4 code

The variation of PSL and quantization level is given in Figure 6.4 for P4 code filtered with MF. Quantization level is varied between 4 and 16 bits. The PSL saturates to its final value after 7 bits.

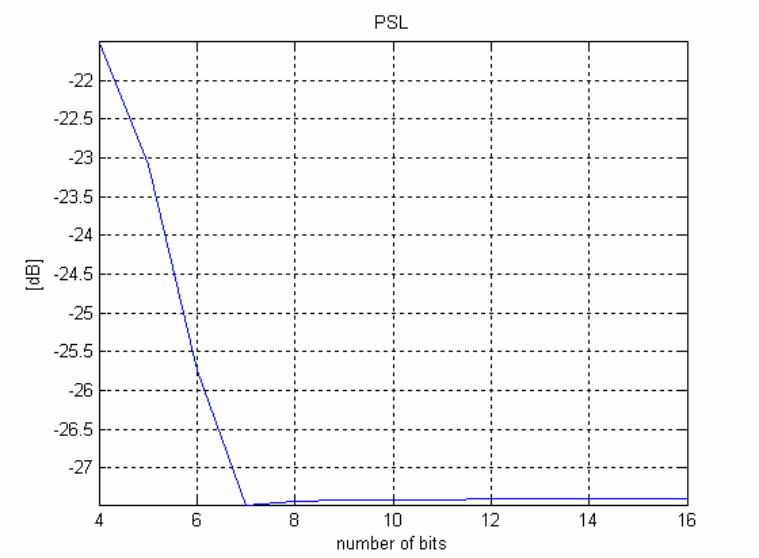

Figure 6.4: PSL versus number of bits for MF

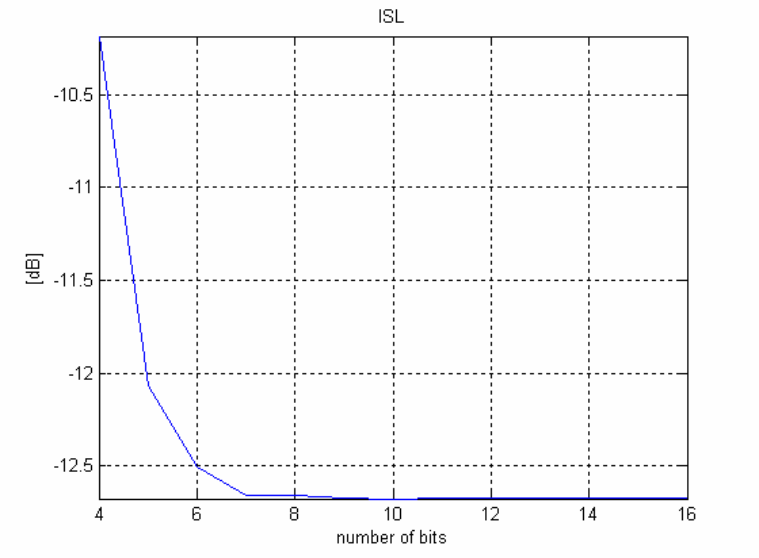

Figure 6.5: ISL versus number of bits for MF

Similar to PSL the ISL of quantized MF system saturates after 7 bits. If the code sequence length is increased the saturation point moves right side. For a code length of 256 the knee point is at 8 bits for ISL and 9 bits for PSL. If

the code length is increased further to 1024 then the knee point remains the same for ISL but moves to 10 bits for PSL. Thus, an increase in the code length also brings an increase in the minimum required bit resolution of quantizer. However, if the code length is to be selected around 128 then 8 bits is sufficient.

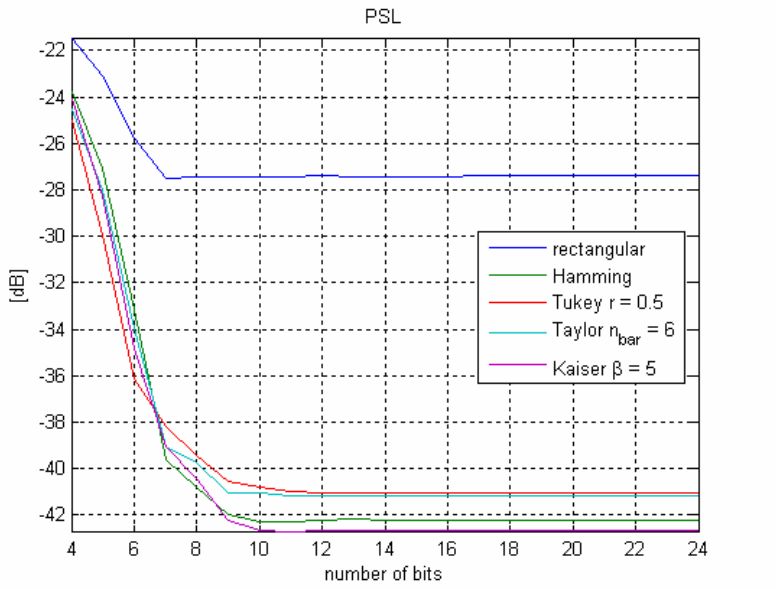

Figure 6.6: PSL versus number of bits for WMF

The effect of quantization on WMF is provided in Figures 6.6 and 6.7. Figure 6.6 depicts PSL versus number of bits used in the quantizers. No window case is also given for reference. The PSL saturates at 10 bits quantization level for most of the windowing functions used. The filter with no window has the knee point at 7 bits which is also given in Figure 6.3. With 7 bit quantization level; the Hamming window has 2.58 dB, Tukey window has 2.87 dB, Taylor window has 2.10 dB and Kaiser window has 3.61 dB higher PSL values compared with the final PSL values. Along with their low PSL values, the window functions also require 3 extra bits to the quantizer

compared with no window. Tukey window gave the worst performance in terms of Doppler shifts in previous chapters. Here again Tukey window saturates at 12 bits which is 2 bits later than the other group.

The variation of ISL with number of bits used in the quantizers is shown in Figure 6.7. The ISL values of WMF system saturates at 8 bits. No window ISL value saturates at 7 bits. Thus, it can be concluded that the effect of quantization on ISL is not as much as the effect on PSL for WMF implementation.

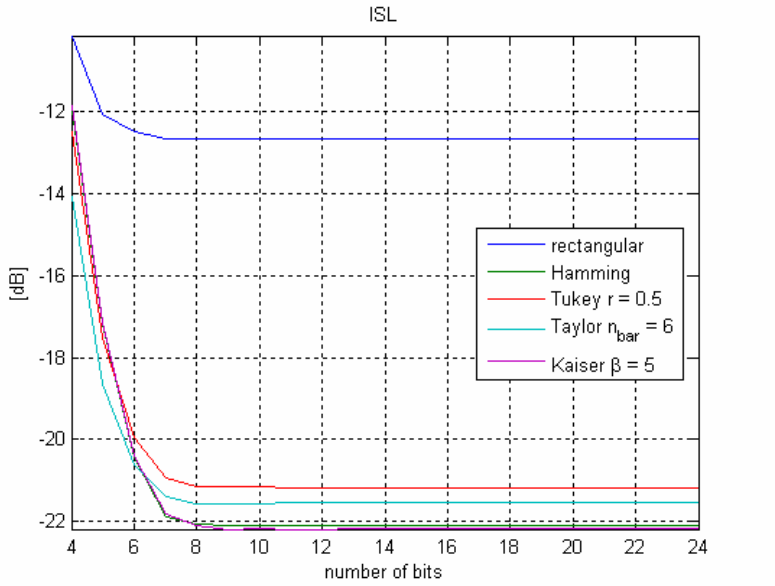

Figure 6.7: ISL versus number of bits for WMF

The IF output of a P4 code with 10 bit of quantization is shown in Figure 6.8. The inverse filter length is taken equal to code length which is 128. The incoming signal and the IF coefficients are quantized with a 10 bit quantizer, i.e. $q_1=q_2=q$. As compared with Figure 5.1 the sidelobe level of IF output has increased even with 10 bits.

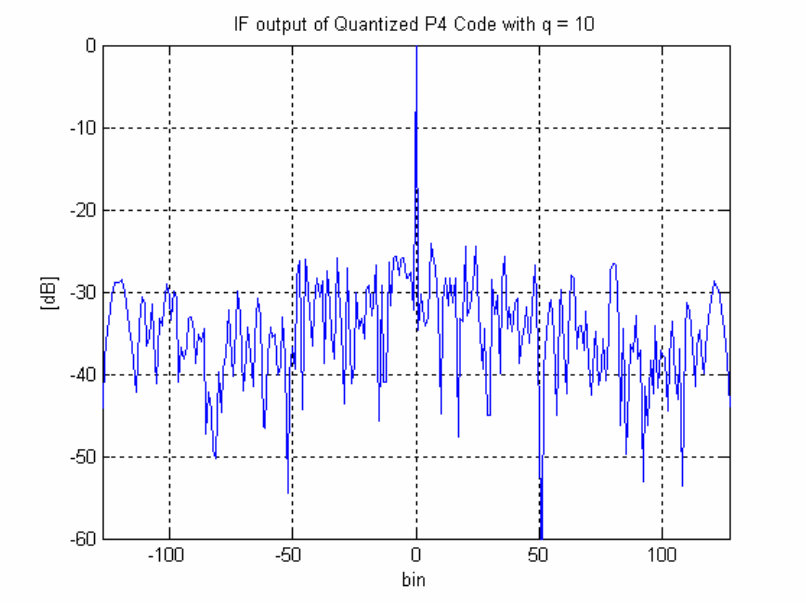

Figure 6.8: IF output of 10 bit quantized P4 code

The variation of PSL with quantization level is plotted in Figure 6.9 for IF method. The PSL of inverse filtered code sequence saturates at 12 bits for IF length of 128 and 14 bits for IF length of 400. MF only case has the knee point at 7 bits of resolution. Thus IF needs 5 to 7 more bits of resolution compared with MF.

ISL versus quantization level is shown in Figure 6.10. The ISL of IF method saturates at 14 bits for IF of length 128 and 16 bits for IF of length 400. This value is 7 to 9 bits more compared with MF knee point. On the overall, the effect of quantization on IF is more compared with MF since IF outputs saturate later compared to MF outputs. If the inverse filter length is increased the knee points of ISL and PSL shifts to the right. Therefore, if inverse filtering is used, depending on IF length, at least 14 or 16 bits of quantizers should be used.

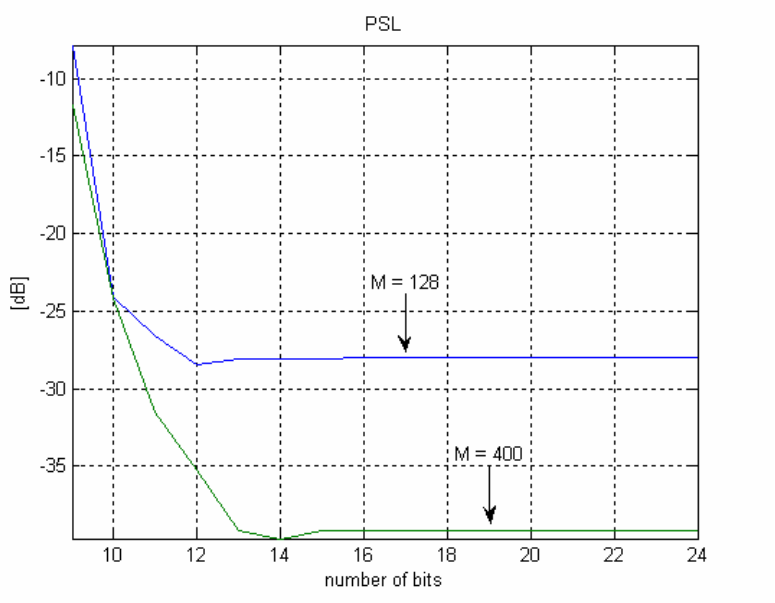

Figure 6.9: PSL versus number of bits for IF

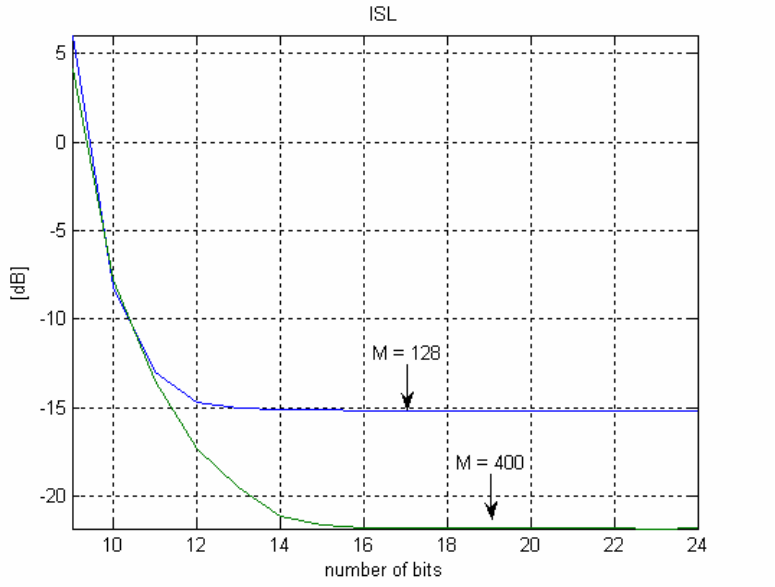

Figure 6.10: ISL versus number of bits for IF

6.3. Quantization Effects on P_D & P_{FA}

In this subsection the effect of quantization on detection probabilities of a radar system is investigated. A standard radar receiver with quantization effects taken into account was given in Figure 6.1. The incoming signal $\overline{u}_n$ after quantization can be written as:

$$\overline{u}_n = u_n + q_n \tag{6.3}$$

where q_n is the quantization noise in received signal.

Similarly, the receiver filter; either MF, IF or WMF can be written as:

$$\overline{h}_n = h_n + e_n \tag{6.4}$$

Then, the output signal $\overline{y}_n$ is equal to:

$$\overline{y}_n = \sum_{k=0}^{M-1} \overline{h}_k \overline{u}_{n-k} = \sum_{k=0}^{M-1} [h_k + e_k][u_{n-k} + q_{n-k}] \tag{6.5}$$

$$\overline{y}_n = y_n + \sum_{k=0}^{M-1} h_k q_{n-k} + \sum_{k=0}^{M-1} e_k u_{n-k} + \sum_{k=0}^{M-1} e_k q_{n-k} \tag{6.6}$$

The output SNR of a radar system was given in (4.5). For the quantized system the output SNR can be rewritten as:

$$SNR_o = \frac{\left|\overline{y}_L\right|^2}{\overline{\sigma}^2 \sum_{k=0}^{M-1} \left|\overline{h}_k\right|^2} \tag{6.7}$$

where L is the ideal sampling position and $\overline{\sigma}^2 = \sigma^2 + \frac{\Delta^2}{12}$ with the quantizer step size of Δ [27].

The received signal in a radar system can be either an echo signal from a target with additive noise or only noise: This can be given by two hypotheses [28]:

$$\begin{aligned} H_0 &: \quad r_i = n_i \\ H_1 &: r_i = m + n_i \end{aligned} \tag{6.8}$$

where $i = 1, 2, .., N_{obs}$ is the number of observations, m is the received signal and n_i are independent zero mean Gaussian noise. Detection and false alarm probabilities for this observation set can be given as [28]:

$$P_D = \int_{\gamma}^{\infty} \frac{1}{\sqrt{2\pi}} e^{-\frac{(l-d)^2}{2}} dl = \frac{1}{2} erfc\left(\frac{\gamma - d}{\sqrt{2}}\right) \tag{6.9}$$

$$P_{FA} = \int_{\gamma}^{\infty} \frac{1}{\sqrt{2\pi}} e^{-\frac{l^2}{2}} dl = \frac{1}{2} erfc\left(\frac{\gamma}{\sqrt{2}}\right) \tag{6.10}$$

where

$$d = \frac{m\sqrt{N_{obs}}}{\sigma} \tag{6.11}$$

and

$$\gamma = \frac{\ln \eta}{d} + \frac{d}{2} \tag{6.12}$$

where η is the threshold that depends on observation probabilities and the costs of the events [28].

For desired values of P_D and P_{FA} the required SNR at the output of the receiver filter can be found using (6.9), (6.10) and (6.11). Then, according to the filter type and quantization level used in the system the input SNR required for that output SNR can be found using (6.7). The output SNR, and therefore, the input SNR of a system without quantization is found in parallel also. Then the extra SNR required for the desired P_D and P_{FA} values in a quantized system can be found by taking the difference in input SNR values of the two systems.

For the computations P4 code with length 128 is used as before. The P_D and P_{FA} are taken as 0.85 and 10^{-6} respectively. Only one observation is assumed $(N_{obs} = 1)$. The results are obtained for MF, WMF and IF.

Figure 6.11 depicts the SNR loss due to quantization in MF. WMF and MF are given on the same plot. All the curves saturate at 10 bits of resolution. The SNR loss of no window case declines to 0 dB. Other curves decline to the SNR loss values given in Table 4.1 after 10 bits. The Hamming and Kaiser window functions give the almost the same loss with all the quantization levels. In the previous chapter PSL of WMF was found to be saturated after 10 bits. Therefore the quantizer should have a resolution of at least 10 bits if the user wants to use windowed MF in the radar receiver for the given detection probabilities.

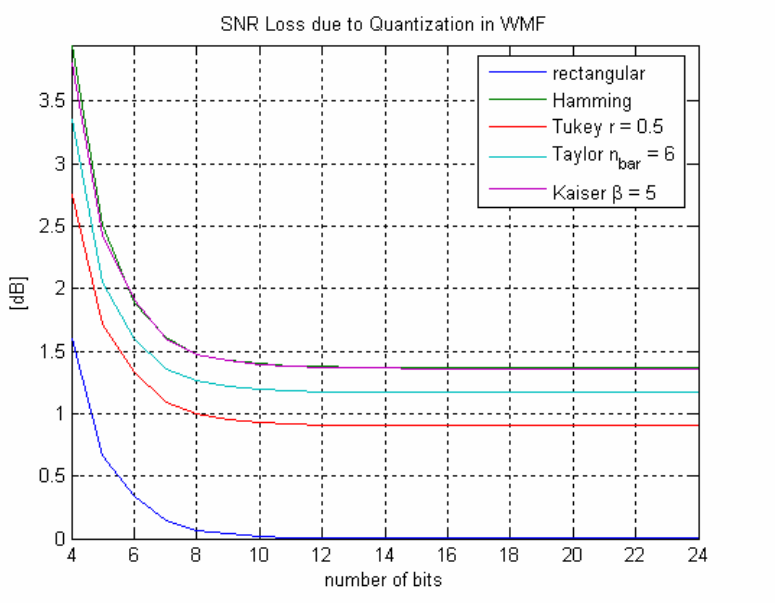

Figure 6.11: SNR loss due to quantization in WMF

The variation of SNR loss with quantizer bit resolution for IF receiver is depicted in Figure 6.12. The curve saturates at 12 bits for both of the inverse filter lengths. The SNR loss of IF of length 128 reaches 0.08 dB after 12 bits as given in Table 5.1. For IF receiver the minimum resolution required was found as 16 bits in the previous chapter. Thus, this result also covers the requirement of SNR loss for detection probabilities and the radar designer should at least use 16 bit quantizers with inverse filter receivers.

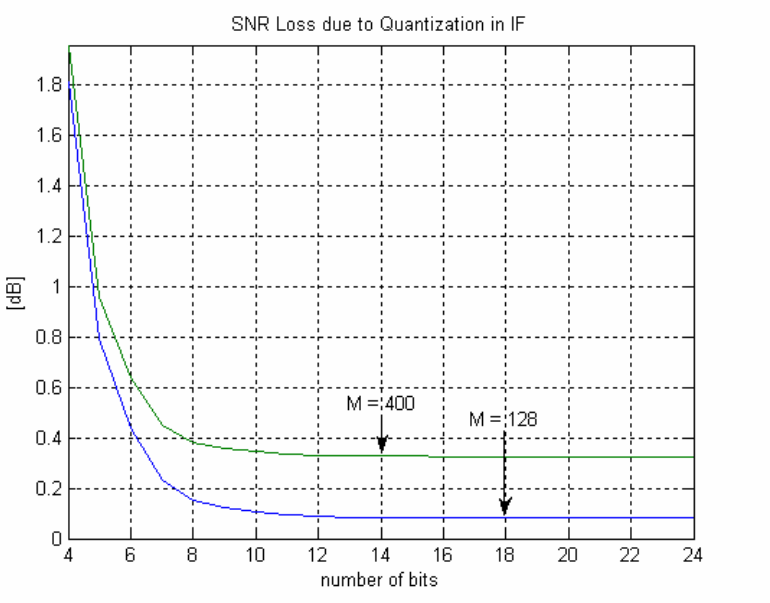

Figure 6.12: SNR loss due to quantization in IF

CHAPTER 7

CONCLUSIONS

We have investigated several design problems for the design of the matched filters used in pulse Doppler radars.

The first problem handled is the hindering of mismatch loss in radar receiver filter which occurs due to the target Doppler in the echo signal. The amount of mismatch loss and the parameters that affect this loss are found. Then two similar methods are proposed to overcome this problem. The methods are based on a parallel filter bank structure in which each filter is matched to a different Doppler shift. The distribution of the parallel filters on the Doppler plane is also given for optimum processing. The results of computations performed with the proposed methods show that the number of parallel filters can vary significantly for a desired maximum mismatch loss and given radar parameters. The number of filters also depends on which of the methods is used.

The second subject studied in this thesis is the reduction of sidelobes of radar receiver filter output. Two different solutions to this problem are considered. The first method considered is the use of classical amplitude weighting window in the matched filter of the radar. The second method is the use of a mismatched filter that minimizes the sidelobe energy. The results of all the methods are obtained and compared with each other. Taylor,

Hamming and Kaiser windows gave the best results with the windowed methods both with and without Doppler shift. It is found that the PSL of the receiver output is lowered by about 15 dB with some of the given windows. The influence of inverse filter on the receiver output is found to be considerable as the inverse filter length is increased over 400 for a 128 length P4 code. It is concluded from computations that the performance of an inverse filter of length 400 is comparable with the performance of the windowed matched filter.

The last part of the thesis is on the quantization effects on the radar performance. The effects of quantization on sidelobe levels and detection probabilities are obtained for the methods studied in Chapter 4 and Chapter 5. It is concluded that 12 bits are sufficient for windowed matched filter methods and at least 14 bits are required for inverse filter receivers.

As a future work, the independent studies conducted in this thesis can be combined to see the overall performance of the receiver with a Doppler shifted echo signal. Also the performance of *P(n,k) codes* [29] with the methods used in this thesis can be investigated.

REFERENCES

[1] IEEE Standard Dictionary of Electrical and Electronic Terms, Std. 100-1984, 1984

[2] F. E. Nathanson, “Radar Design Principles”, McGraw-Hill Inc., NY, 1990

[3] M. Bernfeld, C. E. Cook, J. Paolilli, and C. A. Palmieri, “Matched Filtering Pulse Compression and Waveform Design”, (four parts), Microwave J. 7, pt. 1, pp. 57-64, Oct. 1964, pt. 2, pp. 65-74, Nov. 1964, pt. 3, pp. 75-81, Dec. 1964, pt. 4, pp. 82-90, Jan. 1965

[4] G. L. Turin, “An Introduction to Matched Filters”, IRE Trans., vol. IT-6, pp. 311-329, June 1960

[5] D. O. North, “Analysis of Factors which Determine Signal Noise Discrimination in Radar”, RCA Labs. Princeton NJ, Report PTR-6C, June 1943

[6] Van Vleck, J. H. and D. Middleton, “A Theoretical Comparison of the Visual Aural and Meter Reception of Pulsed Signals in the Presence of Noise”, J. of App. Phys., vol.17, pp. 940-971, Nov. 1946

[7] A. Wald, “Statistical Decision Functions”, John Wiley & Sons Inc., NY, 1960

[8] J. Neyman and E. S. Pearson, “The Problem of the Most Efficient Tests of Statistical Hypotheses”, Phil. Trans., Ray. Sec., vol. 231, Series A

[9] C. E. Cook, M. Bernfeld, “Radar Signals: An Introduction to Theory and Application”, Artech House Inc., MA, 1993

[10] P. M. Woodward, I. L. Davies, “A Theory for Radar Information”, Phil. Mag. 41, 1001, 1941

[11] P. M. Woodward, “Probability and Information Theory with Applications to Radar”, Pergamon Press, Oxford, 1953

[12] B. L. Lewis, F. F. Kretschmer Jr., W. W. Shelton, “Aspects of Radar Signal Processing”, Artech House Inc., MA, 1986

[13] R. L. Frank, “Polyphase Codes with Good Nonperiodic Correlation Properties”, IEEE Trans. on Information Theory, vol. IT-9, pp. 43-45, Jan. 1963

[14] B. L. Lewis, F. F. Kretschmer Jr., “A New Class of Polyphase Pulse Compression Codes and Techniques”, IEEE Trans. on Aerospace and Electronic Systems, vol. AES-17, no. 3, pp. 364-372, May 1981

[15] B. L. Lewis, F. F. Kretschmer Jr., “Linear Frequency Modulation Derived Polyphase Pulse Compression Codes”, IEEE Trans. on Aerospace and Electronic Systems, vol. AES-18, no. 5, pp. 637-641, Sep. 1982

[16] Y. Tanık, “Radar Signal Models”, Project Report, August 2003

[17] B. L. Lewis, “Range-Time-Sidelobe Reduction Technique for FM-Derived Polyphase PC Codes”, IEEE Trans. on Aerospace and Electronic Systems, vol. AES-29, no. 3, pp. 834-840, July 1993

[18] F. F. Kretschmer Jr., L. R. Welch, “Sidelobe Reduction Techniques for Polyphase Pulse Compression Codes”, IEEE International Radar Conference, pp. 416-421, May 2000

[19] J. M. Ashe, R. L. Nevin, D. J. Murrow, H. Urkowitz, N. J. Bucci, J. D. Nespor, “Range Sidelobe Suppression of Expanded/Compressed Pulses with Droop”, 1994 IEEE National Radar Conference, pp. 116-122, Mar. 1994

[20] MATLAB help

[21] A. Ö. Yılmaz, “Linear Frequency Modulation”, Project Report, August 2004

[22] Yu Gen-miao, Wu Shun-jun, Luo Yong-jian, “Doppler Properties of Polyphase Pulse Compression Codes under Different Side-lobe Reduction Techniques”, CIE International Conference on Radar, pp. 524-528, Oct. 2001

[23] M. H. Ackroyd, F. Ghani, “Optimum Mismatched Filters for Sidelobe Suppression”, IEEE Trans. on Aerospace and Electronic Systems, vol. AES-9, no. 2, pp. 214-218, Mar. 1973

[24] J. M. Baden, M. N. Cohen, “Optimal Peak Sidelobe Filters for Biphase Pulse Compression”, IEEE International Radar Conference, pp. 249-252, May 1990

[25] R. B. Rice, “Inverse Convolution Filters”, Geophysics, vol. 27, pp. 4-18, Feb. 1962

[26] Griffin, “Statistical Communication and Detection with Special Reference to Digital Data Processing of Radar and Seismic Signals”, London 1967

[27] G. A. Grey, G. W. Zeoli, “Quantization and Saturation Noise Due to Analog-to-Digital Conversion”, IEEE Trans. on Aerospace and Electronic Systems, pp. 222-223, 1971

[28] Y. Tanık, “EE 535 Lecture Notes”

[29] T. Felhauer, “Design and Analysis of New P(n,k) Polyphase Pulse Compression Codes”, IEEE Trans. on Aerospace and Electronic Systems, pp. 865-874, July 1994